Seismic Vulnerability Assessment of Steel Moment Resisting Frames with Consideration of Mainshock Aftershock Seismic Sequence

Mohammadmehdi Torfehnejad

Submitted to the
Institute of Graduate Studies and Research
in partial fulfillment of the requirements for the degree of

Doctor of Philosophy
in
Civil Engineering

Eastern Mediterranean University
July 2022
Gazimağusa, North Cyprus

Approval of the Institute of Graduate Studies and Research

Prof. Dr. Ali Hakan Ulusoy
Director

I certify that this thesis satisfies all the requirements as a thesis for the degree of Doctor of Philosophy in Civil Engineering.

Prof. Dr. Umut Türker
Chair, Department of Civil Engineering

We certify that we have read this thesis and that in our opinion it is fully adequate in scope and quality as a thesis for the degree of Doctor of Philosophy in Civil Engineering.

Prof. Dr. Serhan Şensoy
Supervisor

Examining Committee

1. Prof. Dr. Yusuf Ayvaz
2. Prof. Dr. Serhan Şensoy
3. Prof. Dr. Cem Topkaya
4. Assoc. Prof. Dr. Mehmet Cemal Geneş
5. Assoc. Prof. Dr. Giray Özay

ABSTRACT

This study assessment of the collapse capacity and mechanism of special steel moment frames (SSMFs) with considering earthquake shock sequences for structures height from 4 to 20 stories. The collapse capacity is expressed in terms of the $S_a(T_1)$ value at which the system reaches the collapse state. Collapse identification relies on the capability of the model to accurately simulate damage of members and the resulting behavior deterioration. The softening in the lateral response expressed in terms of maximum interstory drift (MID) when it is expressed against the $S_a(T_1)$ values is thus used to identify collapse occurrence. The mainshock-aftershock (MS-AS) effect and the uncertainties associated with it are simulated by utilizing a set of 32 natural record pairs. The level of damage induced by MS is represented by two parameters including MID and peak residual story drift (PRSD). Using these parameters, the MS is applied so as to various pre-selected damage levels are imposed. For each MS damage level, an incremental dynamic analysis (IDA) is performed using the AS record that follows MS and a free vibration phase. The AS intensity causing the collapse state is finally identified and respected for evaluating the effect of MS damage level. The correlation between the median collapse S_a's, called aftershock median collapse capacity, and the MS damage indicated by MID and PRSD parameters is quantified. The collapse mechanism under the AS is also investigated by studying the distribution of maximum ductility demand (MDD) and contribution of members in the total hysteretic energy absorption, called energy absorption contribution (EAC). This investigation revealed that the EAC parameter provides better metrics for studying the collapse mechanism which is remarkably affected by the MS-AS sequence. Accordingly, the role of elements experiencing damage under the MS becomes less prominent in absorbing the AS energy and is substituted by contribution of elements with less deterioration under

the MS. The members' EAC is also shown to be affected by the percentage of the energy imposed by each individual shock as a fraction of the total energy imposed by the MS-AS sequence.

Keywords: seismic collapse, mainshock-aftershock sequence, incremental dynamic analysis, median collapse capacity, steel moment frames, energy absorption distribution, inelastic demand distribution

ÖZ

Bu çalışma, 4 ile 20 kat arası yüksekliğe sahip özel çelik moment çerçeveli (ÖÇMÇ'li) yapılar için ardarda oluşan deprem dizileri dikkate alınarak göçme kapasitesinin ve mekanizmasının değerlendirilmesini içermektedir. Göçme kapasitesi, sistemin göçme durumuna ulaştığı Sa(T1) değeri cinsinden ifade edilir. Göçme tanımlaması, oluşturulan modelin her bir elemanının hasar düzeyleri ve bunun sonucunda yapının davranışında oluşan çiddi değişimi doğru bir şekilde simüle etme yeteneğine dayanır. Sa(T1) değerlerine karşı gelen maksimum katlar arası ötelenme (MKÖ) cinsinden ifade edilen yanal tepkideki yumuşama ve aşırı öteleme çökme oluşumunu tanımlamak için kullanılır. Ana şok-artçı şok (AŞ-ARŞ) etkisi ve bununla ilişkili belirsizlikler, 32 doğal kayıt çifti kullanılarak simüle edilmiştir. MS tarafından indüklenen hasar seviyesi, MKÖ ve tepe kalıcı kat ötelenmesi (TKKÖ) dahil olmak üzere iki parametre ile temsil edilir. Bu parametreleri kullanarak, önceden seçilmiş çeşitli hasar seviyelerine ulaşacak şekilde AŞ uygulanır. Her AŞ hasar seviyesi için, AŞ'yi takip eden ARŞ kaydı ve bir serbest titreşim fazı kullanılarak artımsal dinamik analiz (ADA) gerçekleştirilir. Çökme durumuna neden olan ARŞ büyüklüğü nihayet tanımlanır ve AŞ hasar seviyesinin etkisini değerlendirmek için dikkate alınır. Artçı şok medyan çökme kapasitesi olarak adlandırılan medyan göçme Sa (T)'ları ile MKÖ ve TKKÖ parametreleri tarafından belirtilen AŞ hasarı arasındaki korelasyon nicelleştirilir. ARŞ kapsamındaki göçme mekanizması, maksimum süneklik talebinin (MST) dağılımı ve yapı elemanlarının toplam histeretik enerji absorpsiyonuna, enerji absorpsiyon katkısı (EAK) olarak adlandırılan katkısı incelenerek araştırılır. Bu araştırma, EAK parametresinin, AŞ-ARŞ dizisinden önemli ölçüde etkilenen çökme mekanizmasını incelemek için daha iyi ölçümler sağladığını ortaya koydu. Buna göre, AŞ altında hasar

gören elemanların rolü, ARŞ enerjisini emmede daha az belirgin hale gelir ve AŞ altında daha az hasar gören elemanların katkısı ile değiştirilir. Yapı elemanlarının EAK'sinin, AŞ-ARŞ dizisi tarafından uygulanan toplam enerjinin bir bölümü olarak her bir deprem tarafından uygulanan enerjinin yüzdesinden de etkilendiği gösterilmiştir.

Anahtar Kelimeler: sismik göçme, ana şok-artçı şok dizisi, artımsal dinamik analiz, medyan göçme kapasitesi, çelik moment çerçeveler, enerji yutma dağılımı, esnek olmayan talep dağılımı

DEDICATION

To My Late Father

ACKNOWLEDGMENT

I would like to thank Prof. Dr. Serhan Şensoy, Vice Rector of Eastern Mediterranean University, for his continuous support and guidance in the preparation of this study. Without his invaluable supervision, all my efforts could have been short-sighted.

I owe quit a lot to my parents Morteza and Minoo who allowed me to travel all the way from Iran to Cyprus and supported me all throughout my studies.

TABLE OF CONTENTS

LIST OF TABLES

LIST OF FIGURES

LIST OF SYMBOLS AND ABBREVIATIONS

AMCC	Aftershock Median Collapse Capacity
AS	Aftershock
DUCR	Damage To Undamaged Collapse Capacity Ratio
EAC	Energy Absorption Contribution
IDA	Incremental Dynamic Analysis
MID	Maximum Interstory Drift
MDD	Maximum Ductility Demand
MS	Mainshock
PRSD	Peak Residual Story Drift

Chapter 1

INTRODUCTION

1.1 Thesis overview

Investigating the effects of the sequential excitations on special steel moment frame (SSMF) buildings is the topic of the current dissertation. The evaluation focuses on the uncertain aspects of the topic by incorporating multiple mainshock (MS)-aftershock (AS) record pairs and also various intensity levels. To pursue this purpose, this dissertation and the research procedure consists of steps they are organized in a number of chapters. These chapters and their goals are introduced in this short overview section.

Literature review on the effect of MS-AS sequences are completely reviewed in chapter 1 along with a summary of the previous damaging effects observed during MS-AS excitations. The goals and novelties of the study, as well as a brief introduction of the employed methodology are also presented at the end of chapter 1.

Chapter 2 presents complete details about the deployed methodology and procedure it follows for extracting the quantitative results using which the performance of the studied SSMFs is assessed under various MS-AS scenarios in presence of uncertain aspects.

Chapter 3 is devoted to a complete presentation of the numerical method used for representing the SSMFs in OpenSees (Mazzoni, McKenna, Scott, & Fenves, 2004) program. Initial results obtained by subjecting the models to static lateral loads are used for validating the models through comparing their outcomes with previous well-accepted results.

Chapter 4 presents the analytical results obtained by applying the methodology on four SSMFs with 4 to 20 stories. The influence of MS damage on the AS collapse capacity of the SSMFs is one of the main of contribution of this study. The method used in this chapter for representing the MS damage is based on the maximum interstory drift (MID) response imposed by the MSs on the structures.

In chapter 5, an alternative method proposed by the previous studies for representing MS damage is evaluated. This method relies on the peak residual story drift (PRSD) response of the studied SSMFs under the MS-AS sequences.

The mechanism through which collapse of the studies SSMFs is triggered under the applied MS-AS scenarios is the subject of chapter 6. This mechanism is identified by evaluating the distribution of hysteretic energy absorption among various members and along the structures' height.

A summary of the results obtained throughout this dissertation and some suggestions for future studies in this area form the subject of the last chapter, chapter 7.

1.2 Introduction

Some structures may sustain their stability after a mainshock (MS) earthquake but aftershocks (ASs) may cause collapse or remarkable damage. Due to partial or substantial damage to a structure from the MS, a structure becomes more vulnerable to damage during the AS. The possible damage to a structure can therefore be a consequence of the deterioration in behavior caused by the MS, followed by the damage caused by ASs.

Historically, in many evidences, buildings have damaged due to AS excitations. One famous instance of such damaging AS events is the 1997 Umbria-Marche earthquake in central Italy the damage details of which were reported by Del Prete et al. (Del Prete, Guadagno, & Scarascia-Mugnozza, 1998). Another example of buildings damaged under the following ASs is the Church of San Francesco (Figure 1.1). The roof of this building collapsed in an AS, killing four priests while investigating the damage from the MS.

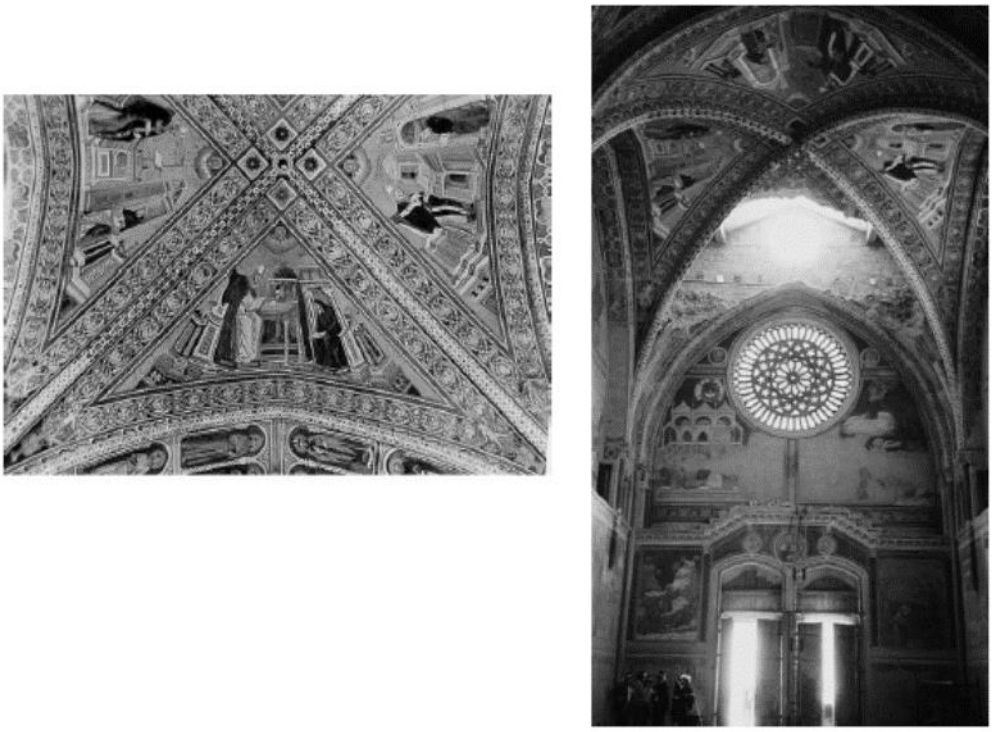

Figure 1.1: The roof of Church of San Francesco after a MS (left). The rubber falls off the roof during an AS (Right) (Prete et al. 2005)

The Foligno Tower (Figure 1.2) is another example of a well-known building that collapsed due to the sequential shocks after the Umbrian earthquakes in the Marche, Italy. Although this structure withstood the shocks of the first and second, the upper part of the structure collapsed during the third shock.

Figure 1.2: The Foligno Tower after fist two sequence shock (Left). The Foligno Tower after the third sequence shock (Prete et al. 2005)

Other instances include the 1999 Kocaeli earthquake in Turkey (Mw 7.4) reported by the USGS (Gross & Phan, 2000) to induce extensive damages due to an AS following the MS in around one month. The same area was also hit by the Duzce earthquake (Mw 7.2) in about four months after the Kocaeli MS and extensive damage was reported by the USGS report (Gross & Phan, 2000) on buildings which had sustained damage under the MS. The Figure 1.3 shows the building that suffered damage from the mainshock (Mw7.4) but collapsed under the AS (Mw5.9) occurred almost a month after the MS (Gross & Phan, 2000).

For predicting the sustainability of a building shocked by a MS followed by an AS, the dynamic features of the structure and its resilience under the MS should be known.

Figure 1.3: A building partially damaged from the mainshock of 1999 Kocaeli earthquake (the upper picture) and completely destroyed under the AS (the bottom picture) (photograph by Thomas L. Holzer (Gross & Phan, 2000))

Figure 1.4, illustrate that a concrete structure that was associated with heavy damage tag after the first earthquake and collapsed after the second earthquake. (Rathje et al.2006).

Figure 1.4: Effect of sequential earthquakes on a concrete building in Turkey (Rathje et al.2006)

The third example can be mentioned as the 2011 Tohoku earthquake (Mw 9.0) in Japan under which many buildings were reported by Nishiyama (Nishiyama, 2011) to suffer intense damage due to AS. Figure 1.5 shows a building which remained intact during the MS on March 11 and collapsed during the AS on April 7.

Figure 1.5: The damaging effects of MS-AS sequence during the March 11 and April 7 shocks of the Tohoku earthquake, Japan

Figure 1.6 shows another evidence confirming that the ASs increased the level of structural damage during the Tohoku earthquake. It was observed that in these constructions, some of the columns remained intact after the MS, but in some of the columns happened shear failure after the ASs, according to the right part of the photo (Nishiyama et al. 2011).

Figure 1.6: Shear crackes in a base-floor column because of ASs of the Tohoku earthquake (Nishiyama et al. 2011)

Conceptually, the inelastic behavior of a structure under the preceding MS leads to residual plastic deformations and stiffness/strength deteriorations that affect its performance under a following AS. Buildings may undergo significant damage under the MS due to degradation of structural stiffness and strength. This reduced structural capacity along with the residual displacements may lead to larger AS displacements, compared to MS, even though a stronger shaking may be imposed by the MS.

One of the important actions to be taken after a MS is evacuating the building for addressing the risk of collapse in the damaged buildings during an AS. The retrofit program of the evacuated buildings may be delayed due to the AS risk even in buildings with minor damage under the MS. An example includes the 7.3Mw magnitude earthquake occurred on November 12, 2017 near Kermanshah province, Iran. During this event, significant financial losses were imposed. The earthquake fatalities were 620 people and more than 70,000 people lost their homes. The risk of collapse in damaged buildings during any likely AS was high and unpredictable. This possibility forced people to stay on the streets continuously and caused major

disruptions to professional places, schools and the social life. This situation is shown in Figure 1.7.

Figure 1.7: Evacuated occupants in Kermanshah earthquake (photograph by Siavosh Ghazi AFP-November 15, 2017)

Based on the MS-AS damage evidences cited above, the seismic effects of the prior damages from MS should be considered in assessing the collapse vulnerability of structures. This requirement is addressed in this dissertation for special steel moment frames. Therefore, a review of the studies on the effects of MS-AS sequences is first presented in the following section.

1.3 Research studies

Investigations on the effects of MS-AS sequences started in 1980 by Mahin (Mahin, 1980) who performed analyses on single degree of freedom (SDOF) systems to prepare design spectra that accounted for inelasticity and AS effects. Studies on SDOF systems continued by Sunasaka and Kiremidjian (Sunasaka & Kiremidjian, 1993) who concentrated on methods for assessment the reliability of building under MS-AS events. Later, Aschheim and Black (Aschheim & Black, 1999) systematically performed over 20,000 SDOF analyses for evaluating of the influence of the pre-earthquake damage on the peak displacement response of SDOF.

Amadio et al. (Amadio, Fragiacomo, & Rajgelj, 2003) also subjected SDOF structures to repeated earthquakes and compared the influence of a single shock on the intact system for variant hysteretic models.

In another study using SDOF systems, Nazari et al. (Nazari, Van De Lindt, & Li, 2013) tried to provide a systematic procedure for integrating AS hazard into the performance-based earthquake engineering (PBEE). They used SDOF systems with varying degradation models that were derived from publicly available experimental data.

Assessments on AS effects were then followed on more sophisticated structural systems by Lee and Foutch (Lee & Foutch, 2004) who performed equivalent static loading on elastic steel models undergoing stiffness degradation as a result of the prior MS earthquakes. These studies took advantage of simplified methods that could be used for upgrading the equivalent SDOF-based design procedures.

To shed more light on the effect of MS-AS excitations, nonlinear time-history analyses of frame structures were conducted for the first time by Luco et al. (Luco, Bazzurro, & Cornell, 2004). They aimed to assessment of the residual collapse capacity of systems, in terms of the first-mode spectral acceleration $S_a(T_1)$ of ASs following certain damage levels induced by MSs. For this purpose, they considered various global drift levels caused by the MS and performed IDA (Vamvatsikos & Cornell, 2002). The IDA method was used for reflecting the record-to-record uncertainties associated with MS-AS sequences. For implementation IDA, structure was subjected to each AS with increasing scales leading finally to collapse of the structure. To see the MS influence on the collapse-inducing intensities of ASs, differently scaled MSs preceded the IDA under AS. The AS intensity leading to collapse of the structure was obtained from the records that applied to structure. The lognormal fragility was fitted to collapse AS intensities. These researchers also tried to propose and calibrate a pushover-based procedure that could predict the residual collapse capacities. They conducted their methodology on a single case-study building in order to elaborate its details.

AS probabilistic seismic hazard analysis (APSHA) was the next major progress in evaluation methods that considered the probability of AS excitations (Yeo & Cornell, 2005). These researchers included the stochastic time-dependent characteristics of ASs and predicted the risk of various AS intensities at different time intervals measured from the MS occurrence time. Probabilistic methods in quantifying AS effects were further developed by Li and Ellingwood (Q. Li & Ellingwood, 2007) who predicted AS intensity as a function of the MS characteristics. The prediction method was utilized for proposing the enhanced uncoupled modal response history analysis which

was used to efficiently analyze high-rise steel buildings under MS-AS sequences. Due to the modal analysis limitations, their study was only focused on elastic structural systems and intended to enhance incorporation of higher modes in the simplified methods proposed by researchers such as Mahin (Mahin, 1980) and Amadio et al. (Amadio et al., 2003).

In the above group of researches, the efficiency provided by utilizing SDOF systems has helped in considering the reliability and probabilistic aspects of the MS-AS effects. The evaluations, however, lacked more accurate multi-degree-of-freedom (MDOF) considerations including the higher vibration modes, the alternative lateral load resisting mechanisms working in a multi-story building and the corresponding collapse mechanisms.

One of the significant experimental research on the influence of AS sequence on multistory structures was performed in 2008 by van de Lindt (van de Lindt, 2008) on wood structures. These researchers studied the effect of wood drywalls on the performance of wood shear wall assemblies affected by MS-AS sequences. In 2010, nonlinear time-history analyses using MS-AS sequences were once again carried out by Hatzigeorgiou and Liolios (Hatzigeorgiou & Liolios, 2010). Their study was focused on typical concrete buildings with regular and vertically irregular (with setbacks) configurations. In addition to five as-recorded seismic sequences recorded within up to three days after the MSs, they also used synthesized MS-AS sequences for the first time. In 2011, the study by Ruiz-García and Negrete-Manriquez (Ruiz-García & Negrete-Manriquez, 2011) used nonlinear response-history analysis to evaluate MID and PRSD of steel moment frames with considering MS-AS sequences. They used 64 as-recorded earthquake record pairs for their analyses. In the same year,

the probabilistic seismic losses induced by excitation sequences on wood structures were investigated by Yin and Li (Yin & Li, 2010). Their results highlighted the significance of ASs on the estimated seismic losses.

In many of the above studies, the selected ground motions were applied at one or a few intensity levels. Therefore, the uncertainties associated with the intensities of the MS-AS sequence were not accounted for. Also, due to the limited intensity levels used, simulation of the highly nonlinear structural response levels such as sidesway collapse was not possible. In 2011, the IDA method was deployed by Ryu et al. (Ryu, Luco, Uma, & Liel, 2011) for probabilistic assessment of MDOF structures hit by MS-AS sequences. They used the same methodology previously deployed by Luco et al. (Luco et al., 2004; Vamvatsikos & Cornell, 2002) for performing the sequential IDAs. In their work, the MS-induced damage was presented by MID parameter. They estimated the AS fragility curves of a typical New Zealand 5-story reinforced concrete moment frame building by regarding various damage states caused by the MS. In 2012, Jeon et al. (Jeon, DesRoches, Brilakis, & Lowes, 2012) used cyclic pushover analyses that imported variant level of MID to simulate the MS-induced structural damage. After each statically simulated MS excitation, the AS was imposed to evaluate the combined effect of the sequential excitation. In 2014, Li et al. (Y. Li, Song, & Van De Lindt, 2014) used repeated, randomized and as-recorded sequences to implement IDAs using a methodology similar to (Luco et al., 2004) and (Ryu et al., 2011). In that work, a single 4-story steel moment frame was regarded as the case study and its collapse capacity was seen to reduce remarkably when the structure was subjected to extensive intensity MS. In addition, the researchers evaluated the influence of MS records, fault types and spectral shapes of ASs on the structural collapse capacity of the studied

structure. Despite the accurate methodology deployed by this research, the dependency between the obtained results and the height of the structural system was not investigated. Furthermore, the macroscopic regimes that influenced the collapse capacity of the studied frame at presence of MS-AS effects were not addressed.

The chronological review of the studies on MS-AS effects continues by a study in 2014 on methods for synthesizing MS-AS record pairs by Han et al. (Han, Li, & van de Lindt, 2014). They evaluated the application of synthesized records. A set of 3 and 6 story non-ductile reinforced concrete (RC) building is considered as a case study. This buildings subjected to multi-shock nonlinear time-history analyses. In 2015, Tesfamariam et al. (Tesfamariam, Goda, & Mondal, 2015) investigated the influence of MS-AS on bare and masonry-infilled RC frames. They treated the MS-AS sequence as a unique excitation scaled to some pre-selected intensity levels and studied the effect of MS on the fundamental period and the MID of the studied structures. Again in 2015, Raghunandan et al. (Raghunandan, Liel, & Luco, 2015) analyzed a set of concrete frame building to MS-AS excitations implementing the IDA-based methodology previously proposed by Luco et al. (Luco et al., 2004) to generate the collapse fragilities of these structures. They used various physical damage measures for representing the structural condition caused by the MS and found that the inter-story drift parameter could best predict the decreased AS collapse capacities for these ductile frames.

In 2017, Hosseinpour and Abdelnaby (Hosseinpour & Abdelnaby, 2017) studied the effect of changing the earthquake direction (polarity) on irregular RC structures with considering the MA-AS sequences. In addition they study the effect of and vertical component to drift demand with considering MA-AS sequences. In an assessment on

a case-study four-story steel framed building, Ruiz-García and Aguilar (Ruiz-García & Aguilar, 2017) studied the effect of uncertain model parameters such as post-yield stiffness and the overstrength ratios on the residual drifts caused by ASs. In another study, Abdollahzadeh et al. (Abdollahzadeh, Mohammadgholipour, & Omranian, 2017) evaluated the plasticity distribution over steel MRFs with heights ranging from 4 to 12 stories. Their study considered multiple naturally-recorded MS-AS sequences by treating each pair as a single excitation scaled to two different hazard levels. The uncertainties that affected the intensities of the MS and AS records were not considered separately. In addition, the structures' performance was not probabilistically assessed regarding pre-defined damage states. Another study performed by Yu et al. (Yu, Li, Lu, & Tao, 2018) in 2018 was also dedicated to evaluation of collapse probability in SDOF systems subjected to MS-AS excitations.

One major limit state considered by seismic design codes, when intense hazard levels are accounted for, is the collapse state. Collapse occurrence itself is a result of the excessive plastic deformations and the damage-induced behavior degradations in the structural members. The loss of strength and stiffness caused by this behavior degradation eventually leads to sidesway instability in presence of the second-order moments imposed by the gravity loads. As a proved fact, the hysteretic energy absorbed by a member plays an important role in degrading the members' characteristics during cycles of a seismic loading (Ibarra, Medina, & Krawinkler, 2005; Rahnama & Krawinkler, 1993). Therefore, the structural collapse state can be comprehensively studied by focusing on two response parameters: i) plastic deformations and ii) hysteretic energy absorption. These parameters have also been considered in representing members' damage by a number of previous researchers

(Park & Ang, 1985; Park, Ang, & Wen, 1985). Such studies have mainly concentrated on the effect of member response on its local damage and predicting this damage through empirical equations. Assessing the influence of these response parameters on the overall collapse of buildings, however, calls for a different class of investigations. Through such appraisals, deterioration occurrence is modelled in the members and a realistic portrait is obtained from the overall collapse event stemming from the spread of local damages occurring in the different members.

1.4 Summary of state-of-the-art

Despite the usefulness of collapse mechanism investigations, very few studies have been devoted to address the collapse mechanism of structural systems. Among these, the most (e.g. (An, Shawky, & Maekawa, 1997; D'Ayala & Speranza, 2003; Kiyono & Kalantari, 2004; Yi, He, & Xiao, 2007)) have considered on distribution of lateral drifts between different stories as an expression of the collapse mechanism. However, as denoted earlier, plastic deformation and hysteretic energy absorption at various parts of the structure are the main causes of structural collapse. Thus, a study on the collapse mechanism that concentrates on distribution of these response parameters throughout the structure is expected to provide more valuable insights. Examples of such evaluations are the two studies performed by Jalali and Darvishan (Jalali & Darvishan, 2019) and Jalali et al. (Jalali, Amini, Mansouri, & Hu, 2020) on steel plate shear wall systems. The latter study is an instance of research on the effect of MS-AS sequence on the collapse mode of structural systems.

In addition to the investigation on the overall collapse mechanism, the probabilistic collapse capacity of more structures should also be evaluated using the methodology developed by previous researchers and reviewed above. Many studies have been

devoted to assessing collapse capacity of various structural systems under single-shock excitations. These include the studies by (Banazadeh, Jalali, & Abolmaali, 2010; Jalali, Banazadeh, Abolmaali, & Tafakori, 2012; Jalali, Banazadeh, Tafakori, & Abolmaali, 2011) on steel moment frames and (Jalali et al., 2020; Jalali & Banazadeh, 2016) on steel plate shear wall systems. However, few studies have been devoted to assessing collapse capacity of various structural systems under sequential excitations. As a result, many structural systems are not still subjected to such assessments. Among these systems is the widely used special steel moment frame (SSMF) system which has only been addressed by Li et al. (Y. Li, Song, & Van De Lindt, 2014) by considering a single 4-story case study.

1.5 Scope of the current study

According to the highlighted summary of state-of-the-art and the significance of studies on the collapse of SSMF structures under MS-AS sequences, this topic is pursued in this study for SSMFs with 4-20 stories by concentrating on the following aspects:

- identifying the probabilistic collapse capacity of SSMFs in terms of the induced seismic intensity,
- expression of collapse mechanism in terms of the distribution of the plasticity demand and the hysteretic energy absorption throughout the structures,
- account of the MS-AS effects and the uncertainties associated with AS intensity and the damage level caused by the preceding MS excitation,
- and, the alternative damage indicator parameters used for scaling MSs.

The first item is an application of the collapse fragility assessment for SSMFs. Regarding the second item, the question to be answered is “to what extent various

members throughout the structures undergo damage and how much they contribute in dissipating the input energy in the response level just before collapse occurrence"? According to the third point, these questions are to be answered by account of the MS-AS effects and should highlight the influence of pre-MS damage on the mechanism and capacity through which the structures undergo collapse.

The last topic addresses the uncertainty associated with the methods used for quantifying the MS effects. Previous researchers have proposed utilization of various response measures for representing the level of damage imposed by a MS. These measures include maximum global drift, maximum interstory drift, (MID), residual global drift and peak residual story drift (PRSD). The latter measure compares the residual interstory drifts of various stories and takes the maximum value as the damage indicator parameter. Utilization of an appropriate damage measure, helps in maximizing the accuracy of the predictive studies that try to forecast the influnce of MS damage on the performance of the structures hit by an AS. Among the alternative damage indicator parameters, the reviewed researches have shown the highest accuracies when MID and the PRSD parameters have been used. To further evaluate utilization of these indicators, the correlation between the AS collapse capacity of the studied SSMFs and the MS damage level is investigated by considering these two MS damage measures.

Two practical applications can be counted for the evaluations to be performed in this study: i) to derive the collapse capacity of the structures when various levels of damage have been caused by the MS, and ii) to provide the insight requirements for design of buildings when effective collapse prevention is of interest. On the other hand, according to the reviewed research studies, the collapse fragilities of SSMFs with 4-

20 stories have not been derived under MS-AS effects. The collapse mechanism of SSMFs are also being evaluated for the first time in presence of the MS-AS effects. The methodology utilized for performing these studies are presented in the following section.

Chapter 2

METHODOLOGY

For assessment of MS damage on the AS collapse capacity and collapse mechanism of SSMF structures, the uncertainties related to sequence records should be addressed appropriately. These uncertainties affect the frequency content (i.e., the spectral shape) and the intensity of each record considered in a MS-AS pair. A wider attention may also consider the number of ASs hitting a structure as the third source of uncertainty. The latter is however neglected in the majority of the studies on MS-AS effects where the number of sequential excitations is limited to two for simplicity purposes.

For reflecting the uncertain spectral shape of the records in a pair, various methods have been considered by previous studies. The first method uses independent random processes to select MS and AS records from a series of preselected natural records. The second approach uses artificial records that use optimization algorithms to maximize the similarity between the spectra of the natural MS and AS records with those of the generated records. The third method assumes a full correlation between the spectral shapes of the MS and AS records and repeats the MS as the AS. Finally, the fourth method tries to comply with the natural relation between MS and AS records by using as-recorded MS-AS pairs. Among these methods, using as-recorded pairs has received the most attention in recent studies due to its adherence to the natural phenomena affecting the spectral shapes of the MS-AS pairs. At the same time, it is

simpler and more efficient compared to the other methods requiring large number of repetitions or generating artificial record pairs.

Regarding the second source of uncertainty, which is the intensity of the MS-AS pair, a well-accepted method is scaling the MS to different target intensity levels (target post-MS damage) and developing IDA to observe variability of AS intensity. This involves implementation the IDA according the methodology that introduced by Luco et al, as will be explain in next section (Luco et al., 2004).

The assessment of MS damage on the AS collapse capacity of SSMF structures and the mechanism governing it is to be studied. For this purpose, the collapse occurrence should be first identified through a reliable method and via nonlinear dynamic analyses. This is achieved by using structural models in which damage-induced degradation is explicitly modelled to allow for direct simulation of model instability due to loss of strength and stiffness in the members. For recognizing the collapse occurrence the ground motions' intensity is scale-up gradually and monitoring the sidesway response of the buildings. This is systematically conducted through the multi-shock IDA method proposed by Luco et al. (Luco et al., 2004) and also deployed by Ryu et al. (Ryu et al., 2011), Li et al. (Y. Li et al., 2014) and Raghunandan et al. (Raghunandan et al., 2015). Using IDA, the collapse state is identified as the stage in which the lateral instability occurs due to excessive second-order moments caused by the gravity loading in presence of lateral displacements. Once the collapse-inducing intensity is identified for an applied MS-AS pair, the nonlinear dynamic response of the structure is regarded for studying the distribution of maximum ductility demand (MDD) and energy absorption contribution (EAC) parameters throughout the structure.

To this end, 4-, 8-, 12- and 20-story structures and numerous ground motion records are utilized that account for different building heights as well as the record-to-record uncertainties.

The MDD parameter is intended as a measure of plasticity undergone by various parts and at the different stories of the structure, at the collapse state. To compute MDD values, a lumped-plasticity model is deployed the explanations of which are introduced at the subsequent chapter of the dissertation. Using this numerical model, the maximum rotation observed at each plastic hinge is divided by its yielding value to compute the ductility demand experienced by that hinge during the analysis. The maximum value of the ductility values observed during the whole ground motion time is regarded as the MDD corresponding to that hinge location. These values are computed for all the hinges throughout the structure.

For assessment the contribution of dissipating different structure members to the input earthquake energy used EAC parameter. For calculating EAC the area under the moment rotation curve is calculated in plastic hinge locations. The energies consumed at the two plastic hinges forming a member are summed to calculate the member's hysteretic energy. The EAC is next obtained by dividing the member's energy by the total hysteretic energy absorbed by the structure during an earthquake. The EAC values are also added together at story level to compute the contribution of different stories to total hysteretic energy absorbed at the collapse state.

The IDA procedure employs multiple ground motion records in order to account for the record-to-record variability. Using each record, the Hunt-Fill algorithm (Vamvatsikos & Cornell, 2002) is used for recursive scaling of the intensity until the

collapse intensity is found within an acceptable tolerance. The MDD and EAC values are finally averaged among all the selected records and their distribution throughout the structure is studied.

To see the multi-shock effects, the 32 real MS-AS pairs previously collected by Han et al. (Han et al., 2014) are utilized. These MS-AS sequences had recorded in the western United States and had AS records that followed the MS within a one-week period. The sequences that had the biggest magnitude choose as AS record. The magnitude of ASs were bigger than 5 .These MS-AS records were occurred on sites that the distant is more than 10 km from the epicenter which means that we can categories these records as far field records. The shear wave velocity range in this site is 200 to 400 meter to second. The range of magnitude for MS is 5.8 to 7.2 and for AS is 5.01 to 6.7. More complete data about the ground motions including the peak ground acceleration (PGA), predominant period (Tr), mean period (Tm), characteristic intensity (Ic), cumulative absolute velocity (CAV) and significant duration (Duration) are provided in Table 2.1 and Table 2.2.

Table 2.1: Summarized data of the MS-AS record pairs

#	Earthquake	Magnitude (Mw)		Record File Name		Station name	Database
		MS	AS	MS	AS		
1	Coalinga	6.36	5.09	NGA_no_368_H-PVY045.AT2	NGA_no_383_A-PVY045.AT2	Pleasant Valley P.P.–Yard	PEER NGA
2	Coalinga	6.36	5.09	NGA_no_368_H-PVY135.AT2	NGA_no_383_A-PVY135.AT2	Pleasant Valley P.P.–Yard	PEER NGA
3	Chalfant Valley	6.19	5.44	ChalfantValley86_CE54171P.V2	ChalfantValley86C_CE54171P.V2	Number 54171	CESMD
4	Chalfant Valley	6.19	5.44	ChalfantValley86_CE54428P.V2	ChalfantValley86B_CE54428P.V2	Number 54428	CESMD
5	Chalfant Valley	6.19	5.44	ChalfantValley86_CE54424P.V2	ChalfantValley86B_CE54424P.V2	Number 54424	CESMD
6	Imperial Valley	6.53	5.01	NGA_no_162_H-CXO315.AT2	NGA_no_195_A-CXO315.AT2	Calexico Fire STA	PEER NGA
7	Imperial Valley	6.53	5.01	NGA_no_174_H-E11140.AT2	NGA_no_199_A-E11140.AT2	El Centro Array 11	PEER NGA
8	Imperial Valley	6.53	5.01	NGA_no_178_H-E03230.AT2	NGA_no_201_A-E03230.AT2	El Centro Array 3	PEER NGA
9	Imperial Valley	6.53	5.01	NGA_no_172_H-E01230.AT2	NGA_no_197_A-E01230.AT2	El Centro Array 1	PEER NGA
10	Imperial Valley	6.53	5.01	NGA_no_169_H-DLT262.AT2	NGA_no_196_A-DLT262.AT2	Delta	PEER NGA
11	Livermore	5.8	5.42	Livermore80A_CE57187P.V2	Livermore80B_CE57187P.V2	Number 57187	CESMD
12	Livermore	5.8	5.42	Livermore80A_CE67070P.V2	Livermore80B_CE67070P.V2	Number 67070	CESMD
13	Livermore	5.8	5.42	NGA_no_212_A-DVD246.AT2	NGA_no_219_B-DVD246.AT2	Del Valle Dam	PEER NGA
14	Livermore	5.8	5.42	NGA_no_214_A-KOD180.AT2	NGA_no_223_B-KOD180.AT2	San Ramon Kodak building	PEER NGA
15	Livermore	5.8	5.42	NGA_no_215_A-SRM070.AT2	NGA_no_224_B-SRM070.AT2	San Ramon	PEER NGA
16	Livermore	5.8	5.42	NGA_no_213_A-FRE075.AT2	NGA_no_220_B-FRE075.AT2	Fremont Mission S.J.	PEER NGA
17	Livermore	5.8	5.42	NGA_no_210_A-A3E236.AT2	NGA_no_217_B-A3E236.AT2	Hayward CSUH Stadium	PEER NGA

18	Mammoth Lakes	6.06	5.94	NGA_no_231_I-LUL090.AT2	NGA_no_250_L-LUL090.AT2	Long Valley Dam UPR L	PEER NGA
19	Mammoth Lakes	6.06	5.7	NGA_no_231_I-LUL090.AT2	NGA_no_243_B-LUL090.AT2	Long Valley Dam UPR L	PEER NGA
20	Mammoth Lakes	6.06	5.69	NGA_no_231_I-LUL090.AT2	NGA_no_234_J-LUL090.AT2	Long Valley Dam UPR L	PEER NGA
21	Northridge	6.69	5.93	NGA_no_963_ORR090.AT2	NGA_no_1676_CASTA090.AT2	Castaic–Old Ridge Route	PEER NGA
22	Northridge	6.69	5.93	NGA_no_1039_MRP090.AT2	NGA_no_1681_MPARK090.AT2	Moorpark	PEER NGA
23	Northridge	6.69	5.28	NGA_no_1005_TEM090.AT2	NGA_no_1712_TEMPL090.AT2	Los Angeles–Temple and Hope	PEER NGA
24	Northridge	6.69	5.93	NGA_no_971_ELI180.AT2	NGA_no_1677_ELIZL180.AT2	Elizabeth Lake	PEER NGA
25	Northridge	6.69	5.93	NGA_no_945_ANA180.AT2	NGA_no_1675_ANAVE180.AT2	Anaverde Valley–City Ranch	PEER NGA
26	Northridge	6.69	5.93	NGA_no_990_LAC180.AT2	NGA_no_1678_CTYTE180.AT2	Los Angeles–City Terrace	PEER NGA
27	Northridge	6.69	5.93	NGA_no_1007_UNI095.AT2	NGA_no_1680_UNIHP090.AT2	LA–Univ. Hospital GR	PEER NGA
28	Petrolia	7.2	6.7	Petrolia_25Apr1992_CE89530P.V2	PetroliaAS2_26Apr1992_CE89530P.V2	Number 89530	CESMD
29	Petrolia	7.2	6.5	Petrolia_25Apr1992_CE89156P.V2	PetroliaAS1_26Apr1992_CE89156P.V2	Number 89156	CESMD
30	Petrolia	7.2	6.5	Petrolia_25Apr1992_CE89509P.V2	PetroliaAS1_26Apr1992_CE89509P.V2	Number 89509	CESMD
31	Whittier Narrows	5.99	5.27	NGA_no_615_A-DWN270.AT2	NGA_no_709_B-DWN270.AT2	Downey	PEER NGA
32	Whittier Narrows	5.99	5.27	NGA_no_663_A-MTW000.AT2	NGA_no_715_B-MTW000.AT2	Mt. Wilson	PEER NGA

Table 2.2: Ground motion parameters of the MS-AS record pairs

#	Earthquake	Record Type	PGA	Tr	Tm	Ic	CAV	Duration
1	Coalinga	Main	0.602	0.5	0.551	0.135	1616.235	8.155
		AS	0.099	0.16	0.426	0.007	93.739	4.88
2	Coalinga	MS	0.525	0.3	0.392	0.127	1541	9.07
		AS	0.211	0.2	0.237	0.013	118.6	1.75
3	Chalfant Valley	MS	0.254	0.24	0.581	0.031	607.59	12.76
		AS	0.183	0.4	0.463	0.013	286.85	14.18
4	Chalfant Valley	MS	0.444	0.2	0.468	0.084	955.287	7.26
		AS	0.16	0.12	0.285	0.01	228.712	7.66
5	Chalfant Valley	MS	0.168	0.08	0.216	0.011	312.784	10.92
		AS	0.032	0.06	0.171	0.013	90.655	10.56
6	Imperial Valley	MS	0.203	0.18	0.409	0.042	798.007	14.81
		AS	0.067	0.16	0.379	0.004	107.077	11.745
7	Imperial Valley	MS	0.367	0.24	0.459	0.086	1128.74	9
		AS	0.097	0.22	0.435	0.007	102.97	4.965
8	Imperial Valley	MS	0.223	0.141	0.497	0.039	730.763	14.15
		AS	0.097	0.14	0.319	0.004	56.687	5.28
9	Imperial Valley	MS	0.136	0.1	0.35	0.017	455.57	19.525
		AS	0.031	0.1	0.207	0.001	33.393	5.255
10	Imperial Valley	MS	0.236	0.48	0.625	0.078	2537.57	51.41
		AS	0.06	0.12	0.209	0.004	105.859	11.58
11	Livermore	MS	0.149	0.62	0.968	0.019	330.69	10.56
		AS	0.279	0.34	0.581	0.021	265.264	5.66
12	Livermore	MS	0.043	0.52	0.68	0.004	173.926	21.08
		AS	0.111	0.26	0.448	0.004	136.534	11.6
13	Livermore	MS	0.256	0.22	0.557	0.017	306.25	7.31
		AS	0.045	0.16	0.337	0.003	94.778	9.25
14	Livermore	MS	0.15	0.62	0.972	0.019	322.644	10.37
		AS	0.28	0.34	0.582	0.021	261.189	5.63
15	Livermore	MS	0.055	0.26	0.591	0.005	219.249	25.24
		AS	0.045	0.4	0.519	0.004	178.503	14.05
16	Livermore	MS	0.045	0.3	0.627	0.004	110.323	10.025
		AS	0.036	0.68	0.627	0.002	64.328	7.25
17	Livermore	MS	0.057	0.2	0.322	0.004	156	10.335
		AS	0.029	0.32	0.341	0.007	59.864	10.885
18	Mammoth Lakes	MS	0.271	0.56	0.415	0.043	678.257	10.845
		AS	0.414	0.16	0.548	0.067	723.947	7.135
19	Mammoth Lakes	MS	0.271	0.56	0.415	0.093	678.257	10.845
		AS	0.159	0.18	0.353	0.016	333.039	7.095
20	Mammoth Lakes	MS	0.271	0.56	0.415	0.093	678.257	10.845
		AS	0.066	0.48	0.464	0.006	183.27	10.275
21	Northridge	MS	0.568	0.26	0.534	0.11	1303.518	9.08
		AS	0.138	0.42	0.459	0.014	256.781	8.12

22	Northridge	MS	0.193	0.26	0.564	0.042	839.434	16.12
		AS	0.14	0.24	0.532	0.014	269.664	10.02
23	Northridge	MS	0.126	0.32	0.488	0.022	525.916	14.6
		AS	0.038	0.08	0.271	0.002	87.187	13.64
24	Northridge	MS	0.109	0.24	0.404	0.018	440.561	11.67
		AS	0.016	0.32	0.361	0.001	57.191	15.11
25	Northridge	MS	0.06	0.36	0.504	0.009	300.465	15.45
		AS	0.012	0.28	0.328	0.001	43.337	13.98
26	Northridge	MS	0.316	0.22	0.319	0.053	867.826	11.86
		AS	0.036	0.2	0.272	0.002	91.358	14.78
27	Northridge	MS	0.214	0.22	0.3	0.032	633.233	12.26
		AS	0.026	0.22	0.302	0.002	84.37	15.43
28	Petrolia	MS	0.226	0.2	0.178	0.03	698.07	16.26
		AS	0.288	0.18	0.231	0.04	543.67	4.5
29	Petrolia	MS	0.662	0.64	0.671	0.126	1550	16.1
		AS	0.439	0.5	0.594	0.059	764.657	6.04
30	Petrolia	MS	0.178	0.52	1.082	0.02	642.155	24.6
		AS	0.052	0.34	0.896	0.006	366.605	32.14
31	Whittier Narrows	MS	0.155	0.7	0.468	0.017	408.185	12.38
		AS	0.061	0.52	0.432	0.007	177.262	12.295
32	Whittier Narrows	MS	0.123	0.04	0.19	0.012	292.357	9.735
		AS	0.145	0.16	0.204	0.008	133.244	3.945

For implementation MS-AF sequence IDA's, the MS record is scaled to the target pre-MS damaged, and, next the AS is applied to MS- damaged frame. The AS intensity is scaled up until the collapse intensity capture. For obtaining the IDA curve used the Hunt-Fill algorithm. The IDAs are expanded for different pre-MS damaged by methodology proposed by Luco et al. and Ryu et al. (Luco et al., 2004; Ryu et al., 2011). This method is a modern methodology for considering the pre-MS damaged to assessment of collapse capacity of structure that described in previous section.

As described in section 1-5, in this study, MS damage is quantified by considering two alternative parameters: maximum interstory drift (MID) and the peak residual story drift (PRSD) experienced by the building during the MS time history analysis. MID is

a convenient physical damage indicator for representing structural and nonstructural building damage, as it is strongly related to damage and repair costs (Porter, Kiremidjian, & LeGrue, 2001).

Seismic events have shown that structures with excessive permanent lateral displacement may need to be demolished at the end of the earthquake, even if they did not suffer severe damage or a partial collapse. In contrast to MID, PRSD is a measurable physical damage indicator after MS, which can be observed during post MS visual inspection, using robotic theodolites (Psimoulis & Stiros, 2007) or even GPS devices (Nickitopoulou, Protopsalti, & Stiros, 2006).

In the current study, the MS's scale is determined in accordance with both the MID (chapter 4) and the PRSD (chapter 5) parameters to evaluate their appropriateness. To reflect variability of MS intensity, the MID parameter takes 0.007, 0.025 and 0.05 values while 0.005, 0.014, and 0.02 are used for PRSD at various analyses. For MID physical damage indicator the pre-collapse MS damage is also considered. This pre - MS damage intensity is belong to one step before MS-induced collapse intensity. Selection of the limit MID values is based on ASCE-41 code (ASCE, 2006) in which three structural performance states are considered. These states are called immediate occupancy (IO), life safety (LS), and collapse prevention (CP) performance limits. According to ASCE-41(ASCE, 2006), the IO, LS and CP limit states are represented by 0.007, 0.025, and 0.05 MID values, respectively.

Selection of the limit PRSD values is based on research that have done with McCormick et al. (McCormick, Aburano, Ikenaga, & Nakashima, 2008) and Iwata et al. (Iwata, Sugimoto, & Kuguamura, 2006). In the first research, the permissible PRSD

equal to 0.005 that beyond which the comfort of the occupants could not be satisfied. The latter research focused on the financial reparability costs associated to different PRSD levels and realized that the PRSD of steel buildings should be limited to about 0.014 to satisfy a reparability limit state. The third limit value is selected based on the suggestion of the FEMA P58 (FEMA-P58, 2012) seismic loss estimation guideline that determines the 0.02 value as the level beyond which a building demolish is necessary.

The multishock-IDA is implemented, in this dissertation, on 4-, 8-, 12- and 20-story SSMFs previously designed by NIST (NIST, 2010). More details about these structures are provided in the next chapter. OpenSees (Mazzoni et al., 2004) software is used for numerically modelling and verification of each structures. Afterward, each structure subjected to a multi-shock IDA using the record pairs presented above. Further description about the modelling and analysis procedures is provided in the following chapters.

Chapter 3

MODELING AND VERTIFICATION

The structural layout used for the SSMFs are adopted from NIST (NIST, 2010) and have also been employed by other researchers (e.g. (Elkady & Lignos, 2015)). This layout is illustrated in Figure 3.1 a. According to this Figure, the lateral load resisting system consisted of two symmetrically located perimeter frames, in each direction. The corner columns of the rectangular plan were excluded from the lateral load bearing systems in order to prevent introduction of columns that received seismic loads from both horizontal directions. The w-shape sections of the ASCE standard were used, and the reduced beam section (RBS) detail was deployed for the beam-to-column connections.

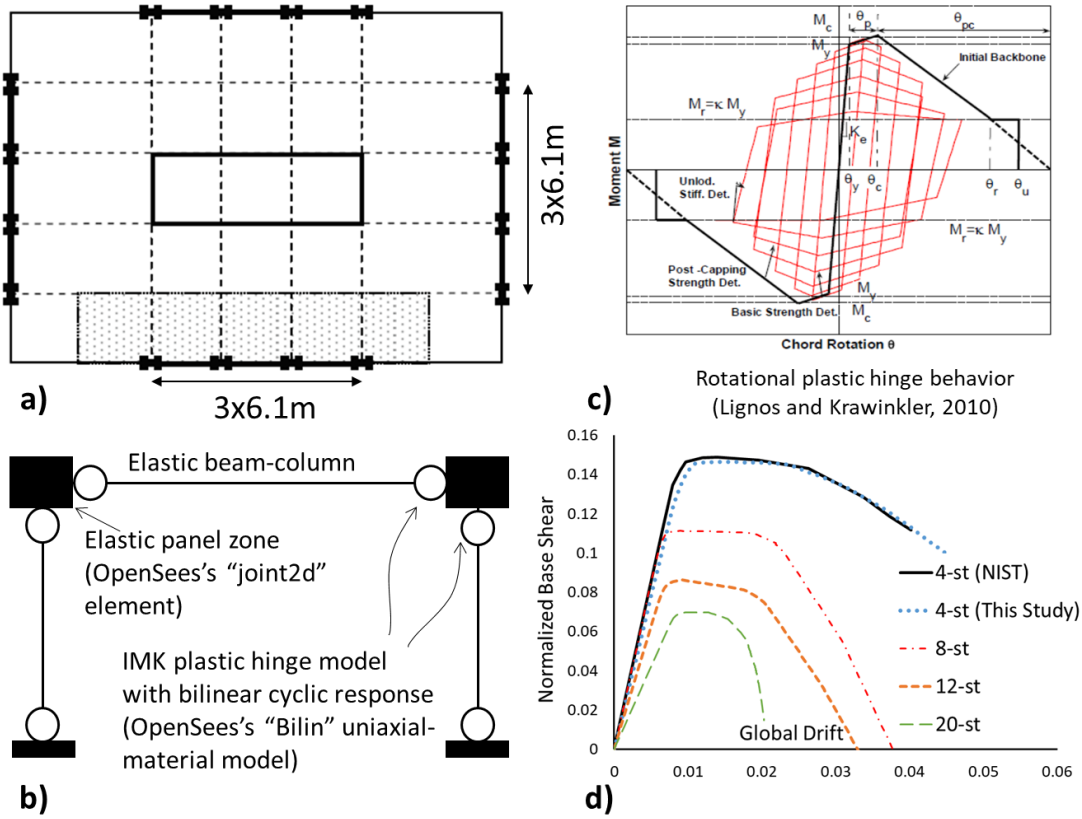

Figure 3.1: a) Plan layout of the studied structures (NIST, 2010); b) a schematic 1-bay-1-story model; c) example cyclic plastic hinge model represented by the IMK model (Lignos & Krawinkler, 2010); and d) the pushover curves of this study along with a comparison against the NIST's (NIST, 2010) curve for the 4-story frame

Buildings were designed to account for the strong-column-weak-beam principle. The structures were 4.6 m and 4.0 m high in the first and other stories, respectively. The dead load was 4.39 KN/m^2 uniformly distributed over each floor and live load was 2.44 KN/m^2. On the roof, the live load was reduced to the 0.97 kN/m^2 while a similar dead load was considered. The structures were seismically loaded following the "response spectrum analysis" method according to the ASCE 7-05 (ASCE, 2005) standard. The building site coefficients were determined so that the structures were designed for the upper bound of the seismic design category D (called D_{max}) per ASCE 7-05 (ASCE, 2005). Table 3.1 presented other description of the buildings such as, R, response modification factor and seismic base shear coefficients

Table 3.1: The design coefficients used by NIST (NIST, 2010) for seismic design of the structures along with their first periods reported by NIST and obtained here

No. of Stories	Design Parameters (NIST, 2010)		First Period (sec.)		
	R	Design Base Shear Coefficient	NIST (NIST, 2010)	This Study	Difference with respect to NIST
4	8	0.067	1.62s	1.54s	4.9%
8		0.039	2.29s	2.13s	7.0%
12		0.037	3.12s	2.94s	5.8%
20		0.037	4.70s	4.36s	7.2%

To minimize the validation concerns, the nonlinear modelling method exactly follows that utilized by the NIST (NIST, 2010) report. That is, a two-dimensional representation of the frames are modelled in OpenSees software by use of the plan symmetry and neglecting the out-of-plane response of the perimeter moment-resisting frames. Therefore, for calculating of seismic mass 50% of total mass is assigned to a lateral resisting frame in each story. The columns are modeled by considering p-delta geometric transformation. For considering the p-delta effect of gravity columns that just carry the gravity load (internal columns) in 3-dimensional structure should be indirectly considered for converted 3-dimensional to 2-dimensional model. Rigid pin-ended columns called “leaning columns” are used for this purpose. These fictitious columns represent the effect of inner gravity columns on amplifying the p-delta forces of the moment frame. These p-delta columns are rigidly linked to the frame model and are subjected to the sum of gravity loads applied on the gravity columns of the half-plan being modelled. As shown in Figure 3.1b, for modelling the nonlinear behavior, the lumped plasticity method is used by employing zero-length rotational springs at the end of each element. The moment-rotation relationship of these hinges is represented through the Ibarra-Median-Krawinkler (IMK) (Ibarra et al., 2005) model and the regression equations provided by Lignos and Krawinkler (Lignos &

Krawinkler, 2010). The cyclic moment-rotation curve of an example section is illustrated in Figure 3.1c.

The initial stiffness of the rotational springs should be considered infinity in order to simulate their actual rigidity before formation of the plastic behavior. However, using infinite rigidity makes the model prone to convergence difficulties. To avoid these difficulties, the elastic stiffness of these springs is reduced and replaced by the member's elastic stiffness multiplied by (N+1) factor where N is an arbitrarily selected positive integer expressing the ratio between spring and chord stiffness values. To compensate for the caused reduction in the overall stiffness of the member, the stiffness of the elastic chord should be amplified by a (N+1)/N factor according to relations governing resultant stiffness of series elements. The applied modification factors are computed so that the resultant stiffness of the series system composed of the rotational springs and the elastic chord equals the elastic stiffness of the original member. These modifications also require some adjustment to the spring behavior in the nonlinear range. These adjustments and the other details related to convenient implementation of lumped plasticity method can be found in (Zareian & Krawinkler, 2006).

While eliminating convergence problems, the above method also leads to inaccuracies one of which is related to the unrealistic distribution of flexural deformations through the element length. The other source of inaccuracy arises from the unreal stiffness assigned to the inner elastic element and is related to the stiffness-proportional damping forces computed for this element. To solve the latter problem, a revised version of elastic beam-column is provided in OpenSees by Zareian and Medina (Zareian & Medina, 2010) in which the stiffness-proportional damping forces are

computed by taking account of the applied stiffness adjustment. The first problem, however, is considered as a compromised drawback of the lumped plasticity method. This compromise is in price of accurate modelling of the cyclic and in-cycle deteriorations not covered by fiber-based distributed plasticity methods.

As shown in Figure 3.1b, the panel zone area is also modelled at the beam-column intersections. According to the post-Northridge design method employed by recent standards, adequate double plates are provided in order to limit the deformation demand and plasticity level of the shear panel. Based on this, the shear force-deformation of the panel zone is simplified in this study by utilization of an elastic model. The utilized results of the pushover analyses performed on the studied structures are presented in Figure 3.1d.

A detailed calibration process was used in the NIST project for the developed models by inspecting the hysteretic response of the hinges and controlling the hinge properties computed using the regression equations provided by Lignos and Krawinkler (Lignos & Krawinkler, 2010). The analytical periods obtained in this study for the first vibration mode are compared against the NIST values in Table 3.1 and show discrepancies that are less than 7% and reveal the good agreement between the models. In addition, the models utilized herein are calibrated against the pushover results provided by the NIST report (NIST, 2010). The pushover curve obtained for the 4-story SSMF is compared against the NIST (NIST, 2010) result in Figure 3.1d to show the exact similarity between the models used in the NIST study and those employed by the current study. Since the models utilized here are based on programming codes, verifying the results of a sample building can be regarded a calibration of the programming code generally used for all the models.

Convergence Problems often occur when nonlinear analyses are run with OpenSees. In this study, smart analyze algorithm is used. This algorithm helps OpenSees model to converge faster. Smart analyze algorithm take the following strategies to help the OpenSees model to converge:

1. If the test norm is not too large, the number of iteration times in test will be increased;
2. If step 1 does not work, algorithm will be changed according to the parameters given by users. For each algorithm, try the strategy in step 1;
3. If all the algorithm do not work, shorten the time step, and iterate again; minimize the time step of analysis. (0.001 or even less), (Note! This may lead to large number of data points that cause a time consuming analysis);
4. If the model still do not converge, return an error message.

Chapter 4

MID-BASED MS-AS EXCITATIONS

The methodology described in chapter 2 is implemented on the models developed following chapter 3's procedure. As previously stated, these analyses aim to evaluate the MS-AS performance of the structures by performing multishock IDAs. These IDAs follow initial IDAs which are performed using the MS record set and establish intensity-MID and intensity-PRSD relationships for these records. Using the established relationships, scaling the MS records so that target MID and PRSD values are achieved becomes possible by use of interpolation method. In this chapter, scaling of the MS is performed following the MID parameter and the comparison between MS damage presentation using MID and PRSD parameters is left for the next chapter.

To conduct the multishock IDA process, the intensity that cause target pre-MS damaged impose to intact frame. Afterwards, the frame is let to rest until the MS-induced response is completely damped.

To determine the duration of the free vibration analysis, which is expected to depend on the various scales used for the MS excitations, an interactive analysis session is deployed. This analysis is performed by employing an OpenSees customization first developed by Jalali (Jalali, 2018) and presented as an open-source github (www.github.com) repository. Using this customization and the added response monitoring commands, the amplitude of drift fluctuation is periodically monitored and

the free vibration is stopped when this fluctuation becomes less than 1e-5 radians in amplitude. This methodology allowed for accurate determination of free vibration duration without need to conservative and time-consuming selections. Next to the free vibration phase, the AS is imposed on the structure and the building response including the MID and PRSD values is extracted.

Since the AS record is applied on a model deformed by the MS, the asymmetry in the AS record, i.e., the variation between the maximum and minimum acceleration histories, will cause differences when it's applied in either 0^o or 180^o direction. That is, the building's response under the AS is polar and sensitive to the applied direction. To account for this polarity effect, each AS is applied twice at the two directions and the direction with the worst damaging effect is regarded. The MS-AS analysis procedure is repeated by increasing the AS scale subjecting to Hunt-Fill algorithm until structural collapse is captured within a 5% tolerance of the $S_a(T_1)$ parameter. The collapse occurrence is identified following FEMA 350 ("FEMA 350: Recommended seismic design criteria for new steel moment frame buildings," 2000) recommendation the last point on the curve with a tangent slope equal to 20% of the elastic slope is defined to be the capacity point or the point with a maximum interstory drift exceeding 10%, whichever occurs sooner. The AS $S_a(T_1)$ values that belongs to the collapse state are extracted and used for deriving the AS collapse fragility curves. These curves are cumulative log-normal curves that present collapse probability at various $S_a(T_1)$ levels.

A remarkable enhancement to the analysis time is also achieved by saving the model state at the end of the free vibration analysis and reloading it several times before applying each scale of the AS.

This procedure is performed using the 32 real MS-AS records presented in methodology section. As stated before, the MS records are scaled so that they induce MID values equal to 0.007, 0.025 and 0.05. In addition the pre-collapse damage level, the state of the structure just before a MS-induced collapse is also considered.

The IDA results, the collapse fragility curves obtained using MS-AS sequences are presented in the following sections.

4.1 IDA results

The obtained IDA curves are shown in Figure 4.1 to Figure 4.4 for SSMFs with 4 to 20 stories. Along with MS IDA, the AS IDA curves are also depicted in the same Figures to show the response of structures in absence of a prior damage by MS. The next IDA curves shown in these Figures are obtained by applying the MS-AS sequences in which MS has been scaled to induce a specific damage level.

To assess the effect of the initial damage caused by the MSs on collapse performance of the SSMFs under AS excitations, the median IDA curves generated for different pre- MS damage levels for SSMFs with different heights are compared in Figure 4.5. In interpreting these curves, one should have in mind that the plotted MID values are only maximized over the AS excitation time and the drift values experienced by the structures during the MS have not been included for obtaining these values. Having mentioned this, the first point to note regarding these curves is the initial drift lag in the IDA curves derived after a damaging level of MS has been applied. This lag is due to the residual story drift experienced by the frames at the end of MS record and increases as the MS damage is intensified. The level of the residual drift at the end of MS (IDA lag) is seen in this Figure to be about 80% of the maximum drift induced

during the MS. For instance, the IDA lag is around 4% when MS is scaled to induce a MID=5% level. It can also be seen that the residual MID is not activated until the 0.025 MS damage level. That is, the residual story drift corresponding to 0.7% damage level is almost zero.

According to median incremental dynamic analysis curve of SSMF, IDA curve is flatted earlier by increasing pre-MS damaged level. For example, IDA curve for 12-story is becoming smooth in around .22 Sa (g) and .12 Sa (g) for no pre-MS damaged and 5% MID pre-MS damaged respectively (Figure 4-5). This phenomena is happened because of this two reason:

i) The behavior deterioration due to the load-deformation cycles imposed by the MS;

ii) The geometry imperfection at the beginning of the AS that tends to amplify the p-delta effects and accelerate accumulation of lateral deformations in the inclined direction.

From the IDA curves, it is also identified that the AS collapse capacity decreases as larger residual drift is imposed by the MS. Further evaluation of this effect is performed by considering the AS fragility curves.

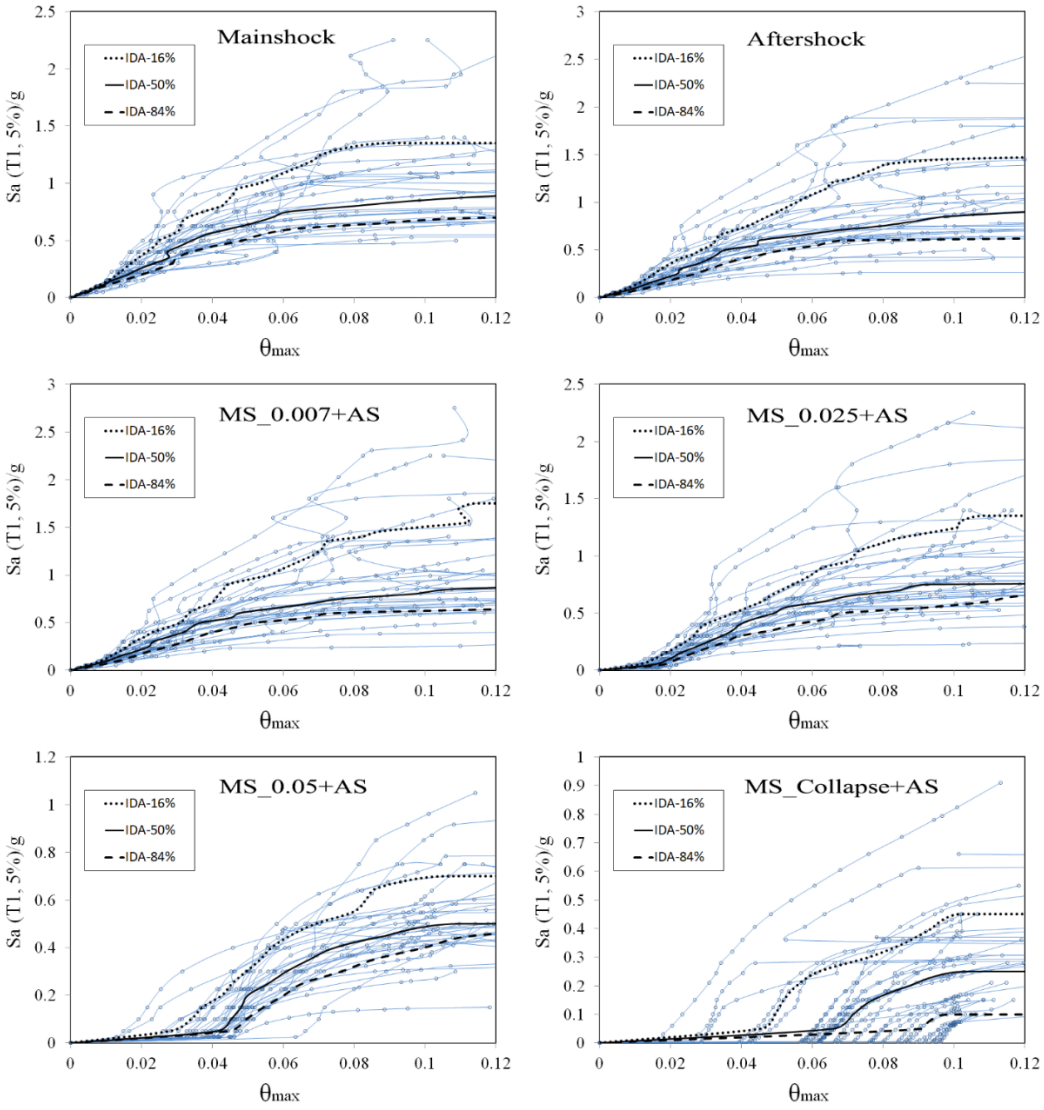

Figure 4.1: Incremental dynamic analysis curves for MS, AS and AS preceded by MSs scaled to various MID levels (4-story SSMF)

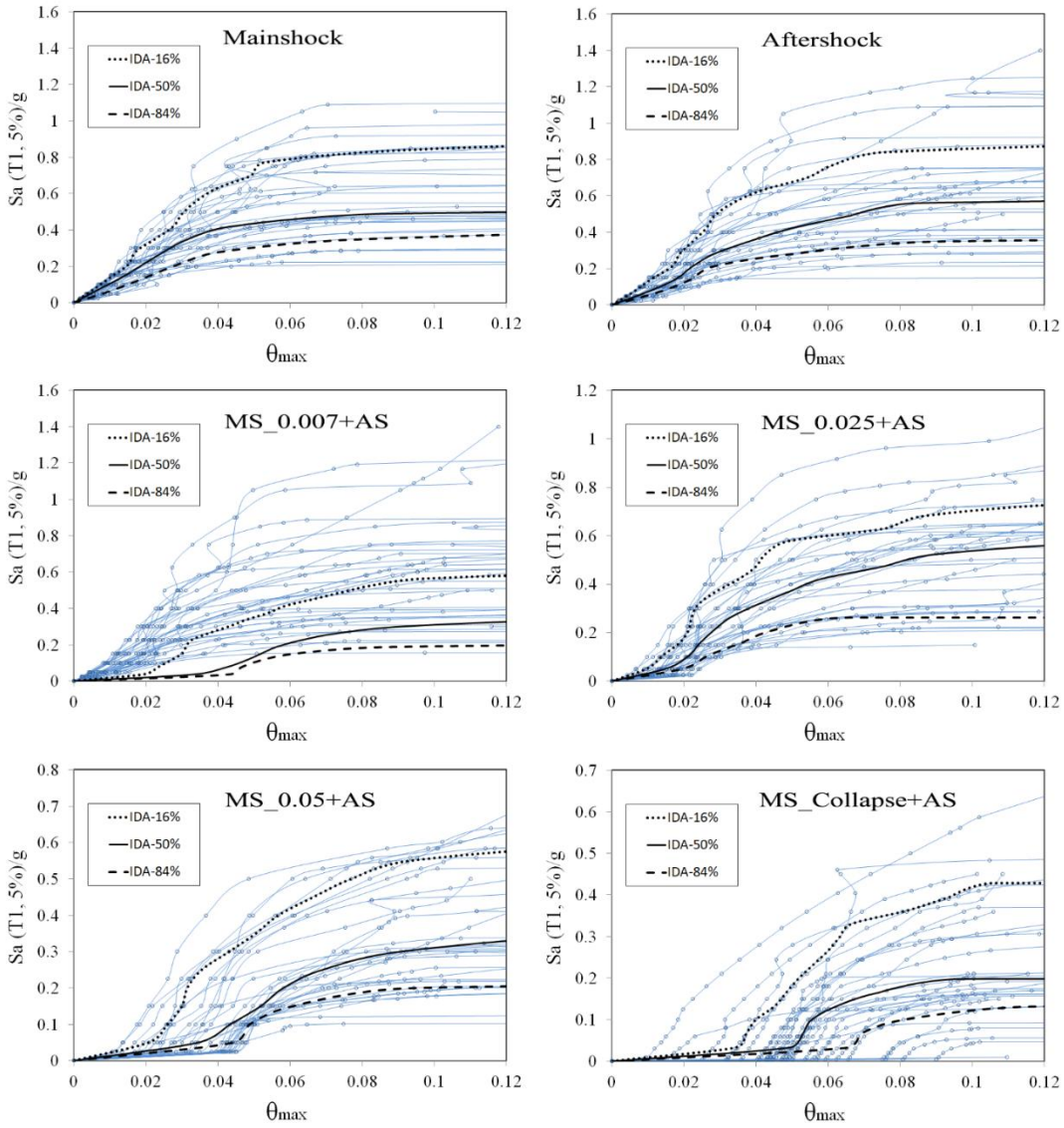

Figure 4.2: Incremental dynamic analysis curves for MS, AS and AS preceded by MSs scaled to various MID levels (8-story SSMF)

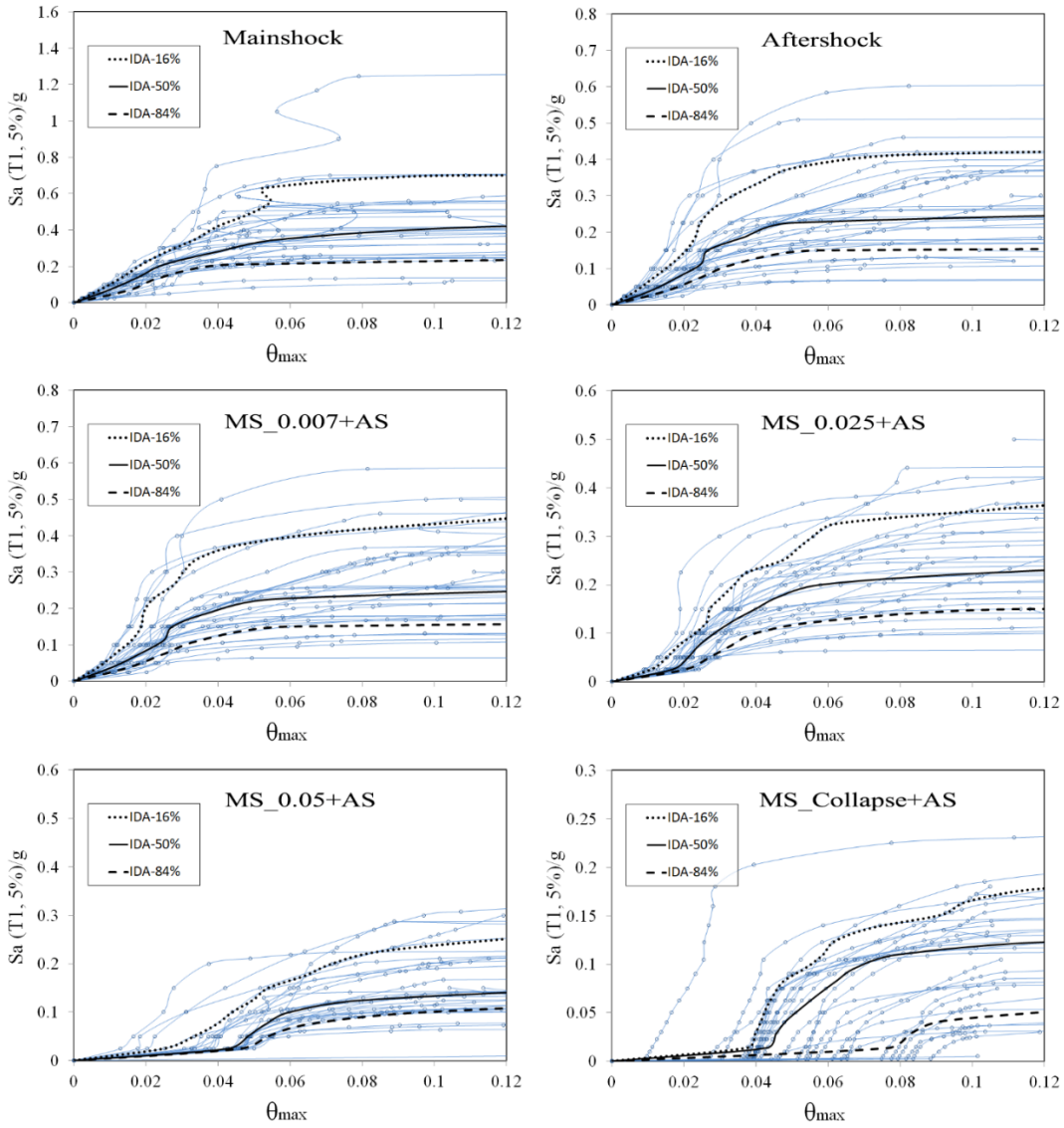

Figure 4.3: Incremental dynamic analysis curves for MS, AS and AS preceded by MSs scaled to various MID levels (12-story SSMF)

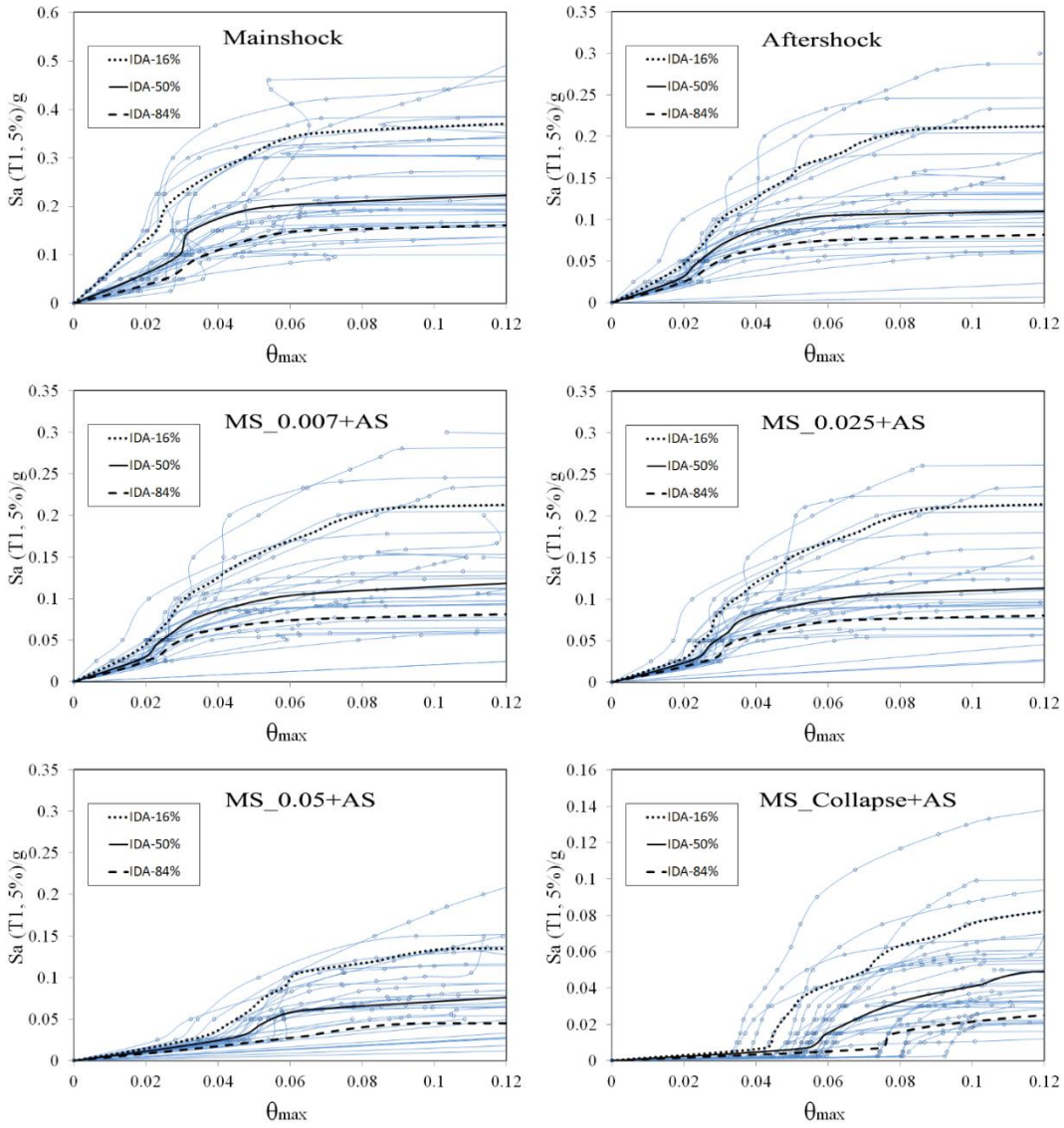

Figure 4.4: Incremental dynamic analysis curves for MS, AS and AS preceded by MSs scaled to various MID levels (20-story SSMF)

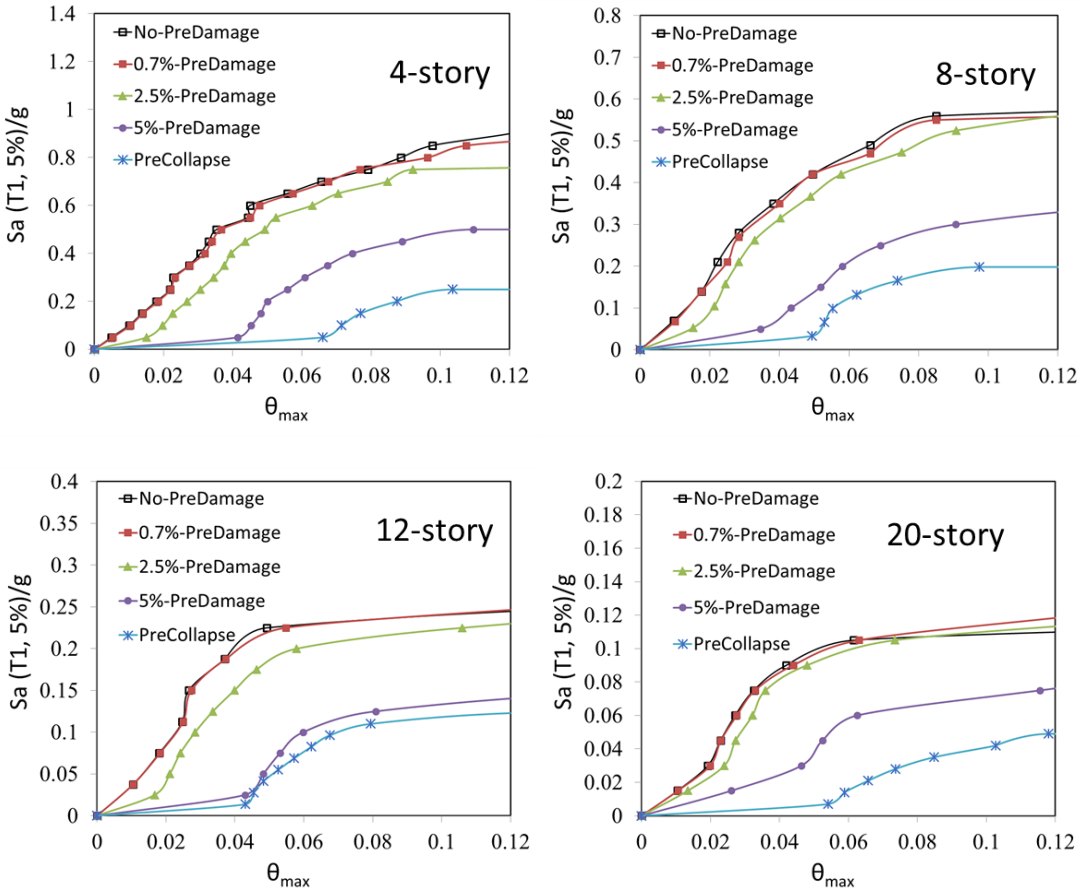

Figure 4.5: Median Incremental dynamic analysis curves of SSMF with different pre-MS damaged

4.2 Drift profile at collapse state

To evaluate the effect of MS excitation on distribution of MID along structures height, the MID values are obtained at the collapse state .This values illustrated in Figure 4.6 to Figure 4.9 for different SSMFs and various MS damage levels.

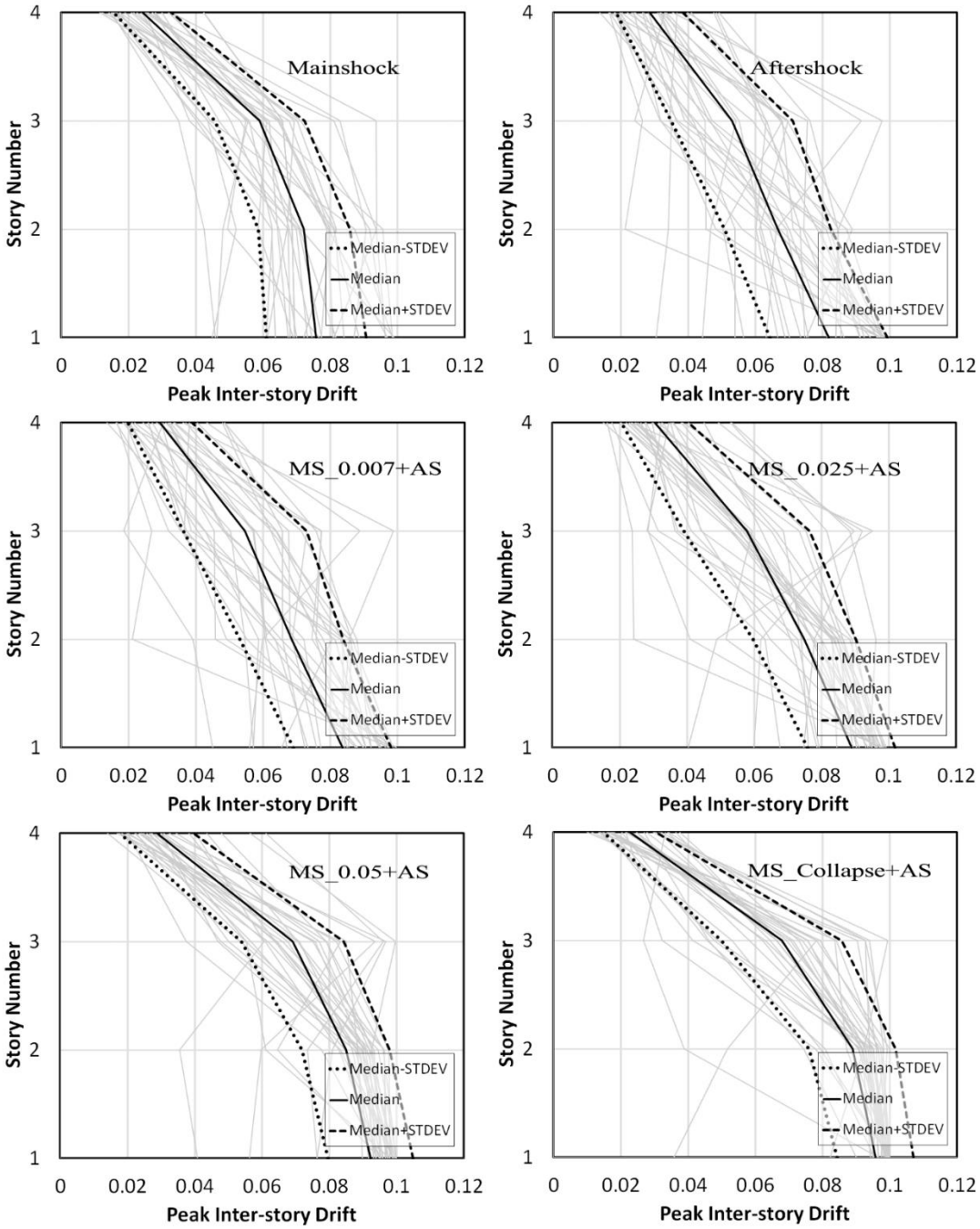

Figure 4.6: Distribution of MID for MS, AS and AS preceded by MSs scaled to various MID levels at collapse state (4-story SSMF)

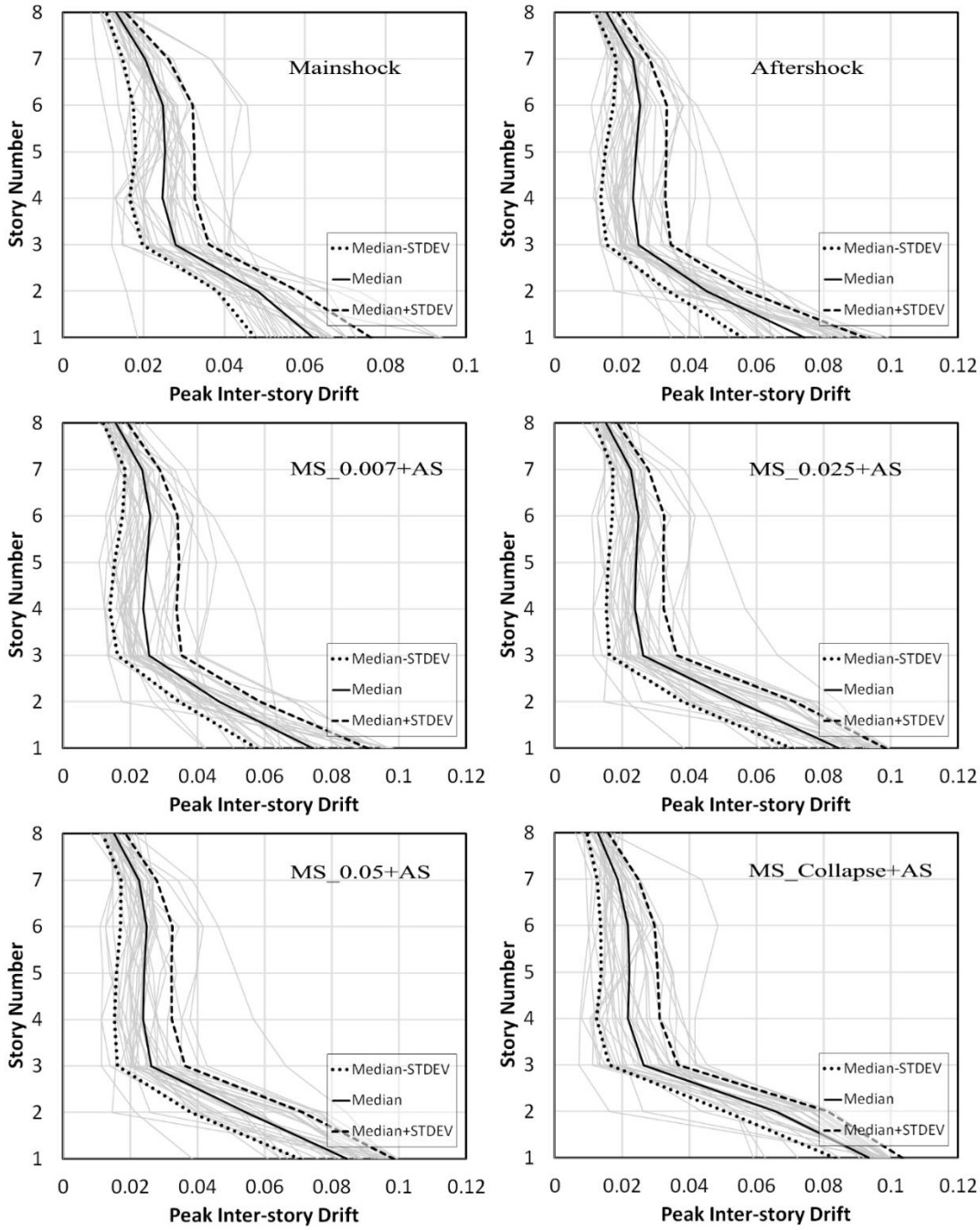

Figure 4.7: Distribution of MID for MS, AS and AS preceded by MSs scaled to various MID levels at collapse state (8-story SSMF)

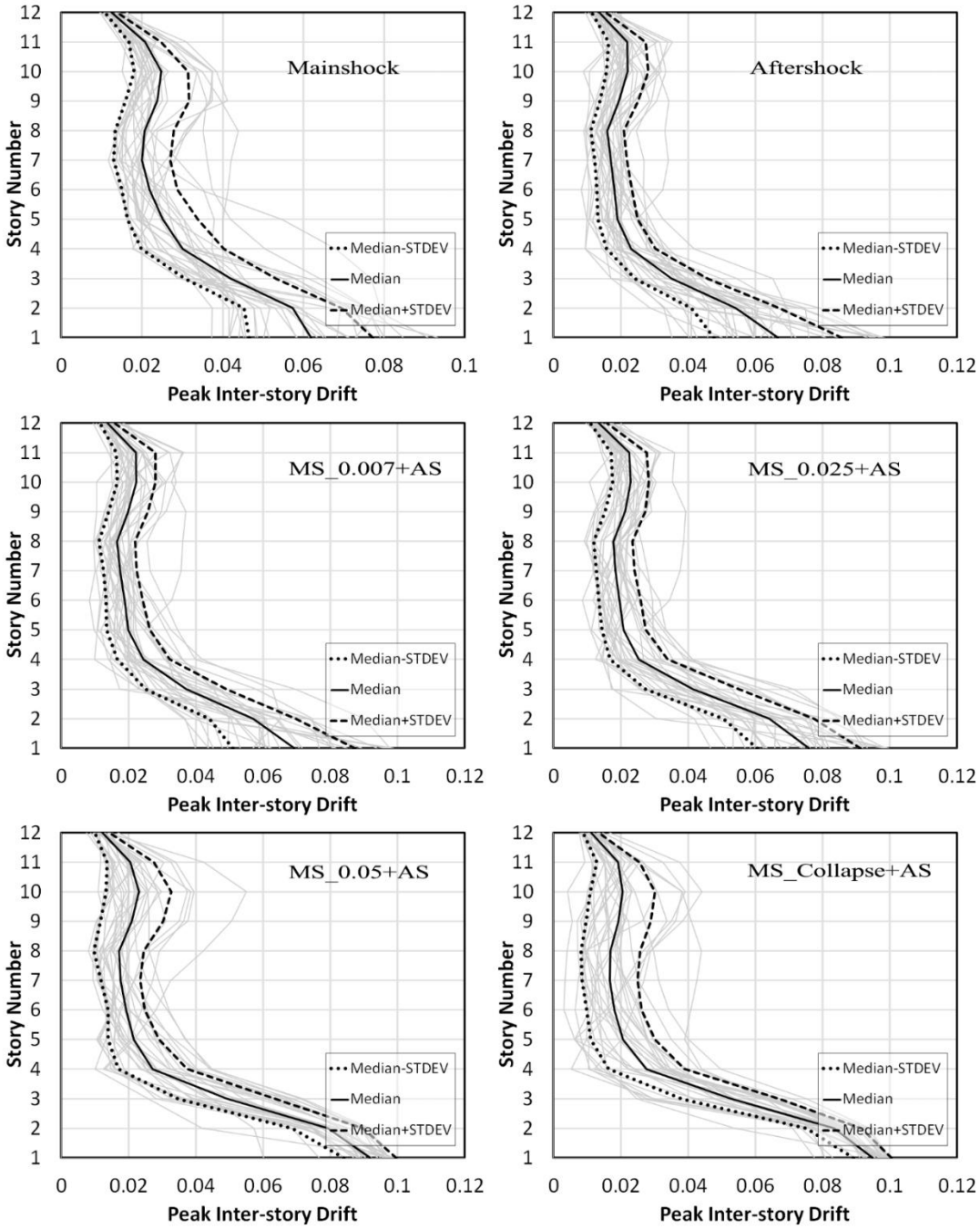

Figure 4.8: Distribution of MID for MS, AS and AS preceded by MSs scaled to various MID levels at collapse state (12-story SSMF)

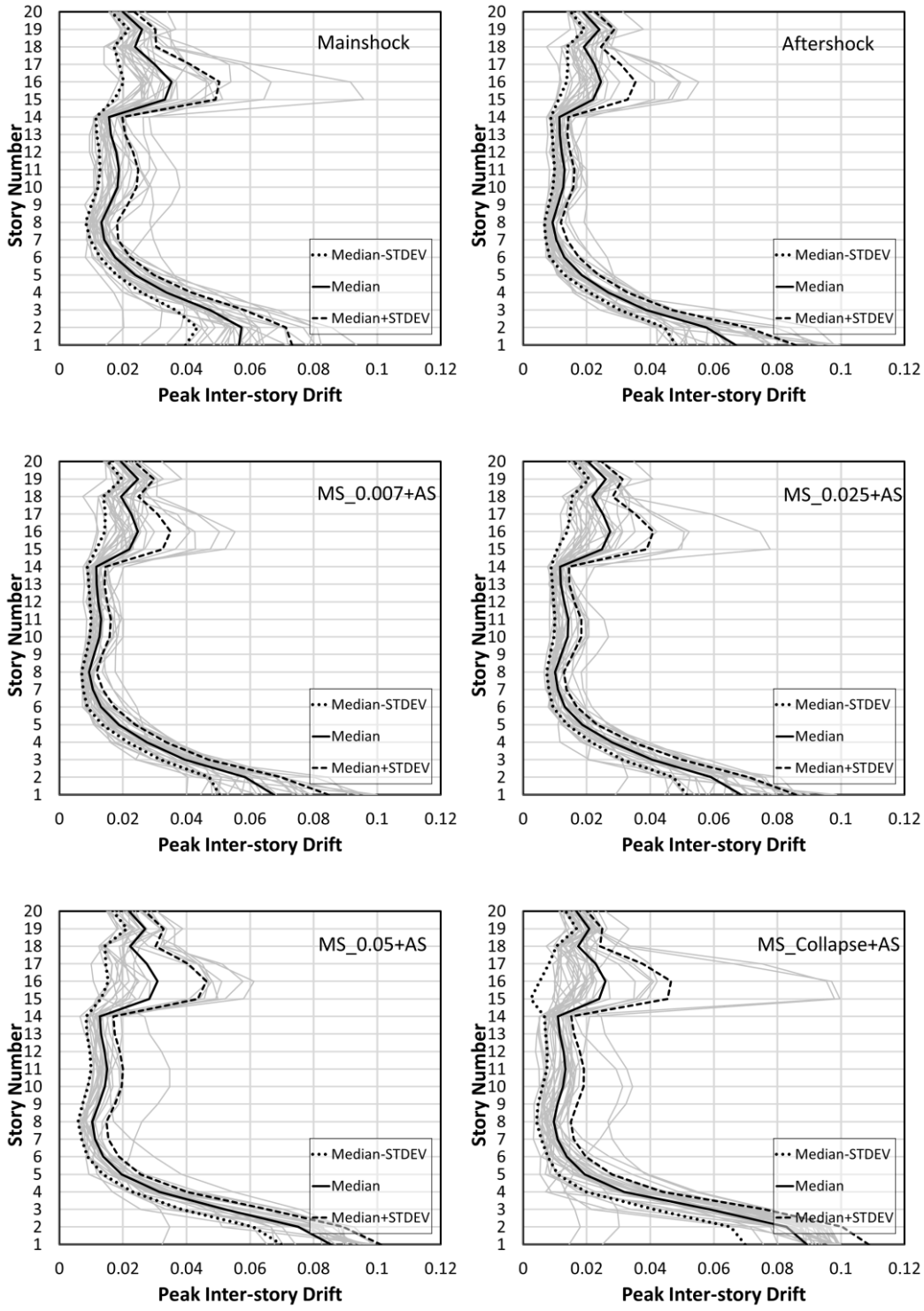

Figure 4.9: Distribution of MID for MS, AS and AS preceded by MSs scaled to various MID levels at collapse state (20-story SSMF)

To allow for a convinient comparison between drift curves related to the diffrenet pre-MS damage and the different structure heights, the median drift profiles are compared in Figure 4.10.To interpret these results, it should be mentioned that, the pattern of

distribution of displacements over building's height plays a significant factor on the capacity of a structure to withstand lateral deformations. This is because the lateral displacements of a structure under seismic excitation lead to second–order p-delta forces under gravitational forces. These second-order effects, in turn, result to the eventual lateral instabilty of the structure, called collapse. The residual story drifts caused by an MS excitation are also likely to alter the final distribution of drifts at which the structure loses its stability at tends towards collapse. As the graphs indicate, except the low-rise 4-story structure, the other SSMFs have collapsed due to concentration of plasticity in quite a few stories. The story at which the maximum drift occurs is not however altered by applying the MS damage and the resulting residual drift.

The maximum of peak inter-story drift is occurred at base story of all structures. The peak inter-story drift for base story is increased by increasing pre-MS damaged level for all of the structures. For example the peak inter-story drift for base story of 12-story increase from 6.5% to 9% by increasing the pre-MS damaged level form no pre-MS damaged to 5% MID pre-MS damaged (Figure 4.10).

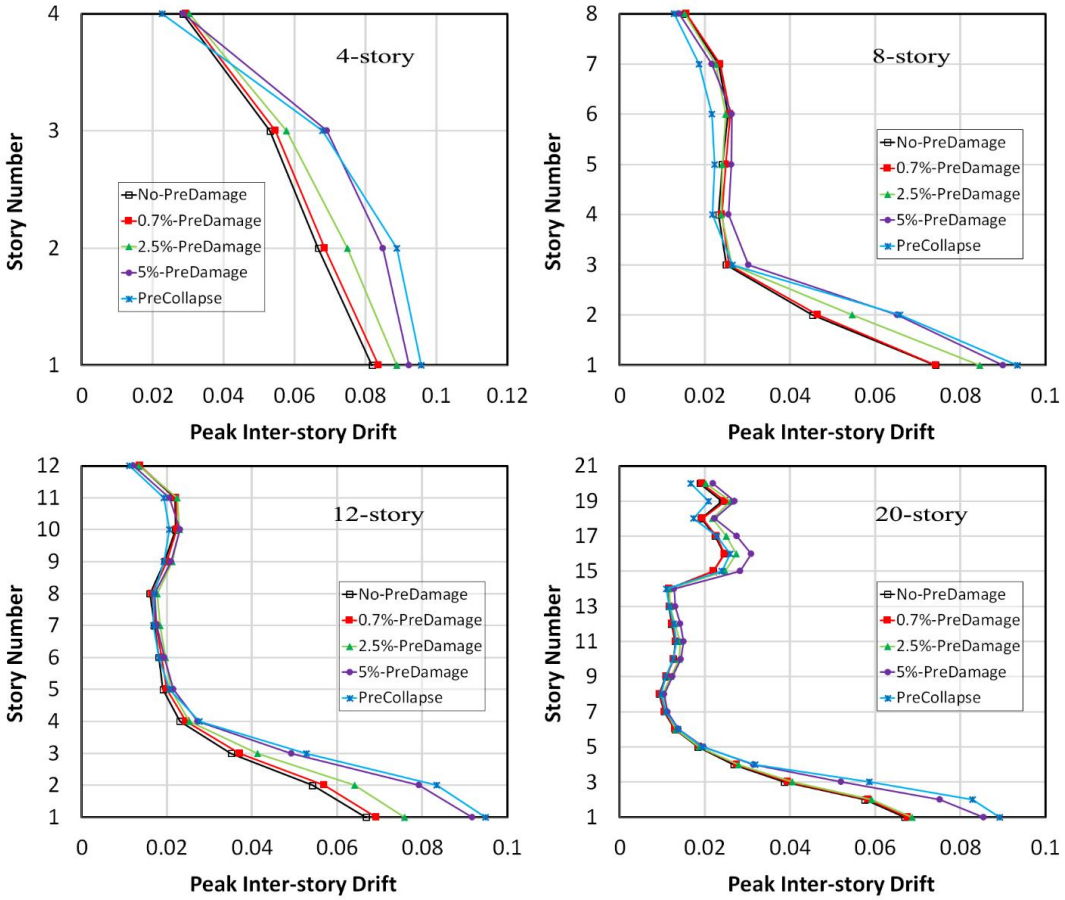

Figure 4.10: Distribution of median MID for AS (No-PreDamage) and AS preceded by MSs scaled to various MID levels at collapse state (4-story to 20-story SSMF)

4.3 AS collapse fragilities

The AS fragility curves are shown in Figure 4.11 to Figure 4.14 for SSMFs with various heights and for different MS damage levels. The fragility curves are compared in Figure 4.15 and the collapse $S_a(T_1)$ associated with a 50% probability is extracted for the various cases.

According to Figure 4.15, for certain value of Sa by increasing the pre-MS damaged the probability of collapse is increased. For example for Sa=0.5g the collapse probability of 4-story SSMF is increased from 10% to 50% by increasing pre-MS damaged from no pre-MS damaged to 5% MID pre-MS damaged.

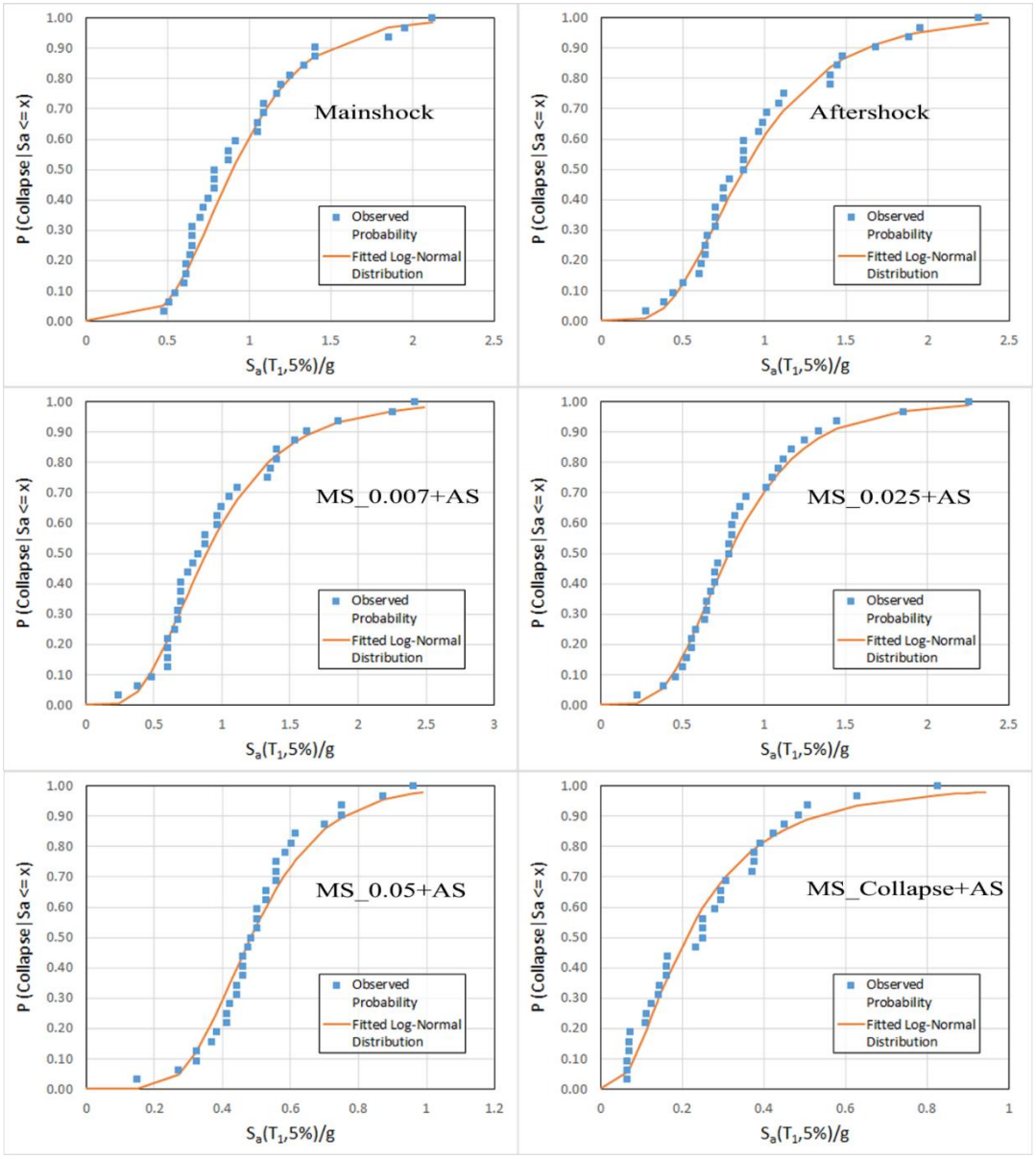

Figure 4.11: AS fragility curves obtained for 4-story SSMF for various MS drift levels

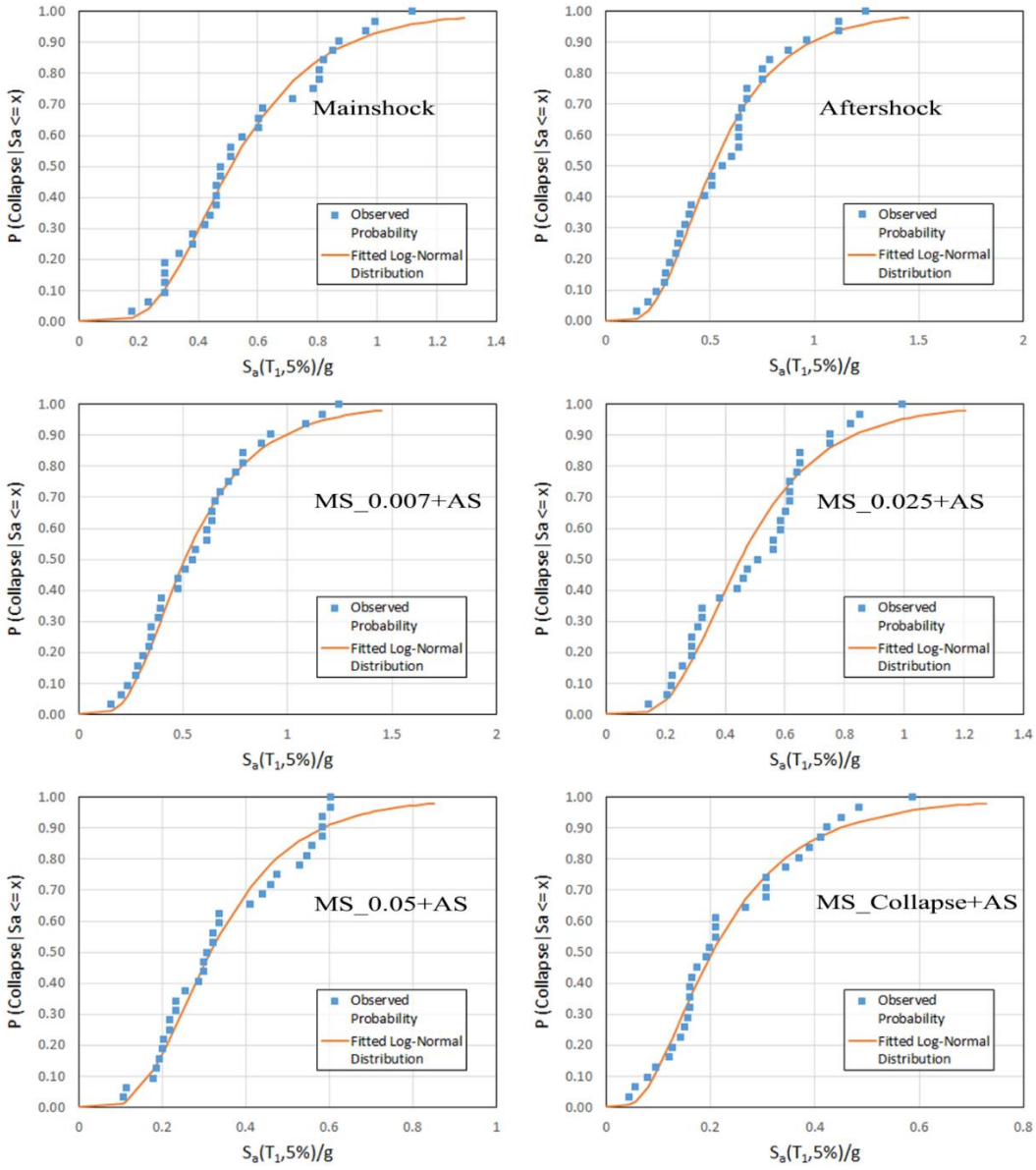

Figure 4.12: AS fragility curves obtained for 8-story SSMF for various MS drift levels

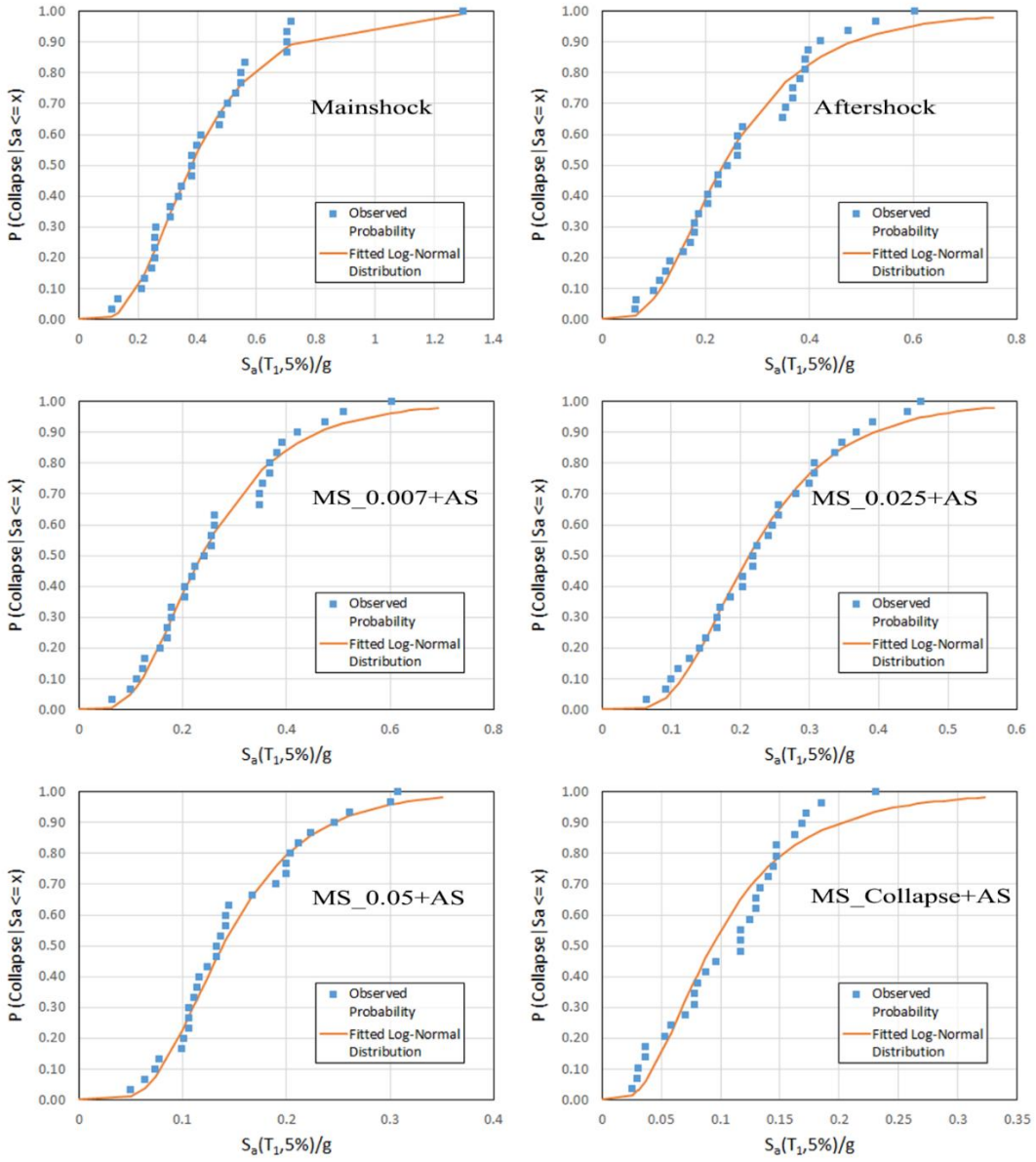

Figure 4.13: AS fragility curves obtained for 12-story SSMF for various MS drift levels

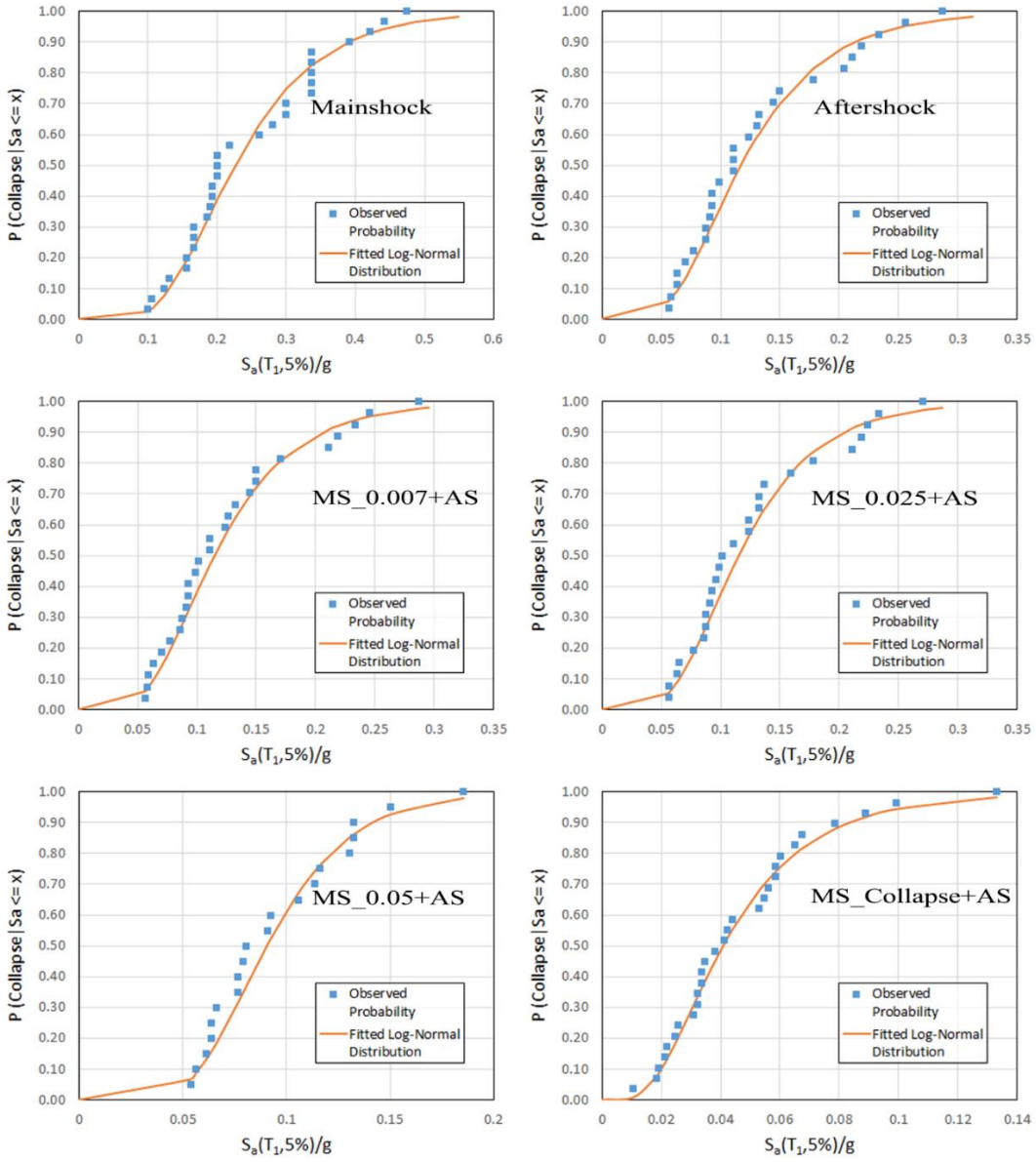

Figure 4.14: AS fragility curves obtained for 20-story SSMF for various MS drift levels

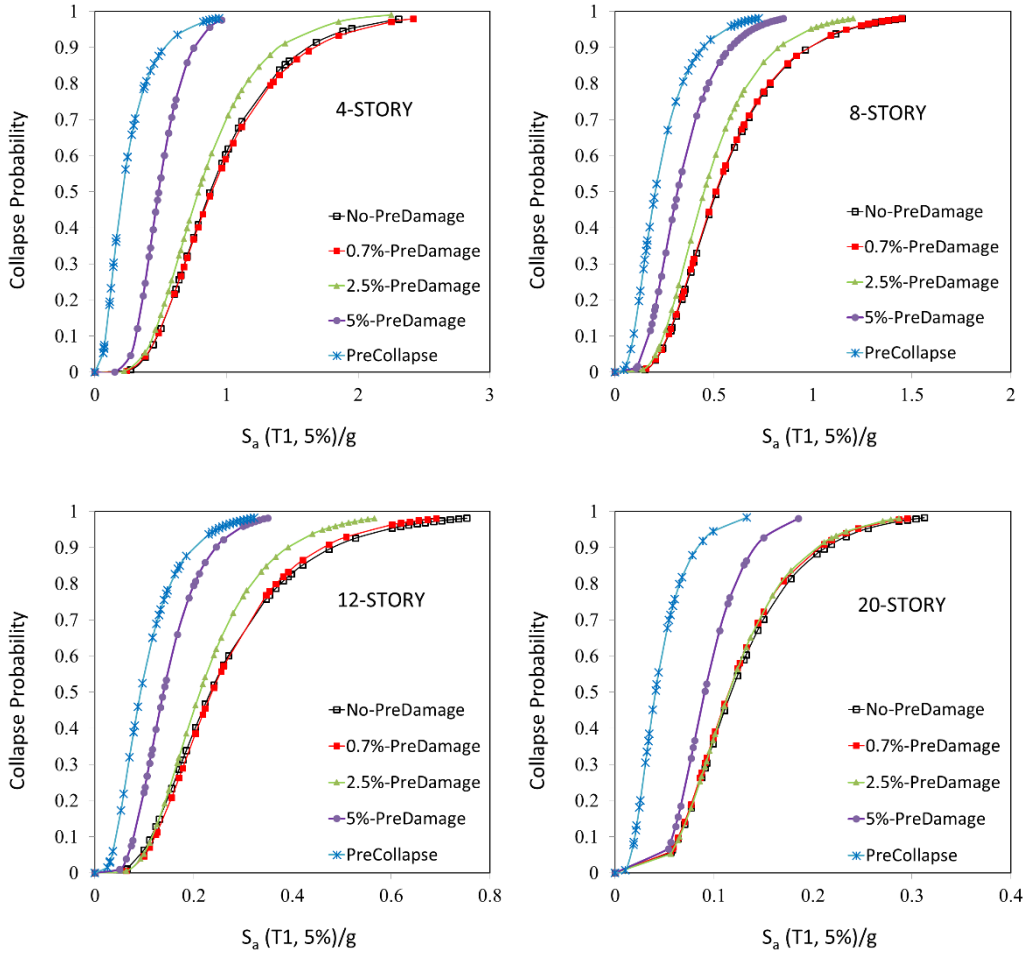

Figure 4.15: AS fragility curves for different pre-MS damaged (4-story to 20-story SSMF)

The so-called AS median collapse capacity (AMCC) are compared in Figure 4.16. As implied by the histogram graphs shown in this Figure, the AMCC value decreases when the level of MS damage is increased. To conduct a more thorough assessment on the effect of MS damage level, the AMCC values are divided to value for intact frames (No-PreDamage) and are compared in Figure 4.17. The derived parameter is named damaged-to-undamaged capacity ratio (DUCR) whose values can help to quantify the influence of pre-MS damaged on the AMCC.

According to Figure 4.17, the studied SSMFs can be categorized into three low-, mid- and high-rise structures including respectively, 4-story, 8 and 12-story, and 20-story

SSMFs. The changes in the DUCR value brought about by altering the MS damage level is almost identical for the low- and mid-rise structures with a minor exception of the pre-collapse case in which a larger sensitivity is observed in the low-rise structure. The high-rise structure, however, shows a different trend; as shown by the Figure, the vulnerability of this structure at the 2.5% initial MID is still slight and does not become pronounced until the 5% initial MID is applied. When the MS drives the high-rise structure to the collapse threshold, the reduction in AS collapse capacity becomes again as much as the low- and mid-rise structures. The sensitivity of the DUCR to a prior collapse is nevertheless thought to be more a function of the collapse detection criteria than the structure's characteristics. Since various drift values are likely to be undergone by various structures at the collapse state, finding a consistent dependency between this damage level and the other drift-defined levels may be difficult. Considering this fact and disregarding the collapse initial damage case, a distinguishable difference can be observed between the sensitivity of high-rise structures and the other structures to a prior MS damage.

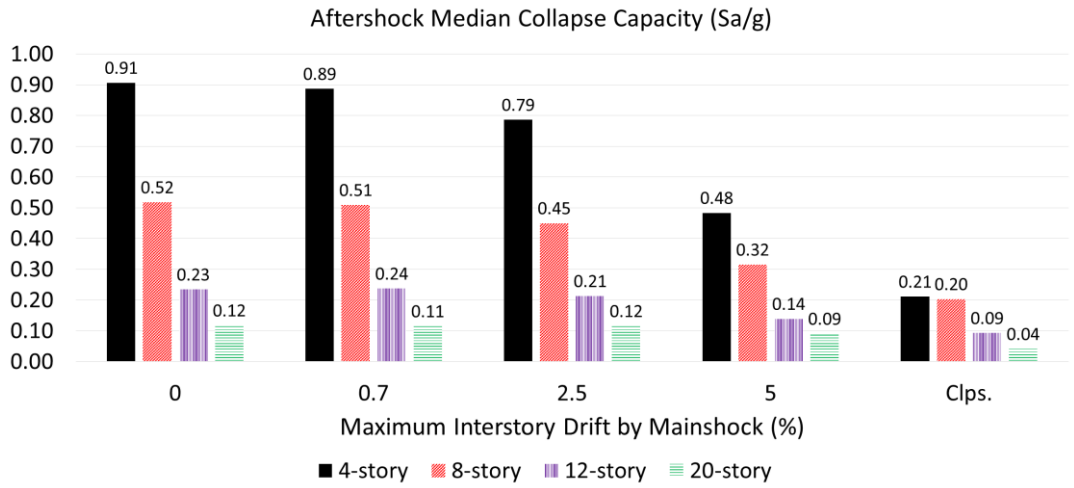

Figure 4.16: AMCC values for SSMFs with different MS damage levels

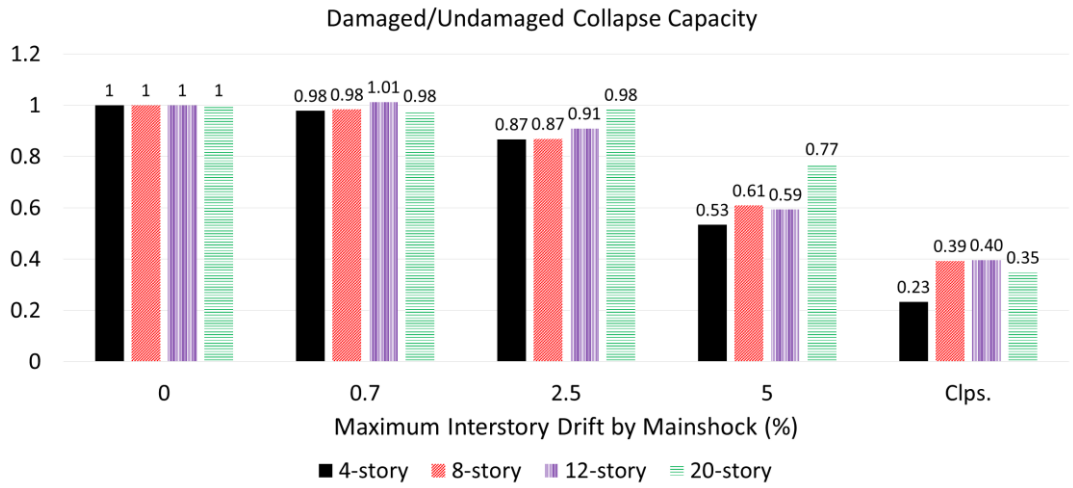

Figure 4.17: Damaged-to-undamaged AMCC ratios for SSMFs with different MS damage levels

According to AMCC results the structural collapse capacity may reduce significantly when the building is subjected to a high intensity MS.

For predicting the DUCR parameter with considering pre-MS damaged, two different datasets related to the low- and mid-rise SSMFs and the high-rise structures are separately considered and used for a regression analysis. The outcome quadratic polynomial curves are illustrated in Figure 4.18 and Figure 4.19. These equations may be used for predicting the effect of various levels of MS damage (expressed in terms of initial MID) on the structure's collapse capacity under a consequent AS.

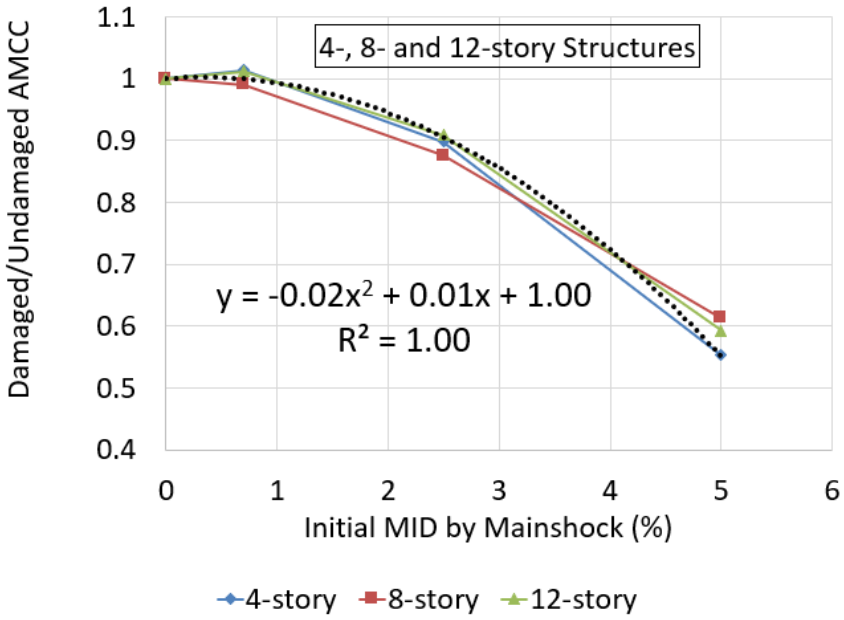

Figure 4.18: Regression equation to predict damaged-to-undamaged AMCC against the MS-induced MID value (4- to 12-story SSMFs)

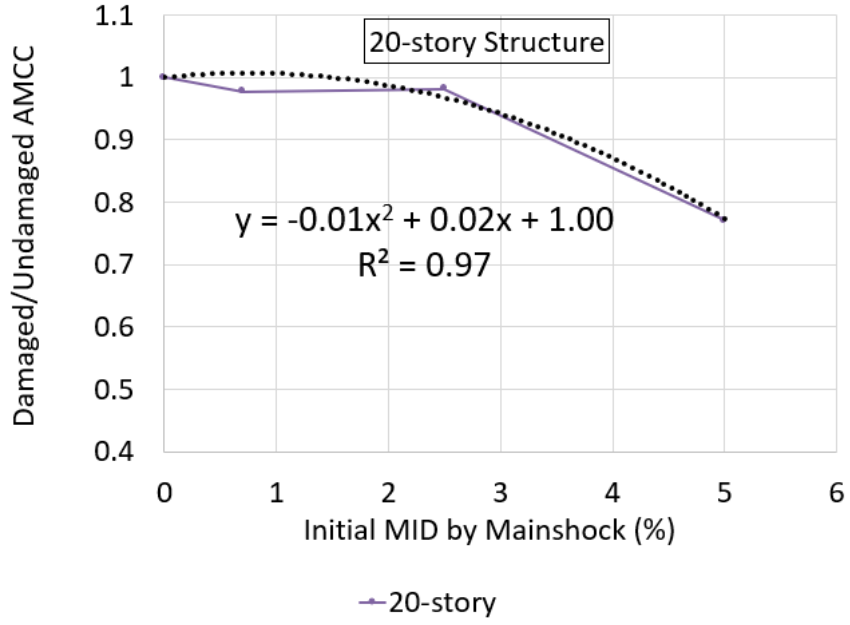

Figure 4.19: Regression equation to predict damaged-to-undamaged AMCC against the MS-induced MID value (20-story SSMF)

The different trends observed for the correlation between the AMCC values of the high-rise SSMFs and those of the shorter structures may be a result of the various correlation between MID and PRSD responses in the two classes of structures. In other

words, the main response parameter affecting the structure's performance when it is hit by an AS is its residual state at the end of MS. Thus, the effect of MS damage could be more directly reflected by use of the PRSD parameter. Since the maximum response reflected by the MID parameter provides an indirect expression of the residual state, the relation between the observed AMCCs and the MIDs is affected by the relation between MID and PRSD responses. While in low-rise structures, a shear mechanism governs the lateral response, for taller SSMFs, the flexural response dominates the lateral collapse. Therefore, the percetage of the maximum drifts that can be recovered during the excitation cycles are also expected to vary for these two classes of structures.

Although good correlation is found between the AMCC values and the MID parameter as MS damage measure, the potentials of the PRSD parameter for expressing the MS damage are also evaluated. This assessment is performed in the next chapter of this dissertation.

Chapter 5

PRSD-BASED MS-AS EXCITATIONS

Utilization of the MID parameter for expressing the damage imposed by an MS excitation was evaluated in the previous chapter. This chapter focuses on substituting the MID with the PRSD parameter for reflecting the MS damage. The PRSD parameter presents the status of the deformations at the end of MS excitation. As stated in previous chapters, the damaging effects caused by an MS consist of i) the behavior deterioration due to the load-deformation cycles imposed by the MS, and ii) the geometry imperfection at the beginning of the AS that tends to amplify the p-delta effects and accelerate accumulation of lateral deformations in the inclined direction.

While the PRSD parameter provides a more direct account of the residual inclination of the structure, it is also beneficial from the measurability aspect. That is, at the end of a MS, the residual drift can be observed and used for predicting the probabilistic effects of the AS. This capability is not provided by the MID parameter since it is a temporary status occurred within the excitation time and not measurable at its end.

Regarding the potential advantages of the PRSD parameter, its utilization as the MS damage indicator is studied in this chapter. As described in earlier chapters, this is done by considering the 0.005, 0.014 and 0.02 PRSD values for expressing the MS damage levels.

Before presenting the PRSD-based IDA results, a discussion is provided in the next section on the relation between the MID and PRSD parameters. This is done with the aid of the structural periods at the end of the MS excitation, called residual period.

5.1 Fundamental period after MS

The effects of the MS excitation were formerly categorized as the damage-induced deterioration in the structural behavior, and the geometry inclination. The first phenomenon plays an important role in also determining the residual displacements forming the inclined geometry of the structure at the end of the MS. Thus, a higher significance should be attributed to the degrading effects caused by a MS excitation. These degradations affect the strength and stiffness of the members at the same time. The strength deterioration caused by a MS can accelerate the entrance of the member into the nonlinear range, and so, the extent of plasticity undergone by it. The effect of MS-induced damage on the members' stiffnesses is also significant in terms of the residual deformations remaining after the seismic loading is ceased. These effects can be quantified by the means of the structural period at the end of MS excitation.

Figure 5.1 schematically shows part of the load-deformation cycles undergone by a typical story under a MS. The points marked as "1" on the curves represent an imaginary peak status along the response history. The unloading and the free vibration regimes are also simply shown in this Figure through points 2-5. While this regime may not immediately follow the peak response in a real situation, this does not affect the role of the peak displacement on the residual deformation of the story. Considering the schematic load cycles, the effect of unloading stiffness on the residual displacement can be identified.

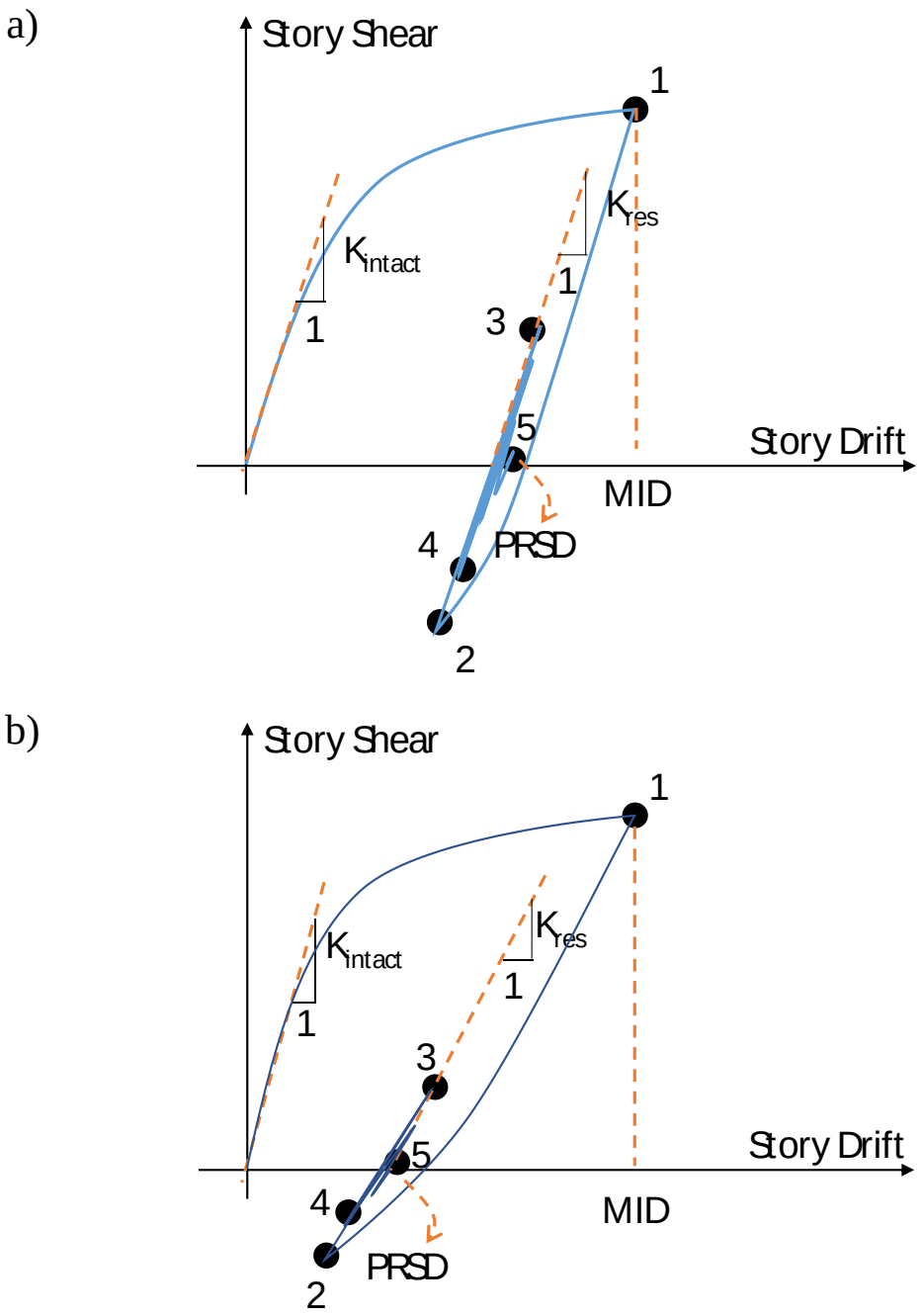

Figure 5.1: The relation between the MID, PRSD and Tres parameters; a) in absence of stiffness deterioration and b) in presence of stiffness deterioration

As shown in Figure 5.1a, in absence of the stiffness deterioration caused by the MS damage, the unloading stiffness nearly equals the elastic stiffness of the story. In such situation, unloading the story shear by removal of the seismic lateral force leads to recovering of a rather small portion of the plastic deformation undergone at the peak point. The reduced unloading stiffness shown in Figure 5.1b, on the other hand, helps

the story to recenter to some smaller residual deformation, compared to the undegraded situtation. An overall portrait of the stories' stiffness at the residual status of the structure can be provided by the first mode vibration period, T_1. When multiple stories with various levels of degradation exist in a structure, the T_1 parameter can only provide an estimate of the mean stiffness and the accuracy of this estimator reduces by increase of the stories number.

According to the role of the unloading stiffness on the residual deformations, it can be said that for a given MID response, the magnitude of the PRSD parameter is tightly correlated with the extent of stiffness degradation undergone within the loading cycles. A higher residual T_1 (T_1 at the end of MS), and the reduced unloading stiffness assciated with it, is thus thought to reflect the higher recentering characteristics of the structure. This leads to lower PRSD levels in the structure compared to one undergoing the same MID but showing smaller residual T_1.

The fundamental period after applying the MS excitation ($T_{1,\,MS}$) of the 4- to 20-story SSMFs are there for studied in this section. These values are computed through performing eigen analysis after the MS excitations. The average and standard deviation of the $T_{1,\,MS}$ values obtained for various MS records are reported in Table 5.1 along with their minimum and maximum values. The changes in the average T_1 brought about by the MS excitation are also graphically presented in Figure 5.2.

According to Figure 5.2, for the low-rise (4-story) SSMF, the average change in the period is approximately as low as 7% irrespective of the MS damage level. For taller structures, the effect of the MS damage becomes more significant and shows considerable sensitivity to the applied MS damage.

According to the above descriptions, these observations indicate the more closeness of the MID and PRSD responses in the low-rise 4-story SSMF in which low period change is observed. The low change in the structural stiffness can also be taken as a sign of the minor deterioration in the behavior of the 4-story SSMF. This in turn indicates that the MS effect mainly appears by inclining the geometry of the structure and amplifying the p-delta effects.

For the mid-rise 8-story SSMF, the period elongation is obvious and indirect relation with the MS damage level. In range of the taller structures, this trend intensifies and a sudden period increase is observed when MS damage elevates from 0.5% to 1.4%. Further increase of MS-induced PRSD to the 2% level does not, however, show the same level of period elongation and shows some sort of saturation in the extent of deterioration induced by the MS at the 1.4% level.

Table 5.1: The average, standard deviation, minimum and maximum values of fundamental periods after applying different levels of MS damage

Model	Target PRSD level	Intact fundamental period, T_1 (s)	Fundamental period (s) after MS earthquake $T_{1,MS}$				
			Ave	Stdv	Min	Max	MS-induced change
4st	0.005	1.54	1.660	0.239	1.577	2.630	7.70%
	0.014		1.634	0.172	1.577	2.486	6.10%
	0.02		1.658	0.198	1.577	2.486	7.70%
8st	0.005	2.13	2.360	0.451	2.174	3.692	11.00%
	0.014		2.367	0.470	2.174	3.692	11.00%
	0.02		2.394	0.470	2.174	3.692	12.39%
12st	0.005	2.94	3.151	0.574	3.016	6.230	7.00%
	0.014		3.596	1.851	3.016	12.846	22.00%
	0.02		3.732	1.886	3.016	12.847	26.94%
20st	0.005	4.36	4.764	0.818	4.505	8.051	9.20%
	0.014		5.221	1.557	4.505	9.466	20.00%
	0.02		5.410	1.844	4.505	10.223	24.09%

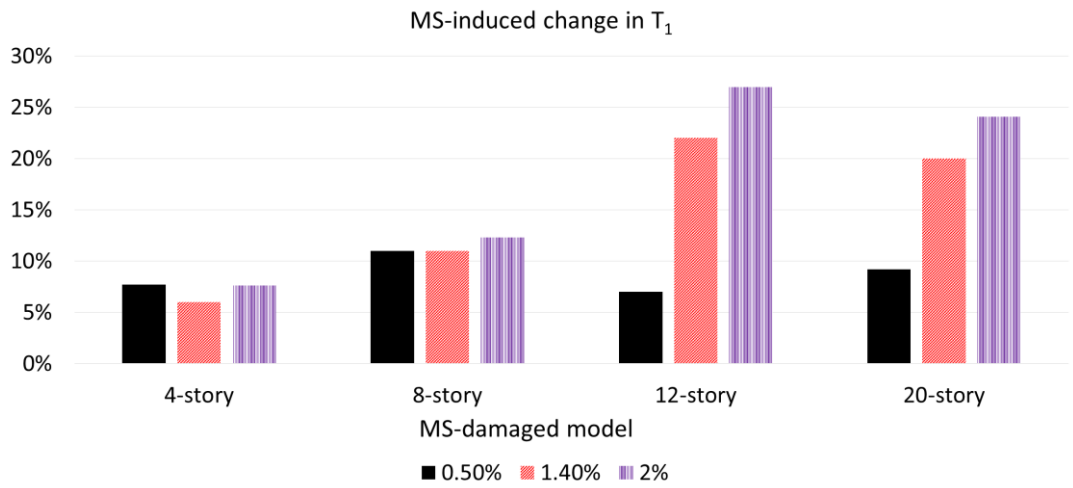

Figure 5.2: The average MS-induced change in the structures' fundamental periods

5.2 IDA results

The PRSD-based IDA results obtained for the 4- and 8-story SSMFs are presented in Figure 5.3 while Figure 5.4 shows these results for the 12- and 20-story structures. For the sake of brevity, complete IDA curves are only presented for the two extreme cases, i.e., the AS-only and the MS-AS sequence with MS scaled to the 0.02 PRSD value. To accommodate to the MS damage expressed by PRSD parameter, the presented IDA curves employ PRSD as the demand parameter. The median IDA curves of the structures are compared in Figure 5.5 to Figure 5.8 for all MS-AS combinations.

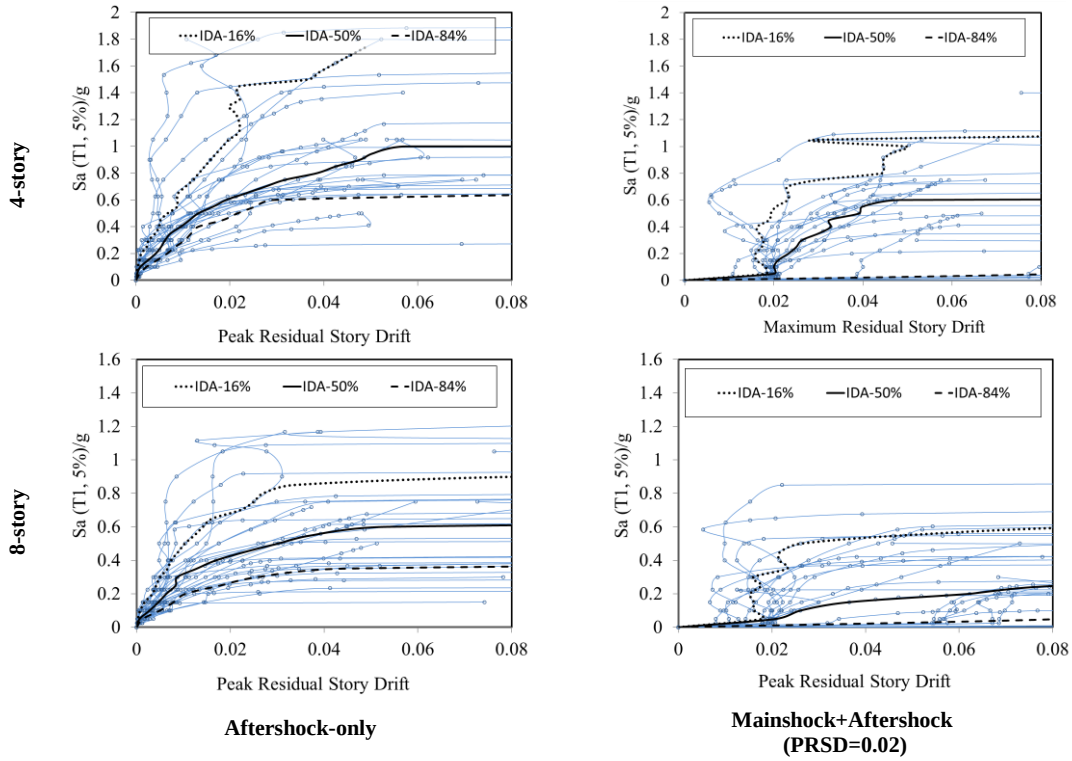

Figure 5.3: IDA curves obtained for SSMFs subjected to AS-only and AS preceded by MSs scaled to PRSD=0.02 (4- and 8-story SSMFs)

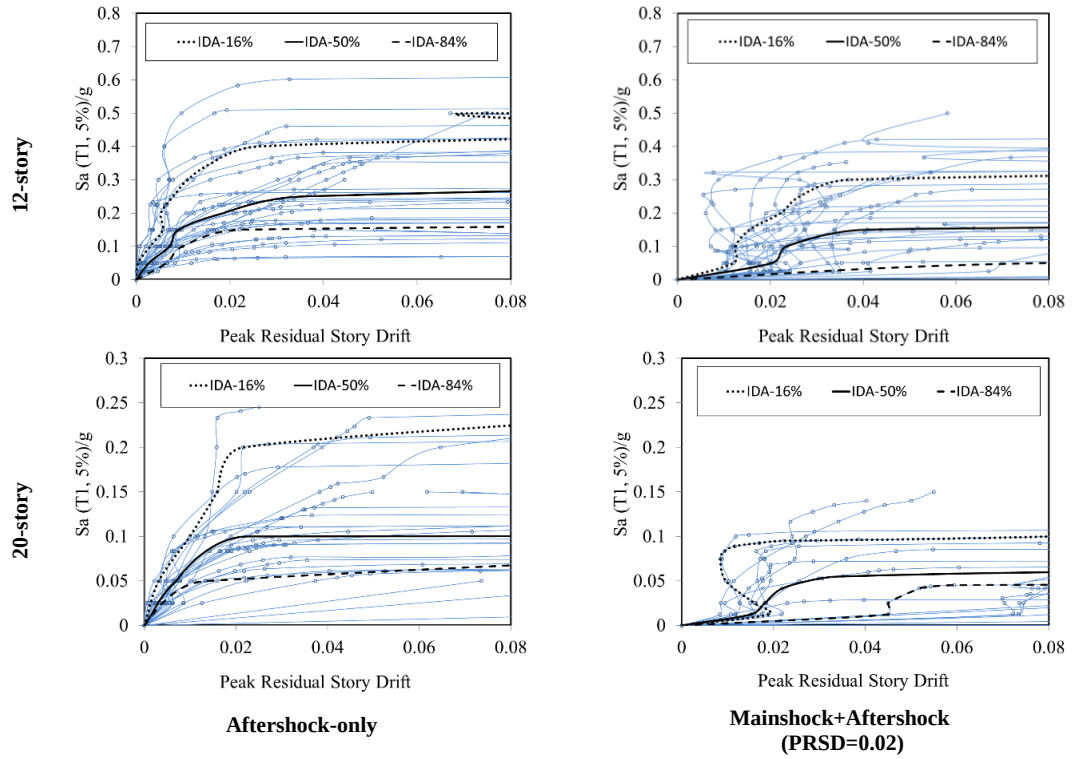

Figure 5.4: IDA curves obtained for SSMFs subjected to AS-only and AS preceded by MSs scaled to PRSD=0.02 (12- and 20-story SSMFs)

As was shown for the case of MID-represented damage in chapter 4, the influence of the pre-MS damaged on the IDA curves appears as an initial lag in the PRSD values. In other words, the PRSD value that presented in IDA curves is always greater than or equal to the value induced by the MS. Thus, these initial lags equals the PRSD occurring at the end of MS excitation and increases by scaling the MS level. In spite of the MID-based IDA curves, the observed initial lag is directly correlated to the MS damage being expressed using PRSD parameter.

As was discussed for the case of MID-represented damage in chapter 4, the median incremental dynamic analysis curve of SSMF is flatted earlier by increasing pre-MS damaged level. For example, IDA curve for 12-story is becoming smooth in around .25 Sa (g) and .15 Sa (g) for no pre-MS damaged and 2% PRSD pre-MS damaged respectively (Figure 5.4). This phenomena is happened because of this two reason:
i) The behavior deterioration due to the load-deformation cycles imposed by the MS
ii) The geometry imperfection at the beginning of the AS that tends to amplify the p-delta effects and accelerate accumulation of lateral deformations in the inclined direction.

5.3 AS collapse fragilities and PRSD profiles

The AS collapse fragility curves derived by using PRSD as MS damage indicator are shown in Figure 5.5 to Figure 5.8 for the considered MS-AS combinations. As is expected and was also shown in the previous chapter, an increased collapse probability is observed at given $S_a(T_1)$ intensities for MSs with higher damage level and larger PRSDs. According to Figure 5.5, for certain value of Sa by increasing the pre-MS damaged the probability of collapse is increased. For example for Sa=0.5g the collapse

probability of 4-story SSMF is increased from 10% to 60% by increasing pre-MS damaged from no pre-MS damaged to 2% PRSD pre-MS damaged.

The height profile of the PRSDs occurring at various stories at the AS-induced collapse state are shown at the bottom parts of Figure 5.5 to Figure 5.8. According to these graphs, the prior MS damage changes the maximum PRSD value of the structures at their collapse state. The pattern of PRSD distribution along buildings height is not, however, altered by changing the MS damage level. Irrespective of the MS effects, comparison between residual drift curves obtained for various structures reveals remarkable PRSD concentration at some stories of the structures with 8 stories and higher. This observation is related to the already known fact about the plasticity localization in high-rise structures that makes their collapse mechanism more like the buckling failure of a slender column.

The maximum of peak inter-story drift is occurred at base story of all structures. The peak inter-story drift for base story is increased by increasing pre-MS damaged level for all of the structures. For example the peak inter-story drift for base story of 12-story increase from 2.6% to 3.7% with is increased the pre-MS damaged level from no pre-MS damaged to 2% PRSD pre-MS damaged (Figure 5.7).

Mechanically, the magnitude of the lateral deformations at the collapse state has a direct relationship with the second-order moments caused by gravity loads. These moments, together with the earthquake dynamic effects, including the internal forces and the behavior deteriorations, trigger the final collapse of the structure. When the collapse state's lateral deformations and the resulting second-order moments enlarge in magnitude, the dynamic affects are also expected to change in order to accommodate

to the constant dynamic capacity of the structure. These trends are all governed by the collapse mechanism whose study is the subject of chapter 6.

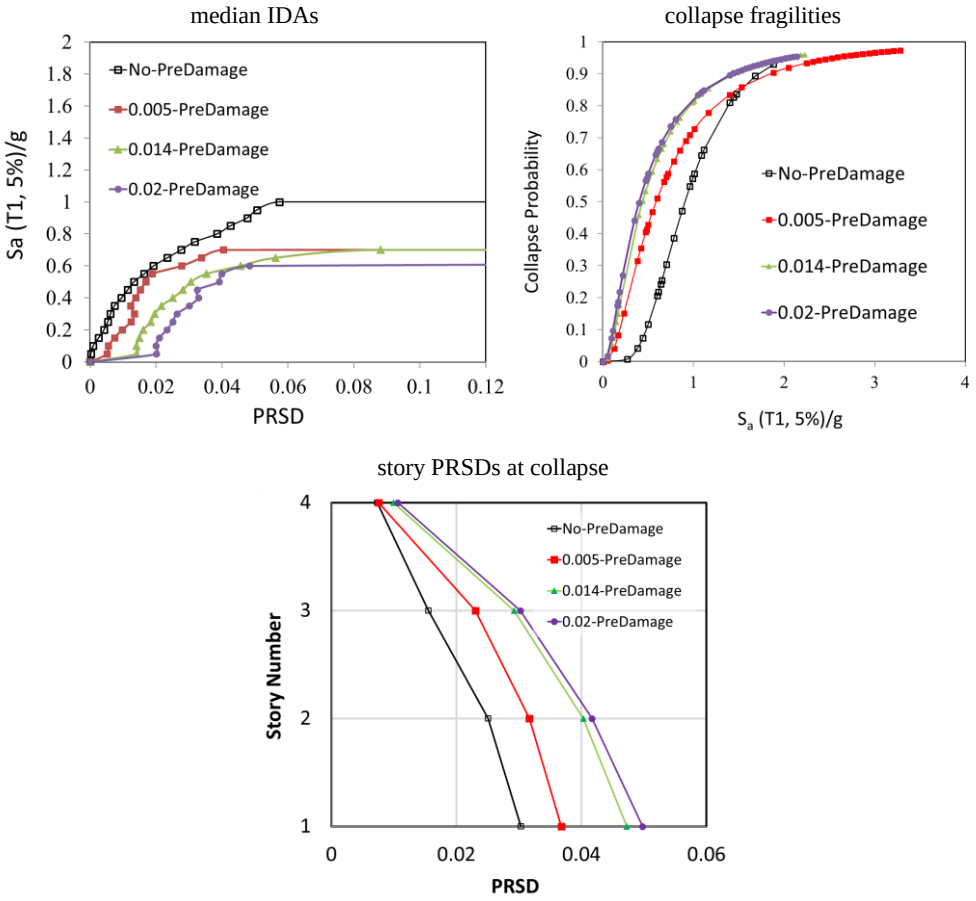

Figure 5.5: Median IDAs, fragilities, and PRSD profile at AS-induced collapse of 4-story SSMF

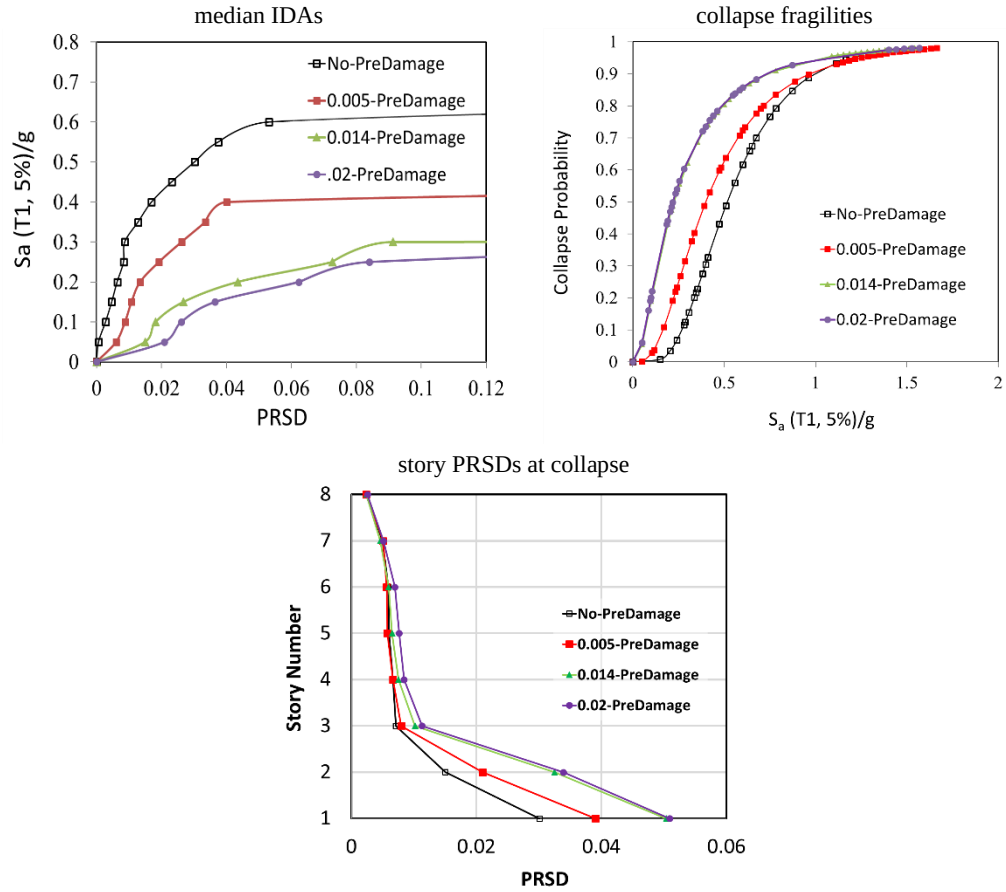

Figure 5.6: Median IDAs, fragilities, and PRSD profile at AS-induced collapse of 8-story SSMF

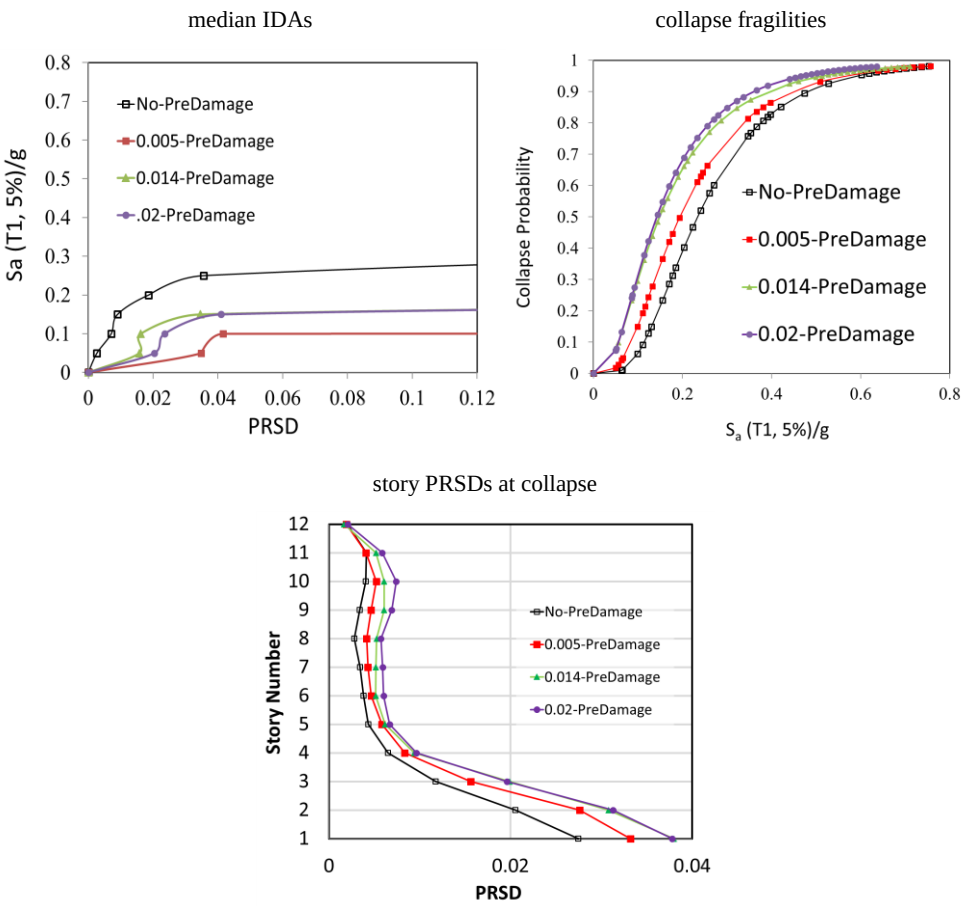

Figure 5.7: Median IDAs, fragilities, and PRSD profile at AS-induced collapse of 12-story SSMF

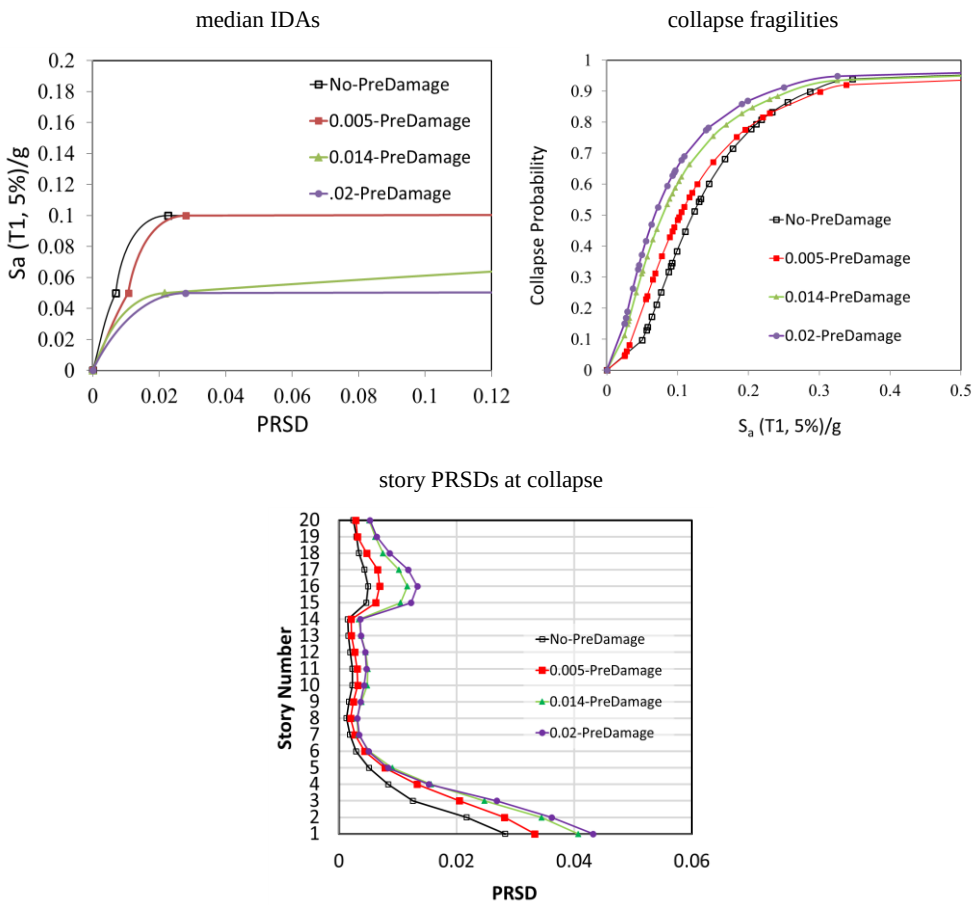

Figure 5.8: Median IDAs, fragilities, and PRSD profile at AS-induced collapse of 20-story SSMF

5.4 AMCC-PRSD correlation

As in the previous chapter, the AS median collapse capacities (AMCCs) derived from the fragility curves are compared in Figure 5.9 for the various frames and the various MS-AS scenarios. To evaluating the influence of pre-MS damaged on the observed capacities, the damaged-to-undamaged capacity ratio (DUCR) are again derived and illustrated in Figure 5.10. Considering the reduction ratios of the 4-story SSMF, a remarkable drop (around 40%) in the building's collapse capacity under AS is found when the MS damage is as low as 0.5%. Comparing this observation with the previous chapter's results provided in terms of MS' MID response, reveals the relative high effect of minor PRSD values on low-rise structures. Further increase of the MS's

PRSD does not however result in the same order of capacity reduction as in the 0.5% damage level.

For the SSMFs with higher story numbers, the mentioned abrupt drop in the collapse capacity occurs at the 1.4% PRSD level of the MS. The lowered sensitivity of these structures' collapse to MS PRSD should be attributed to their flexure-dominated behavior. According to AMCC results the structural collapse capacity may reduce significantly when the building is subjected to 1.4% pre-MS damaged level. This result confirm the study that have done by Iwata et al. (2006) that shows the PRSD should be limited to about 0.014 to satisfy a reparability. Further assessment of this issue requires the collapse mechanism of the studied SSMFs to be evaluated. This evaluation is the subject of the next chapter of this dissertation.

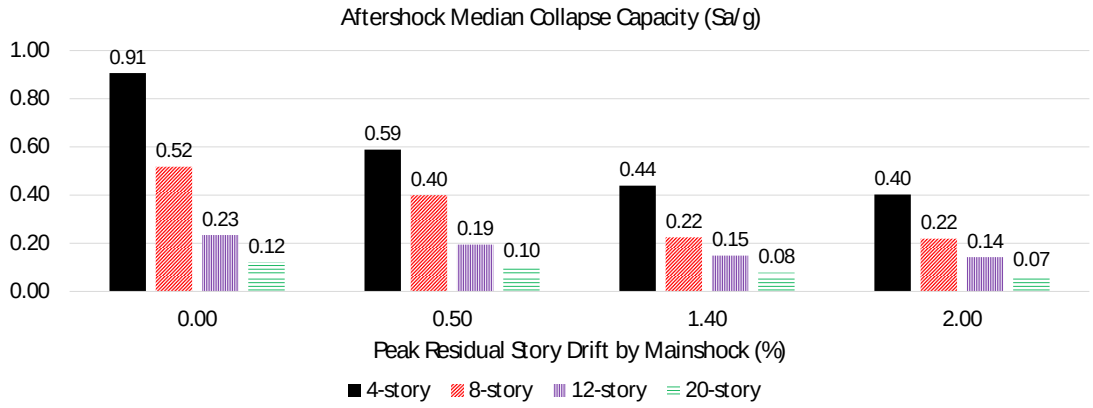

Figure 5.9: AMCC values for SSMFs with different MS damage levels

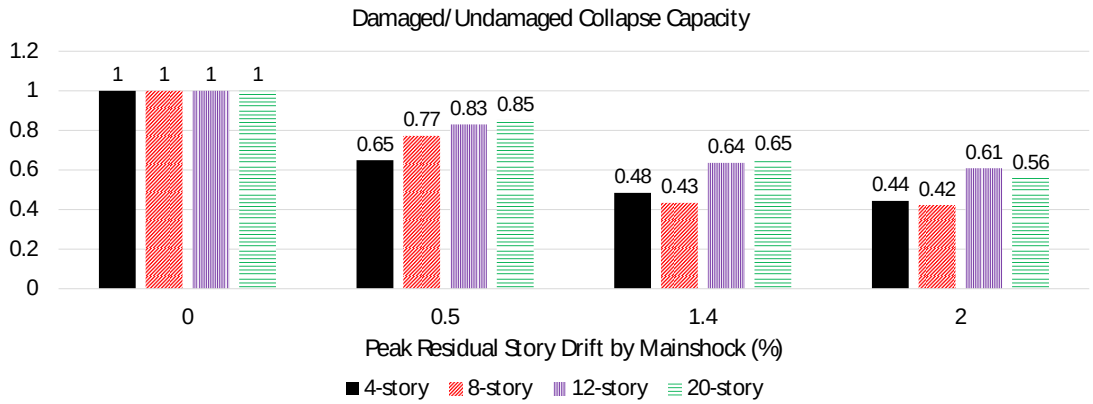

Figure 5.10: Damaged-to-undamaged AMCC values for SSMFs with different MS damage levels

To better quantify the trend governing the AMCC-PRSD relationship, a mathematical equation is used. This could be optimally achieved by deploying polynomial trendlines that are shown in Figure 5.11 and Figure 5.12. According to these plots, the trendlines related to the 4- and 8-story SSMFs show relative similarities according to which they are plotted together in Figure 5.11. The quantitative regime describing the AMCC-PRSD relationship of the 12- and 20-story SSMFs are also depicted in Figure 5.12.Recalling the polynomial trendlines derived for describing the AMCC-MID relation in Figure 4.18 and Figure 4.19 of previous chapter, it can be identified that utilization of PRSD parameter for expressing MS damage is more sensitive to changes in the height of the SSMFs. In case of the MID-expressed damage, very close predictive curves were obtained for the 4- to 12-story SSMFs. For the PRSD, however, considerable differences can be identified when the structures height change. The good accuracy provided by the AMCC-MID trendlines (denoted by their $R^2 \approx 1$ values) can also be a sign of the better predictively of this relationship compared to the AMCC-PRSD relation.

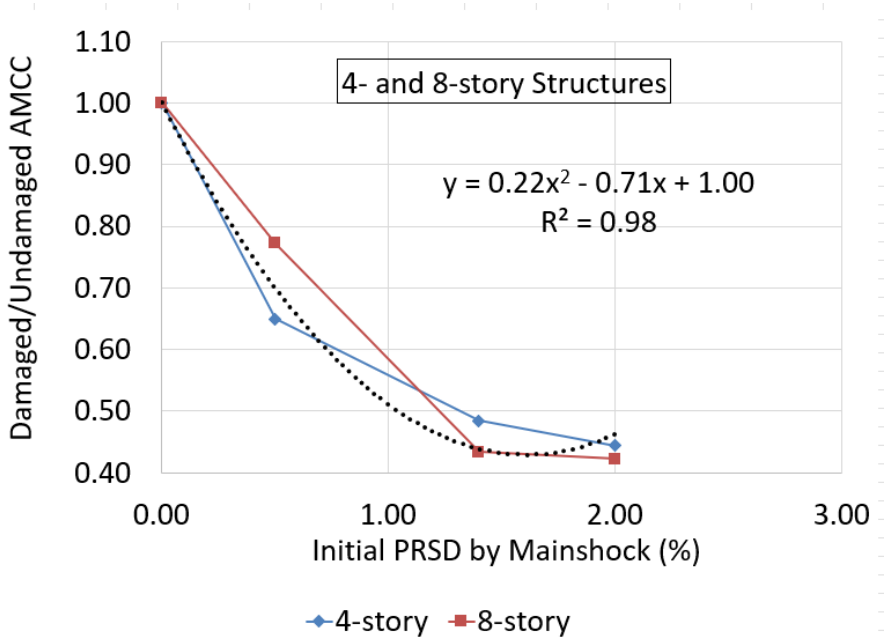

Figure 5.11: Regression equation to predict damaged-to-undamaged AMCC against the MS-induced PRSD value (4- and 8-story SSMFs)

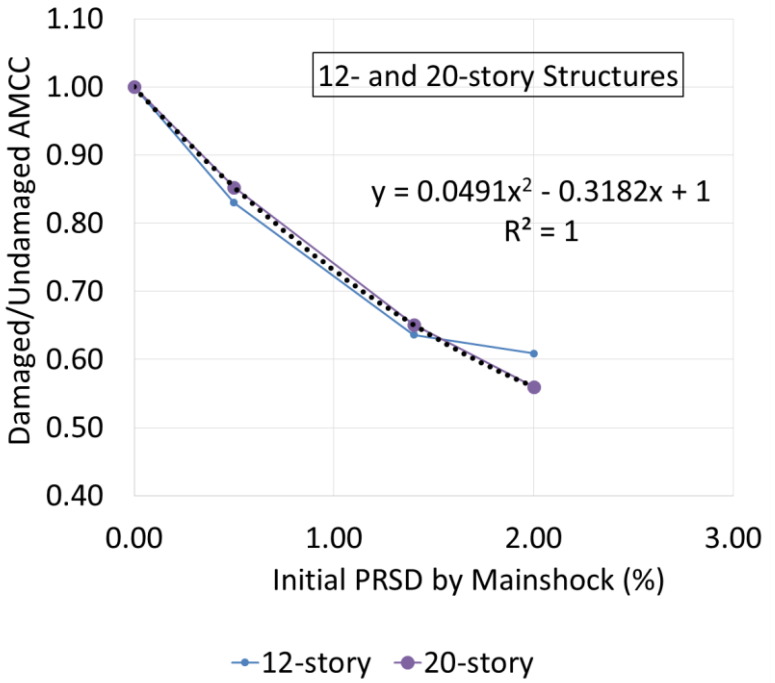

Figure 5.12: Regression equation to predict damaged-to-undamaged AMCC against the MS-induced PRSD value (12- and 20-story SSMFs)

For rapid evaluation the post-earthquake safety of SSMF buildings according to PRSD observed after the mainshock can be used of these Regression equation. DUCR would

be to associate for safety tagging. For example, we can assume that red tags (unsafe) are associated with mainshock damage that DUCR less than 0.6 , and yellow tags (restricted use) are associated with mainshock damage that DUCR less than 0.8. For example, if the PRSD observed after MS for 12-story is equal to 1%, the DUCR is equal to 0.72 by using regression equation to predict damaged-to-undamaged AMCC against the MS-induced PRSD value (Figure 5.12).This damaged structure would be associated with yellow tag (restricted use).

Chapter 6

COLLAPSE MECHANISM OF SSMFS UNDER MS-AS EXCITATIONS

As was described in the previous chapters, many aspects of the performance provided by structures under MS-AS excitations at the collapse state, can be described by considering the mechanism dominating the collapse of the structures. Thus, this chapter focuses on evaluating the mechanisms that govern collapse of the studied SSMFs under AS excitations following MS damage.

To study the mechanisms dominating collapse of the studied SSMFs, the distribution of plasticity and energy absorption contribution should be studied at various conditions. This is pursued in the following using the MDD (maximum ductility demand) and EAC (energy absorption contribution) parameters described before.

The evaluations performed in this chapter use the PRSD parameter for expressing the MS damage level. The main reason behind this selection is the measurability feature of the PRSD parameter. As denoted in the previous chapters, this feature allows AS performance predictions to be performed at the end of a MS by observing the actual residual drifts of a damaged structure.

6.1 Ductility demand distribution

The ductility demand parameter expresses the ratio of inelastic deformation imposed by an earthquake to a structural component over its yield deformation. For computing the MDD parameter, the maximum rotational deformation undergone at the two ends of various members is recorded during the AS analysis leading to collapse of the structures. This value is normalized by dividing over the yield rotation of the hinge in order to compute the MDD. For estimating the yield rotation, yielding bending moment of the member and its bending stiffness should be approximated. For estimating the yield bending moment in presence of axial loads, a zero axial force is assumed in beams while the combined gravitational axial force is employed for the columns. After computing the collapse MDD for each MS-AS record pair, the obtained values are averaged over all record pairs to see the effect of ground motion variability.

Distribution of average MDD values obtained at the collapse state of 4-story SSMF are summarized in Figure 6.1 using a contour presentation (colors reflect MDD values). For evaluating the effect of MS-AS sequences, the AS-only results (Figure 6.1a) can be best compared against the PRSD=0.02 MS-AS case (Figure 6.1b). Comparing distribution of colors across the two contours, relatively similar MDD distributions are identified for the two cases at the collapse state. According to Figure 6.2, Figure 6.3 and Figure 6.4 contours, similar observations can also be made for the 8-, 12- and 20-story structures regarding the AS-only and the PRSD=0.02 MS-AS results. To address these changes more accurately, representative story values are regarded in Figure 6.5 for all structures and MS-AS scenarios.

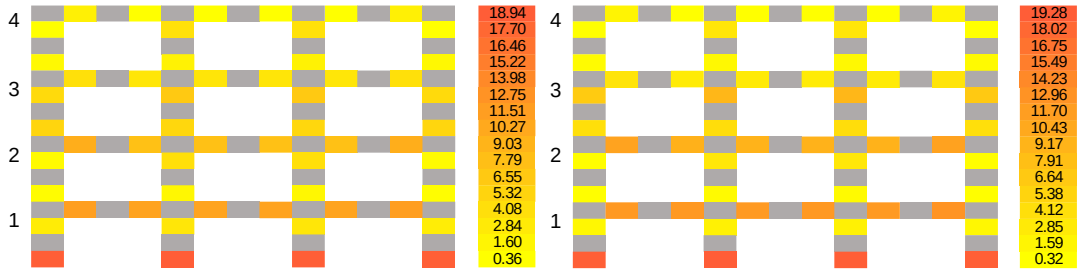

a) b)

Figure 6.1: Maximum ductility demand for AS and AS preceded by MSs scaled to specific PRSD levels at collapse state (a) AS-only and (b) AS preceded by MS with PRSD=0.02 (4-story SSMF)

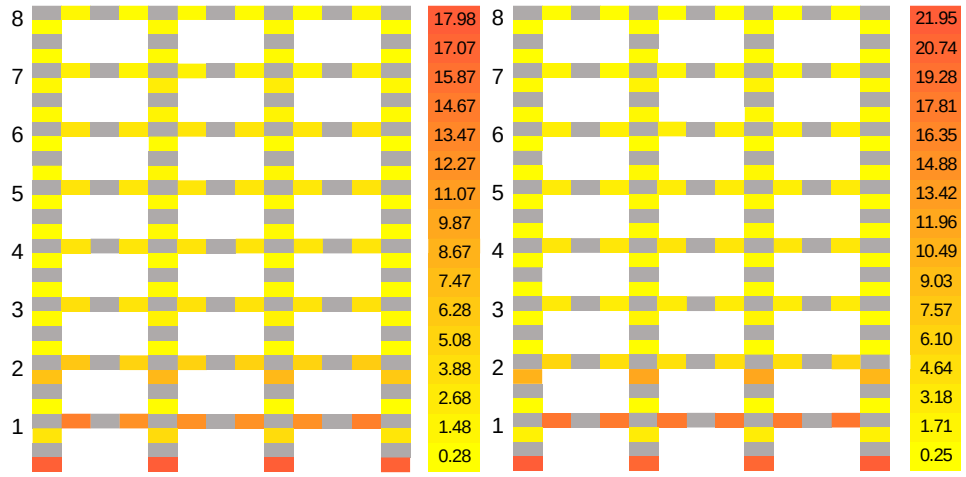

a) b)

Figure 6.2: Maximum ductility demand for AS and AS preceded by MSs scaled to specific PRSD levels at collapse state (a) AS-only and (b) AS preceded by MS with PRSD=0.02 (8-story SSMF)

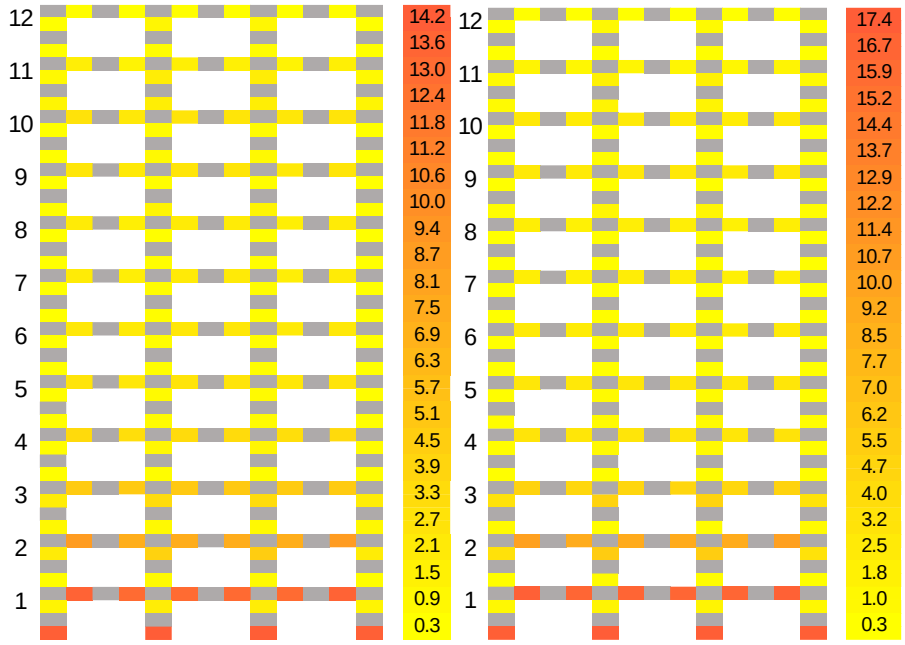

Figure 6.3: Maximum ductility demand for AS and AS preceded by MSs scaled to specific PRSD levels at collapse state (a) AS-only and (b) AS preceded by MS with PRSD=0.02 (12-story SSMF)

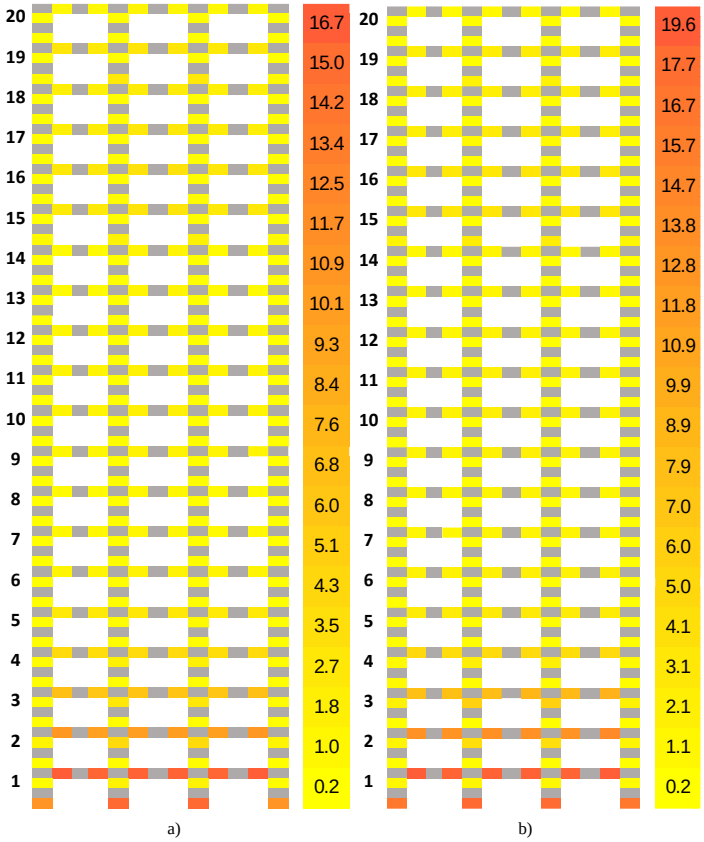

Figure 6.4: Maximum ductility demand for AS and AS preceded by MSs scaled to specific PRSD levels at collapse state (a) AS-only and (b) AS preceded by MS with PRSD=0.02 (20-story SSMF)

Figure 6.5 provides more clear views of changes in the maximum MDDs of beams and columns located in various stories. The effect of the MS damage levels not shown in previous Figures can be seen in these Figures as well. According to these graphs, altering MS damage level has led to minimal changes in the patterns governing MDD distribution along the heights of the structures. Still, there are minor changes in MDDs due to change in the MS damage level which are differently pronounced in various stories.

For the 4-story structure, intensifying MS damage is almost ineffective until the damage corresponding to the PRSD = 0.014 is reached. Any further increment in MS damage is also shown to be ineffective and the damage level corresponding to PRSD=0.014 forms the threshold damage limit. A change in PRSD from 0.005 to 0.014 has led to around 12% increase in the beam MDDs undergone in the two first stories while almost equal MDDs are experienced at the topper stories. Regarding the column MDDs, this change has led to MDD increment in the third story while the MDDs of other stories have remained unchanged.

The observations made regarding the 8-story SSMF unveil nearly the same trends except that the columns' MDDs are also increased in the lower two stories and the upper stories have undergone no changes due to increase in the MS damage. These observations are also repeated for the two taller 12- and 20-story SSMFs. For all cases, where an MDD increment is observed in the stories its value is limited to a maximum of about 12%.

According to the MDD results, the mechanism that dominates the collapse of the structures is not much affected by the preliminary damage by the MS. However, when

this mechanism feels some effect, these effects lead to an increase in the deformation of the lower 25% of the structures' height. Further interpretation about this complex variation can be best done using the EAC results presented in the following.

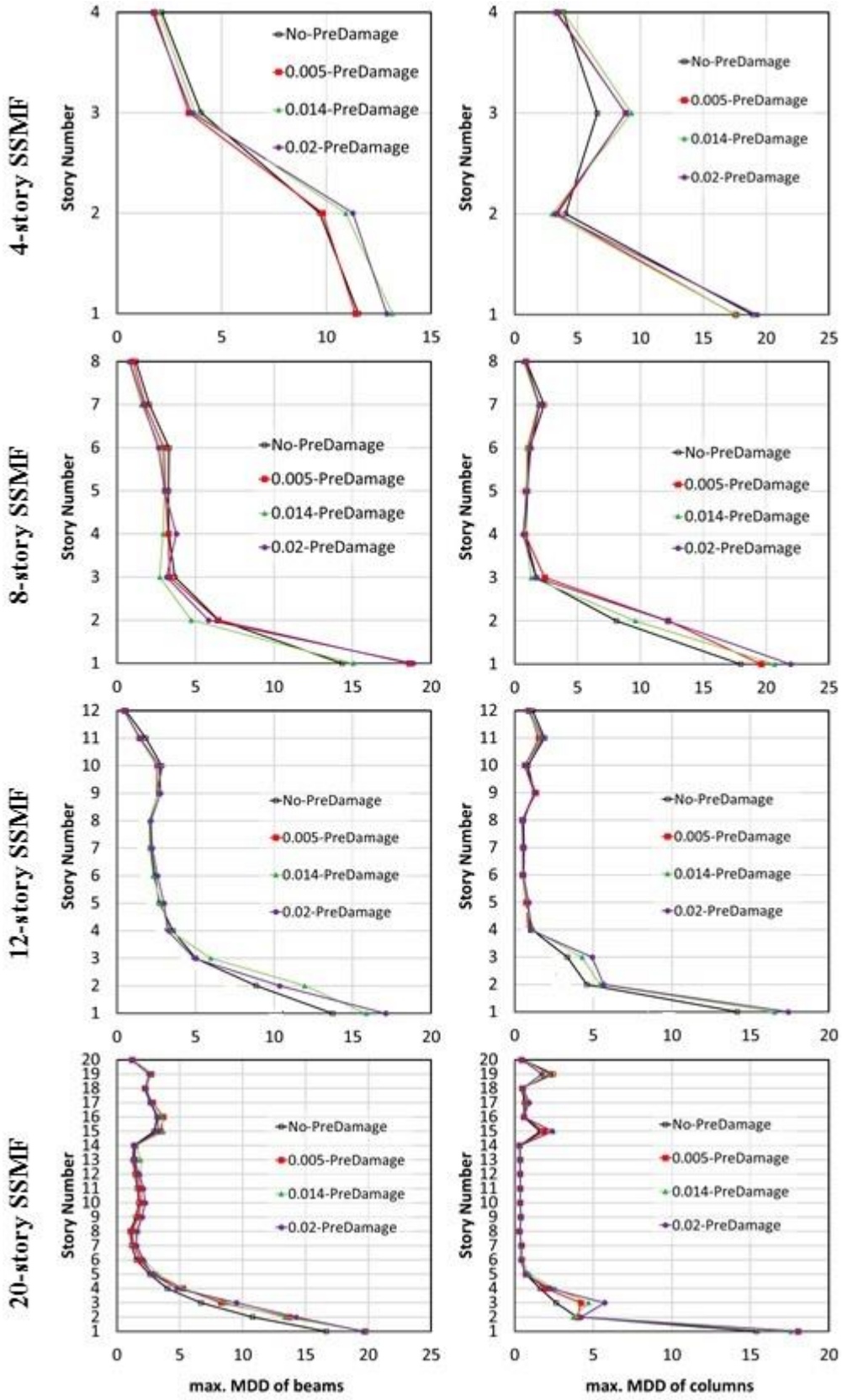

Figure 6.5: Profile of beams and columns MDDs obtained at the collapse state of SSMFs under different MS damage levels

6.2 Energy absorption contribution

As described in chapter 2 the hysteretic energy absorbed by various members is computed and divided over the total dissipated energy to compute the EAC parameter for each member during an analysis. For multi-shock analyses, the absorbed energy is computed for the total analysis time including both MS and AS excitations. The average of all records, computed at their collapse states, are finally considered for evaluating the effect of MS damage on the collapse mechanism of the studied structures. The EAC contours are presented in Figure 6.6 to Figure 6.9 for SSMFs with 4 to 20 stories. The first observation made regarding these results is the much higher sensitivity of the EAC values to the imposed MS damage. This is in spite of the MDD parameter which showed minimal sensitivity to the changes in the MS damage level. According to this observation, it can be concluded that the EAC parameter provides a more suitable metric for studying the collapse mechanism of SSMFs.

According to the complexity of the trends shown by the contour results, the EAC results are further interpreted by considering sum of story values and the changes occurring along the height of the structures.

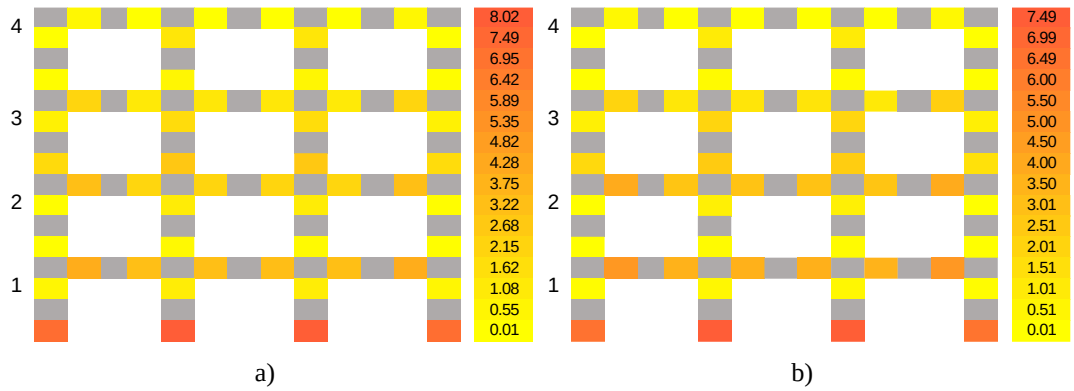

a) b)

Figure 6.6: Energy absorption distribution for AS and AS preceded by MSs scaled to specific PRSD levels at collapse state (values in %) (a) AS-only and (b) AS preceded by MS with PRSD=0.02 (4-story SSMF)

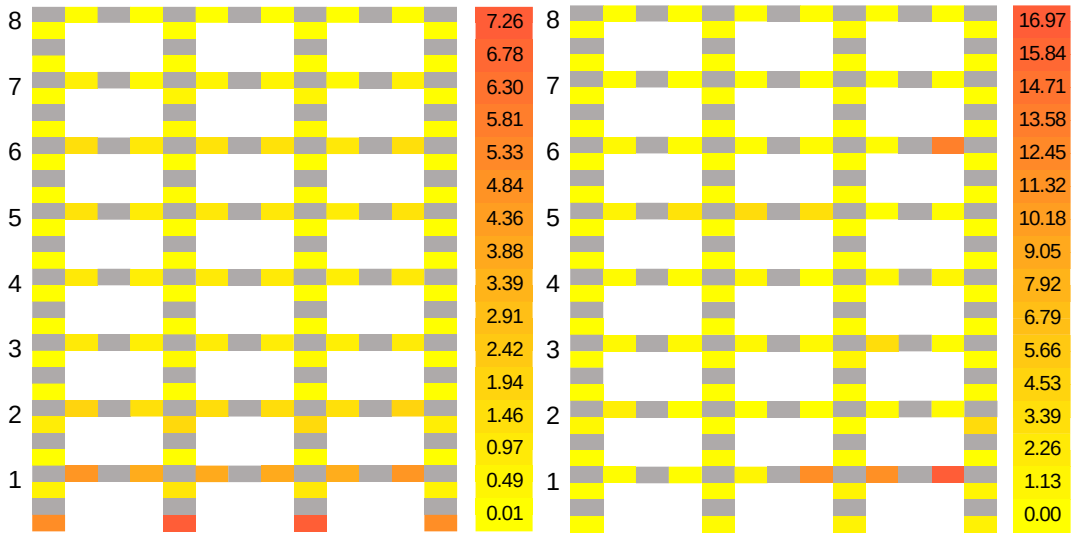

a) b)

Figure 6.7: Energy absorption distribution for AS and AS preceded by MSs scaled to specific PRSD levels at collapse state (values in %) (a) AS-only and (b) AS preceded by MS with PRSD=0.02 (8-story SSMF)

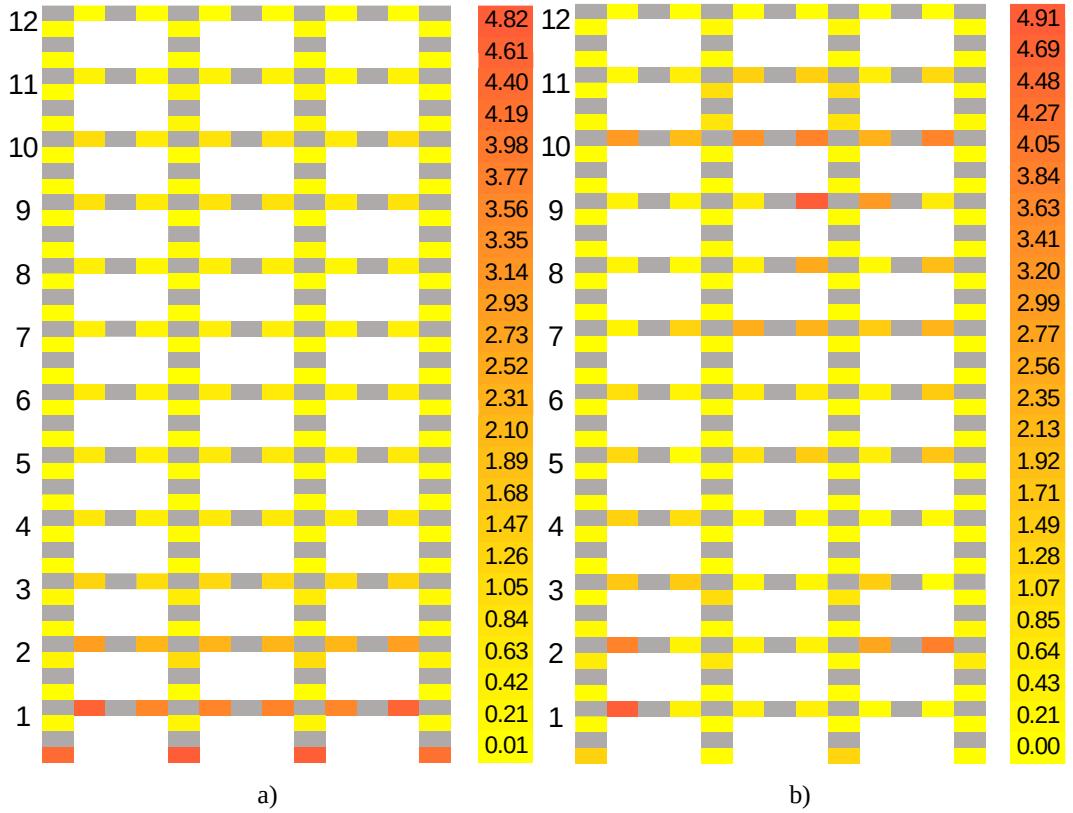

a) b)

Figure 6.8: Energy absorption distribution for AS and AS preceded by MSs scaled to specific PRSD levels at collapse state (values in %) (a) AS-only and (b) AS preceded by MS with PRSD=0.02 (12-story SSMF)

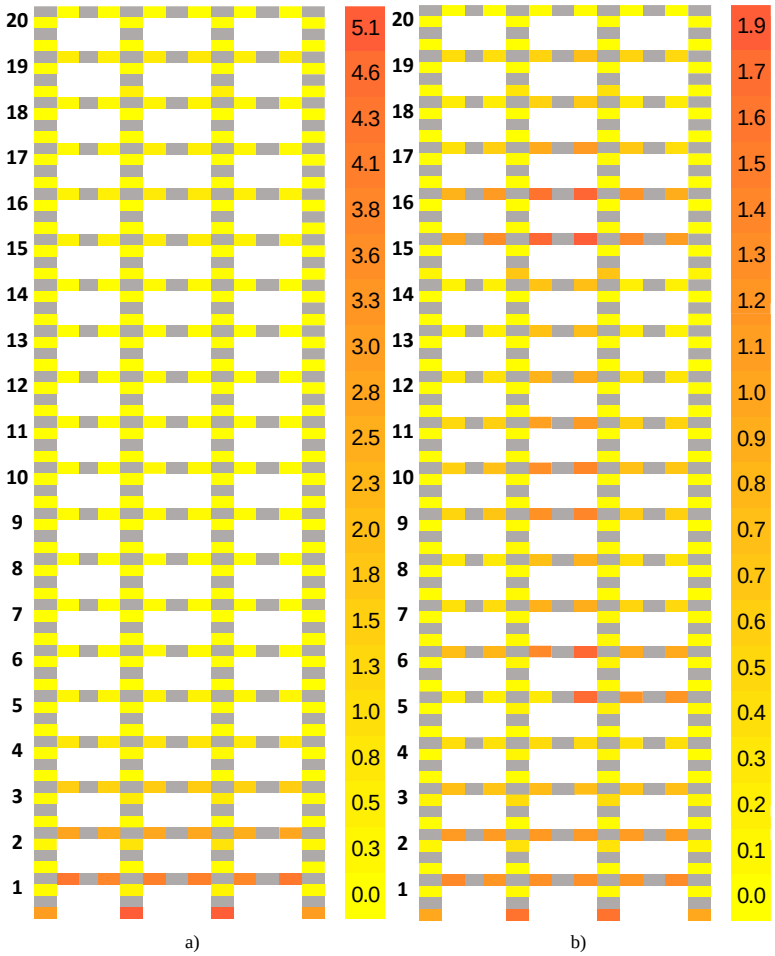

Figure 6.9: Energy absorption distribution for AS and AS preceded by MSs scaled to specific PRSD levels at collapse state (values in %) (a) AS-only and (b) AS preceded by MS with PRSD=0.02 (20-story SSMF)

According to the total story EACs shown in Figure 6.10 to Figure 6.13 for various SSMFs, distribution of EACs between stories follows patterns that depend on the MS damage level. To describe the reason for these changes, it should be noted that the energy absorbed by a member is the area under the force-deformation hysteresis. Thus, three factors can be named that govern the amount of energy absorbed by a member during an excitation.

I) The MS-induced damage undergone by a member and the resulting strength deterioration reduces its energy absorption capacity under the AS.

II) The balance between the input seismic energy and the internal energy absorbed by the members leads to EAC elevation in some members in order to compensate for the EAC decrease in other members; the energy absorption reduction mentioned in (I) is thus accompanied by EAC increments in some other members.

III) According to the series systems rules, the overall distribution of flexibility throughout the structure affects the distribution of deformation demands. That is, among various candidate members, EAC compensation mentioned in (II) occurs in members with larger flexibilities.

The role of MS excitation in posing damage to the members and thereby affecting the energy absorbed by them during an AS is reflected by (I). Important instances of this observation can be named that include reduction in the first story EACs due to increase in the MS damage level. In other words, in the first story of all structures, increase of MS damage has led to a decrease in contribution of story in absorbing total input energy. Regarding (I), this reduction is attributed to the large damage posed to the first story members under MSs.

To accommodate to the above EAC changes caused by MS damage, EAC should elevate in undamaged stories, with reference to (II). That is, other stories should provide larger contributions in absorbing the input energy to compensate for the reduction caused in the stories damaged by the MS. However, different stories do not contribute equally in this elevation and the EAC increase is a function of the flexibility possessed by various stories. Considering total story EAC results provided for the 4-story frame (Figure 6.10), the decrease in the first story is mainly compensated in the second story and the upper stories contribution is almost zero. According to (III), larger

contribution of the second story is a result of its larger flexibility and the tendency of the deformations to concentrate in it. This can be confirmed by MDD results provided in Figure 6.5 for this structure. By considering total columns EAC and total beams EAC in Figure 6.10, the beams are seen to have effectively contributed to the compensation provided by this story. Recalling (III), the low flexibility of columns has prevented them from undergoing large-enough deformation demands and providing further contribution to the story's EAC. We should also bear in mind that the flexibility of the members is a function of their geometry itself being affected by the residual deformations caused by the MS. The above three principles can also be used to describe other examples of trends found in the EAC data.

While the above principles can be clearly used in some cases for description of the observed results, there are still complexities that call for further considerations in order to be described.

Considering the 8-story results reveals one of these complex situations in which the effect of increased MS damage on EAC distribution is not clear. As in Figure 6.11, an increase in the MS damage from "no-damage" to "PRSD=0.014" is accompanied with a mentioned decrease in the first story EAC. As expected, this decrease is compensated by an increase in higher stories EACs including story 6. However, further increase in PRSD from 0.014 to 0.02 leads to a surprising increase of EAC in the first story and the corresponding decrease in story 6.

To describe this observation, we should account for the changes in the energy imposed by the AS excitation. Thus, increasing PRSD from 0.014 to 0.02 leads to an increase to the MS energy while the AS energy reduces. The EAC values, on the other hand,

are computed by considering the total energy absorbed under both MS and AS. Accordingly, damaged members located in the first story absorb large energies under MS and negligible values under AS. For upper stories' members, on contrary, energy absorption only occurs under AS since inelastic response is not stimulated in them by MS. This is while the AS energy is of a much lower order compared to MS and thus the EAC of the upper stories is not of a great magnitude.

As is seen, the increase in the MS intensity has increased the portion of energy dissipated at the lower stories while it has decreased the share of the upper stories. To reflect this observation, we introduce the (IV) principle as:

IV) The contribution of members in absorbing total (MS and AS) energy depends on the portion of energy induced by each excitation and the absorption provided by a member under each excitation.

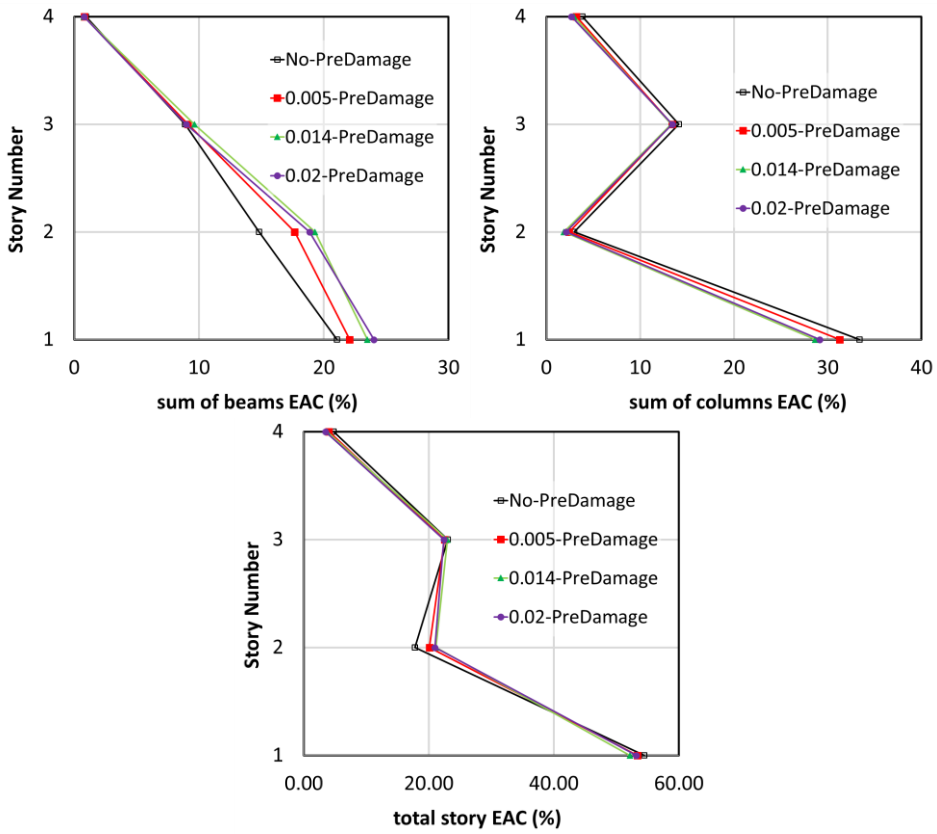

Figure 6.10: Profile of beams, columns and story energy absorption distribution under different pre-MS damaged at the collapse state (4-story SSMF)

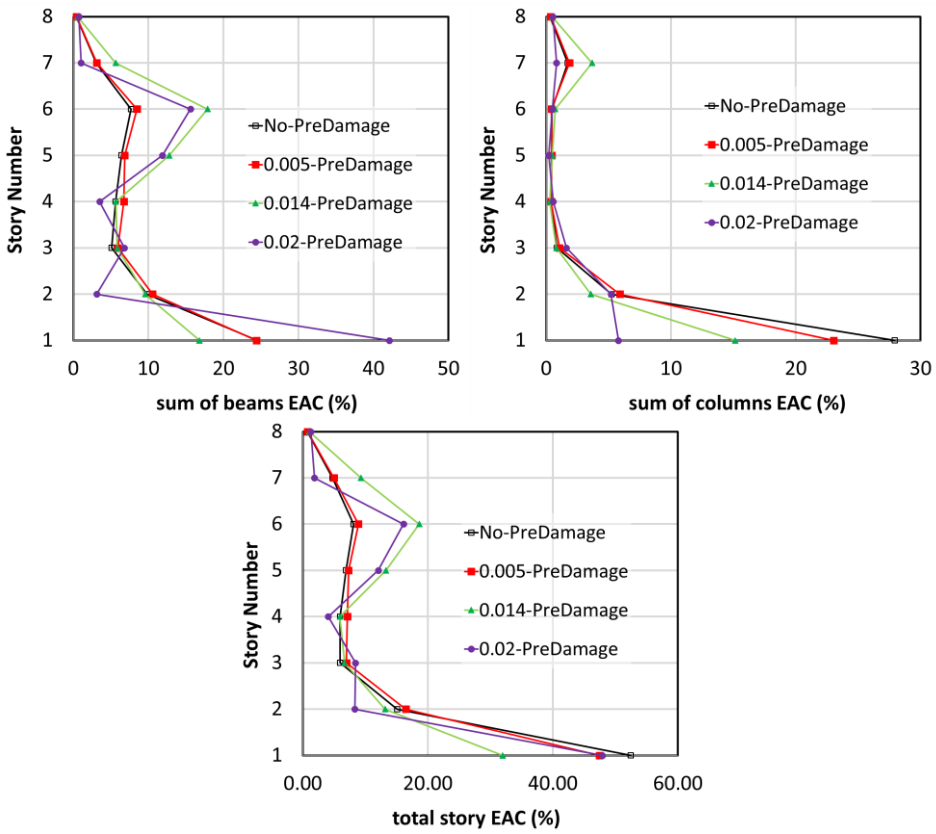

Figure 6.11: Profile of beams, columns and story energy absorption distribution under different pre-MS damaged at the collapse state (8-story SSMF)

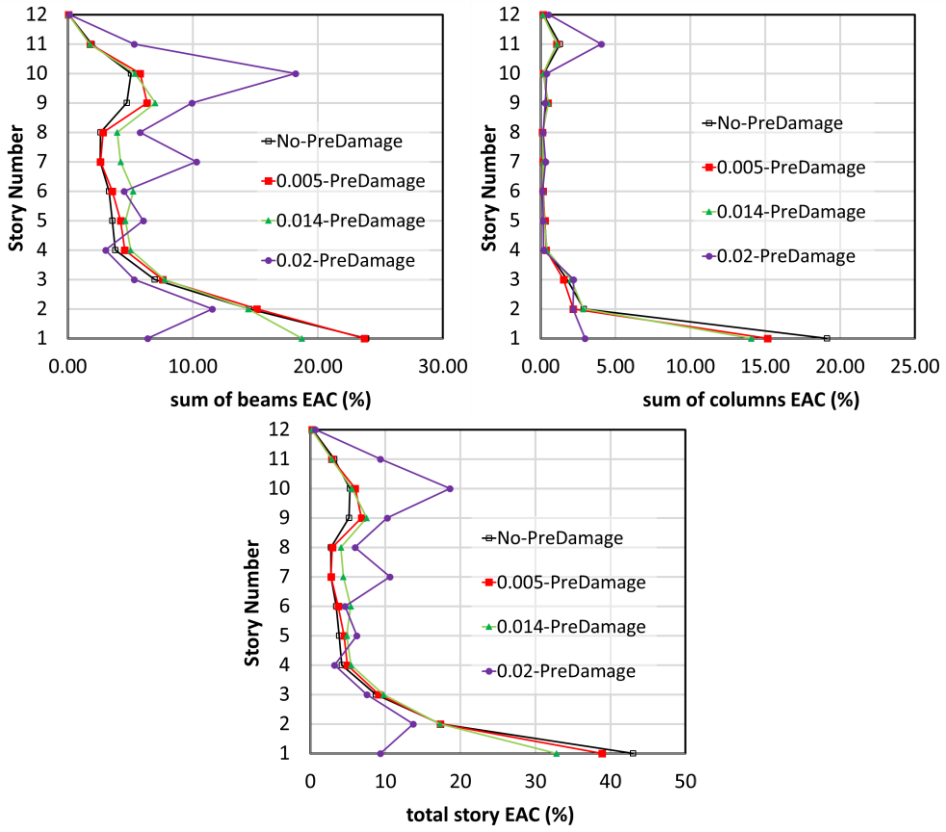

Figure 6-12 Profile of beams, columns and story energy absorption distribution under different pre-MS damaged at the collapse state (12-story SSMF)

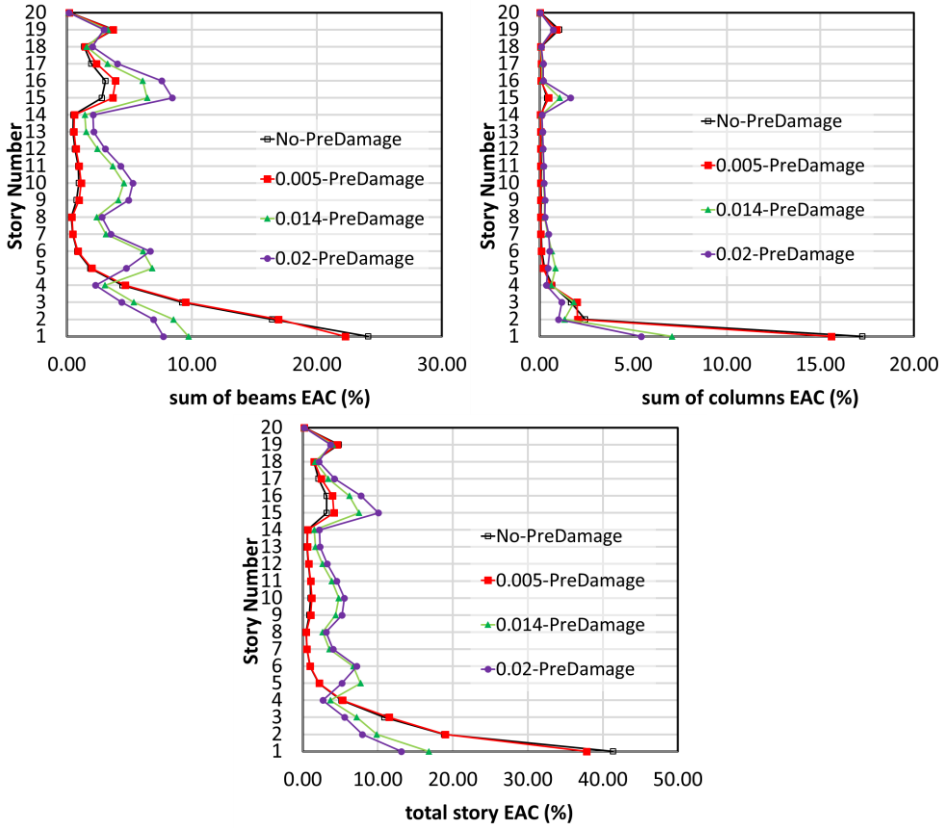

Figure 6.13: Profile of beams, columns and story energy absorption distribution under different pre-MS damaged at the collapse state (20-story SSMF)

To achieve an overall comparison between the total EACs provided by the beams and columns, Figure 6.14 is depicted. According to this Figure and by comparing the circle charts related to the different SSMFs, the EAC provided by the beams increases from 46% in the 4-story SSMF to 75% in the 20-story, reflecting a 63% elevation. This indicates that for taller building the beams dissipating hysteric energy is more pronounced.

This observation is attributed to the fact that the shear mechanism dominating the lateral behavior of low-rise moment frames is substituted by a flexural behavior mode in the taller ones. In a shear mode, the beams only behave as collector elements that transfer horizontal loads via their axial action. In a flexural mode, on the other hand,

the beams play a coupling role as well, and undergo flexural demands that increase as the columns' bending moments grow.

The mentioned 60% difference between the beams and columns does not change with increase of MS damage to the maximum considered level of PRSD=0.02. However, despite the AS-only case, in the PRSD=0.02 MS damage level, very minor differences are observed between the total beam EACs related to SSMFs with 8 stories and more.

By comparing the charts related to the different MS damage levels, the role of the beams in providing energy absorption increases again by enlarging the MS damage. This increase is about 15%, irrespective of the buildings height, when the no MS damage is compared with the PRSD=0.02 level. As described earlier, this should be attributed to the reduction of columns' energy dissipation capacity due to the MS damage. Neglecting the changes in the energy input by various MS-AS scenarios, the aforementioned increase in the beams' EAC should be accompanied by a reduction in the columns' values to keep the total dissipated energy constant. The circle charts provided in Figure 6.14 approve this assumption.

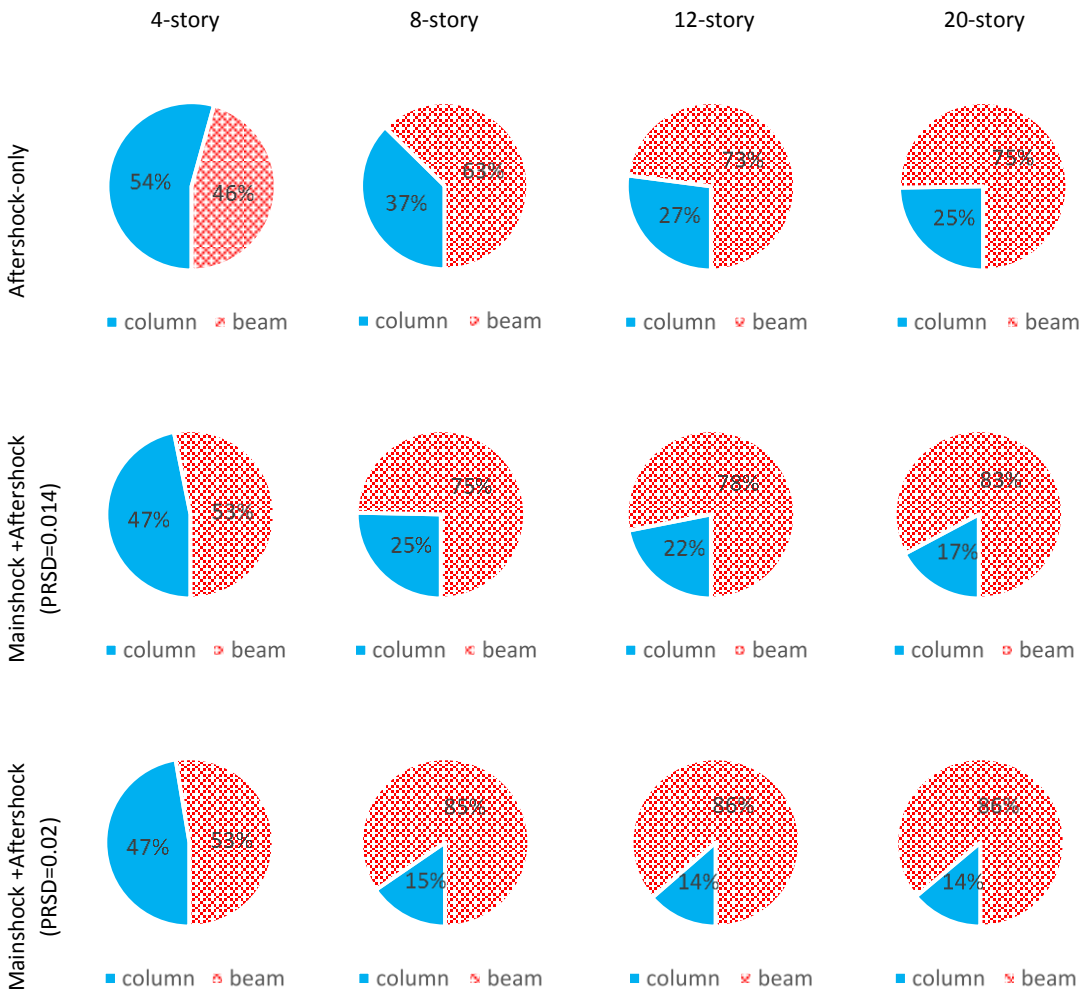

Figure 6.14: Total EAC provided by the beams and columns under various MS-AS scenarios and in the different SSMFs

Chapter 7

CONCLUSIONS AND FUTURE DIRECTIONS

In this study, the effect of MS damage on seismic collapse of special steel moment frames (SSMFs) was evaluated by using a set of 32 real MS-AS records. The AS collapse capacity of the structures was obtained using IDA method for a set of 4-,8-,12- and 20- story SSMFs. A summary of the study method and the obtained results are presented at this chapter. In the last section of this chapter, some suggestions are also provided for future investigations on the effect of MS-AS excitations.

7.1 Summary and conclusions

The AS median collapse capacities (AMCCs) were obtained by applying AS records after different levels of damage were induced by the MS. To evaluate the appropriateness of various parameters for expressing the MS damage level, two response parameters were regarded for scaling the MS record. These were the maximum interstory drift (MID) and the peak residual story drift (PRSD) parameters. For the MID parameter, the damage levels corresponding to the 0.7%, 2.5% and 5% values were selected. The PRSD values corresponding to the same damage levels were taken as 0.5%, 1.4% and 2%.

The obtained AMCC results identified two various regimes for the effects of MS damage on the AS collapse capacities. The first regime dominated low- to mid-rise structures and showed that the MS damage became significant when MIDs as low as 2.5% were applied. The second regime governing the high-rise structure, however,

started when MS MID surpassed a value as large as 5%. To aid in quantifying the MS damage effects, two predictive regression equations were also derived that provided the ratio of damaged-to-undamaged AMCCs for various MID and PRSD values.

According to AMCC results the structural collapse capacity may reduce significantly when the building is subjected to a high intensity MS.

A comparison between the trendlines presented by the regression equations developed in terms of the MID and PRSD variables was used for evaluating the appropriateness of these parameters. Accordingly, the MID parameter showed more predictable trend when the effect on the AMCC was observed. The PRSD parameter was, however, said to be useful in the sense that its value could be measured just after an MS excitation and could thus aid in decision making about an immediate retrofit action.

Evaluating the influence of pre-MS damaged in the collapse state on distribution of story drifts, the story at which plasticity concentrated was shown to remain unchanged after a MS damage was induced.

The damaged vibration period of the structures hit by the MS were also calculated and used in line with the other observations. This parameter was found helpful in identifying the extent of stiffness deterioration caused by the MS. A reduced stiffness was discussed to increase the part of MID response that could be recovered after removing the seismic loads. Thus, for a constant MID response, a lower PRSD value occurred when a significant period elongation was seen.

The last part of the study was devoted to investigating the MS effect on the mechanism through with the AS caused structural collapse. For this purpose, distribution of two inelastic response measures was studied throughout the height and in various members of the studied SSMFs. These parameters included maximum ductility demand (MDD) and energy absorption contribution (EAC). These response measures were computed for each member at the AS-induced collapse state by averaging the results of the various AS records. The results of this assessment can be summarized as below:

I) The MDD parameter reflecting the extent of plasticity undergone by various members within different stories showed minimal sensitivity to the changes in the MS damage level. Since this sensitivity was highly pronounced in terms of the EAC, this parameter was concluded to provide a better metric for studying the collapse mechanism.

Study of the mechanisms dominating the collapse of SSMFs under various MS damage levels unveils that EAC values are not affected by a single and simple trend. While this precludes providing quantitative summaries regarding the effect of MS, studying the prominent trends results in the following remarks:

II) The damage imposed by the MS on a member and the resulting behavior degradation reduce its energy absorption capacity at the collapse stage caused by the AS. Thus, comparing the EAC distribution of AS-only collapse stage with the MS-preceded collapse, shows EAC reduction in the members undergoing large MDDs under the MS. This EAC reduction is compensated by EAC increase in some other members so that the energy imposed by the MS-AS sequence can be dissipated. The compensating members are those with

unremarkable contribution in absorbing the MS energy and thus with small MDD values under it.

III) Among different candidate members, the energy absorption compensation, described in (II), is provided by the stories and members with the highest potential for receiving additional deformations. Since the lateral strengths provided by the various stories form a series system of resisting elements, the rule managing series systems should be regarded for selecting the candidate story for compensating the unbalanced input energy. Amid the various elements resisting within a story, however, a parallel relation exists in which larger forces are transferred to elements with higher rigidities. In such circumstances, energy compensation is provided by members with larger rigidities.

IV) According to (II), elements cannot provide equal energy dissipations under the MS and AS excitations. Thus, two regimes are identified for dissipating the seismic input energy by the elements and stories. In regime i, members absorb large energies under the MS and stay in rest under the AS while regime ii is vice versa and a large energy absorption is provided under the AS after a period of low energy absorption under the MS. When comparing the energy absorptions provided by the members obeying either of these regimes, the percentage of the total seismic energy imposed by each of the excitations in a MS-AS sequence has a determining effect. When AS poses the larger portion of the energy, the members forming the regime ii show the larger EACs and vice versa. This consideration should be taken alongside the previously mentioned facts for describing the collapse mechanism with respect to the energy absorption contributions.

A study on the total EACs provided by the beams and columns of different SSMFs shows that the beams EAC increase by about 60% in absence of the MS damage when the short 4-story SSMF is compared with taller 12- and 20-story structures. This observation is attributed to the flexural load bearing mechanism becoming more dominant in taller structures in comparison with the shear mechanism that dominates short structures. An increase in the MS damage is also seen to lead to an elevation in the beams EACs undergone by a certain structure. This elevation reaches an amount of 15% irrespective of the structure height.

Regarding the significance of the energy dissipation mechanisms in identifying the collapse of SSMFs, this study can be further extended by account of the energy absorption provided by inherent viscous damping. Subtraction of these dissipated energies from the input seismic energy to compute the kinetic energy of the structures at various stages can also shed light on the collapse mechanism of SSMFs especially when MS-AS effects are considered.

7.2 Future directions

The study presented in this dissertation can be further extended and completed by performing the following evaluations:

- Evaluation of the seismic losses caused by MS-AS sequences; the repair costs, casualties and downtimes are surely affected when more than one excitation hits a structure. Quantifying these loss measures when various MS-AS scenarios are considered can be useful for an accurate prediction of earthquake consequences.
- More complete evaluation of the energy absorption mechanisms in SSMF structures hit by MS-AS sequences. The only energy parameter considered at

this study was the hysteretic energy dissipation. However, evaluating the energy flow in the structures at the collapse state requires simultaneous consideration of other energy values that reciprocally affect the hysteretic energy. These additional energy terms include the viscous energy dissipated due to inherent damping of the structure, the input motion energy applied to various parts of the structure, and the kinetic energy appearing as the part of input energy not dissipated by the absorbing mechanisms.

REFERENCES

Abdollahzadeh, G., Mohammadgholipour, A., & Omranian, E. (2017). Seismic evaluation of steel moment frames under mainshock–aftershock sequence designed by elastic design and PBPD methods. *Journal of Earthquake Engineering*, 1-24.

Amadio, C., Fragiacomo, M., & Rajgelj, S. (2003). The effects of repeated earthquake ground motions on the non-linear response of SDOF systems. *Earthquake Engineering & Structural Dynamics, 32*(2), 291-308.

An, X., Shawky, A. A., & Maekawa, K. (1997). The collapse mechanism of a subway station during the Great Hanshin earthquake. *Cement and concrete composites, 19*(3), 241-257.

ASCE. (2005). Minimum design loads for buildings and other structures.

ASCE. (2006). ASC3 41: Seismic rehabilitation of existing buildings: American Society of Civil Engineers.

Aschheim, M., & Black, E. (1999). Effects of prior earthquake damage on response of simple stiffness-degrading structures. *Earthquake Spectra, 15*(1), 1-24.

Banazadeh, M., Jalali, S., & Abolmaali, A. (2010). *Seismic performance of reduced beam section moment frames considering record-to-record uncertainties.* Paper

presented at the 9th US national and 10th Canadian conference on earthquake engineering.

D'Ayala, D., & Speranza, E. (2003). Definition of collapse mechanisms and seismic vulnerability of historic masonry buildings. *Earthquake Spectra, 19*(3), 479-509.

Del Prete, M., Guadagno, F., & Scarascia-Mugnozza, G. (1998). Earthquake induced damage in an historic area: the September–October 1997 seismic sequence which affected Assisi, central Italy. *Bulletin of Engineering Geology and the Environment, 57*(1), 101-109.

Elkady, A., & Lignos, D. G. (2015). Effect of gravity framing on the overstrength and collapse capacity of steel frame buildings with perimeter special moment frames. *Earthquake Engineering & Structural Dynamics, 44*(8), 1289-1307.

FEMA-P58. (2012). *Seismic Performance Assessment of Buildings. FEMA p58*.

FEMA 350: Recommended seismic design criteria for new steel moment frame buildings. (2000). FEMA-350, SAC Joint Venture Washington, DC.

Gross, J. L., & Phan, L. T. (2000). *Implications for earthquake risk reduction in the United States From the Kocaeli, Turkey, Earthquake of August 17, 1999*.

Han, R., Li, Y., & van de Lindt, J. (2014). Assessment of seismic performance of buildings with incorporation of aftershocks. *Journal of Performance of Constructed Facilities*, *29*(3), 04014088.

Hatzigeorgiou, G. D., & Liolios, A. A. (2010). Nonlinear behaviour of RC frames under repeated strong ground motions. *Soil Dynamics and Earthquake Engineering*, *30*(10), 1010-1025.

Hosseinpour, F., & Abdelnaby, A. (2017). Effect of different aspects of multiple earthquakes on the nonlinear behavior of RC structures. *Soil Dynamics and Earthquake Engineering*, *92*, 706-725.

Ibarra, L. F., Medina, R. A., & Krawinkler, H. (2005). Hysteretic models that incorporate strength and stiffness deterioration. *Earthquake Engineering & Structural Dynamics*, *34*(12), 1489-1511.

Iwata, Y., Sugimoto, H., & Kuguamura, H. (2006). Reparability limit of steel structural buildings based on the actual data of the Hyogoken-Nanbu earthquake. *Proceedings of the 38th Joint Panel. Wind and Seismic effects. NIST Special Publication*, *1057*, 23-32.

Jalali, S. A. (2018). Commits to OpenSees in github repository.

Jalali, S. A., Amini, A., Mansouri, I., & Hu, J. W. (2020). Seismic Collapse Assessment of Steel Plate Shear Walls Considering the Mainshock–Aftershock Effects. *Thin-Walled Structures*.

Jalali, S. A., & Banazadeh, M. (2016). Computer-based evaluation of design methods used for a steel plate shear wall system. *The Structural Design of Tall and Special Buildings, 25*(17), 904-925.

Jalali, S. A., Banazadeh, M., Abolmaali, A., & Tafakori, E. (2012). Probabilistic seismic demand assessment of steel moment frames with side-plate connections. *Scientia Iranica, 19*(1), 27-40.

Jalali, S. A., Banazadeh, M., Tafakori, E., & Abolmaali, A. (2011). Seismic performance assessment of steel moment frames with generic Locally Reinforced connections. *Journal of Constructional Steel Research, 67*(8), 1261-1271.

Jalali, S. A., & Darvishan, E. (2019). Seismic demand assessment of self-centering steel plate shear walls *Journal of Constructional Steel Research, 162*. doi:10.1016/j.jcsr.2019.105738

Jeon, J., DesRoches, R., Brilakis, I., & Lowes, L. (2012). *Aftershock fragility curves for damaged non-ductile reinforced concrete buildings.* Paper presented at the 15th World Conference on Earthquake Engineering.

Kiyono, J., & Kalantari, A. (2004). Collapse mechanism of adobe and masonry structures during the 2003 Iran Bam earthquake. *Bull. Earthq. Res. Inst. Univ. Tokyo, 79*(157), 161.

Lee, K., & Foutch, D. A. (2004). Performance evaluation of damaged steel frame buildings subjected to seismic loads. *Journal of Structural Engineering, 130*(4), 588-599.

Li, Q., & Ellingwood, B. R. (2007). Performance evaluation and damage assessment of steel frame buildings under main shock–aftershock earthquake sequences. *Earthquake Engineering & Structural Dynamics, 36*(3), 405-427.

Li, Y., Song, R., & Van De Lindt, J. W. (2014). Collapse fragility of steel structures subjected to earthquake mainshock-aftershock sequences. *Journal of Structural Engineering, 140*(12), 04014095.

Lignos, D. G., & Krawinkler, H. (2010). Deterioration modeling of steel components in support of collapse prediction of steel moment frames under earthquake loading. *Journal of Structural Engineering, 137*(11), 1291-1302.

Luco, N., Bazzurro, P., & Cornell, C. A. (2004). *Dynamic versus static computation of the residual capacity of a mainshock-damaged building to withstand an aftershock.* Paper presented at the 13th World conference on earthquake engineering.

Mahin, S. A. (1980). *Effects of duration and aftershocks on inelastic design earthquakes.* Paper presented at the Proceedings of the 7th world conference on earthquake engineering.

Mazzoni, S., McKenna, F., Scott, M. H., & Fenves, G. L. (2004). *OpenSees users manual*: PEER Center, University of California, Berkeley.

McCormick, J., Aburano, H., Ikenaga, M., & Nakashima, M. (2008). *Permissible residual deformation levels for building structures considering both safety and human elements.* Paper presented at the Proceedings of the 14th world conference on earthquake engineering.

Nazari, N., Van De Lindt, J., & Li, Y. (2013). Effect of mainshock-aftershock sequences on woodframe building damage fragilities. *Journal of Performance of Constructed Facilities, 29*(1), 04014036.

Nickitopoulou, A., Protopsalti, K., & Stiros, S. (2006). Monitoring dynamic and quasi-static deformations of large flexible engineering structures with GPS: Accuracy, limitations and promises. *Engineering Structures, 28*(10), 1471-1482.

Nishiyama, I. (2011). *Building damage by the 2011 off the Pacific coast of Tohoku earthquake and coping activities by NILIM and BRI collaborated with the administration.* Paper presented at the The 43rd Joint Meeting of United States-Japan Panel on Wind and Seismic effects, 2011.

NIST. (2010). Evaluation of the FEMA P-695 Methodology for Quantification of Building Seismic Performance Factors: National Institute of Standards and Technology, NIST GCR 10-917-8.

Park, Y.-J., & Ang, A. H.-S. (1985). Mechanistic seismic damage model for reinforced concrete. *Journal of Structural Engineering, 111*(4), 722-739.

Park, Y.-J., Ang, A. H.-S., & Wen, Y. K. (1985). Seismic damage analysis of reinforced concrete buildings. *Journal of Structural Engineering, 111*(4), 740-757.

Porter, K. A., Kiremidjian, A. S., & LeGrue, J. S. (2001). Assembly-based vulnerability of buildings and its use in performance evaluation. *Earthquake Spectra, 17*(2), 291-312.

Psimoulis, P. A., & Stiros, S. C. (2007). Measurement of deflections and of oscillation frequencies of engineering structures using Robotic Theodolites (RTS). *Engineering Structures, 29*(12), 3312-3324.

Raghunandan, M., Liel, A. B., & Luco, N. (2015). Aftershock collapse vulnerability assessment of reinforced concrete frame structures. *Earthquake Engineering & Structural Dynamics, 44*(3), 419-439.

Rahnama, M., & Krawinkler, H. (1993). *Effects of soft soil and hysteresis model on seismic demands*: John A. Blume Earthquake Engineering Center.

Ruiz-García, J., & Aguilar, J. D. (2017). Influence of modeling assumptions and aftershock hazard level in the seismic response of post-mainshock steel framed buildings. *Engineering Structures, 140*, 437-446.

Ruiz-García, J., & Negrete-Manriquez, J. C. (2011). Evaluation of drift demands in existing steel frames under as-recorded far-field and near-fault mainshock–aftershock seismic sequences. *Engineering Structures, 33*(2), 621-634.

Ryu, H., Luco, N., Uma, S., & Liel, A. (2011). *Developing fragilities for mainshock-damaged structures through incremental dynamic analysis.* Paper presented at the Ninth Pacific Conference on Earthquake Engineering, Auckland, New Zealand.

Sunasaka, Y., & Kiremidjian, A. S. (1993). *A method for structural safety evaluation under mainshock-aftershock earthquake sequences*: John A. Blume Earthquake Engineering Center.

Tesfamariam, S., Goda, K., & Mondal, G. (2015). Seismic vulnerability of reinforced concrete frame with unreinforced masonry infill due to main shock–aftershock earthquake sequences. *Earthquake Spectra, 31*(3), 1427-1449.

Vamvatsikos, D., & Cornell, C. A. (2002). Incremental dynamic analysis. *Earthquake Engineering & Structural Dynamics, 31*(3), 491-514.

van de Lindt, J. W. (2008). Experimental investigation of the effect of multiple earthquakes on woodframe structural integrity. *Practice Periodical on Structural Design and Construction, 13*(3), 111-117.

Yeo, G. L., & Cornell, C. A. (2005). *Stochastic characterization and decision bases under time-dependent aftershock risk in performance-based earthquake engineering*: Pacific Earthquake Engineering Research Center Berkeley, CA.

Yi, W., He, Q., & Xiao, Y. (2007). Collapse performance of RC frame structure. *Jianzhu Jiegou Xuebao/Journal of Building Structures, 28*(5), 104-109.

Yin, Y.-J., & Li, Y. (2010). Seismic collapse risk of light-frame wood construction considering aleatoric and epistemic uncertainties. *Structural Safety, 32*(4), 250-261.

Yu, X.-H., Li, S., Lu, D.-G., & Tao, J. (2018). Collapse capacity of inelastic single-degree-of-freedom systems subjected to mainshock-aftershock earthquake sequences. *Journal of Earthquake Engineering*, 1-24.

Zareian, F., & Krawinkler, H. (2006). *Simplified performance-based earthquake engineering.* Stanford University Stanford, CA, USA.

Zareian, F., & Medina, R. A. (2010). A practical method for proper modeling of structural damping in inelastic plane structural systems. *Computers & Structures, 88*(1-2), 45-53.